








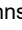








REVIEW ARTICLE | AUGUST 22 2023

# National Diagnostic Working Group (NDWG) for inertial confinement fusion (ICF)/high-energy density (HED) science: The whole exceeds the sum of its parts **FREE**

Special Collection: [Diagnostics for inertial confinement fusion](#)

J. D. Kilkenny ; W. W. Hsing ; S. H. Batha ; G. A. Rochau ; T. C. Sangster ; P. M. Bell ; D. K. Bradley ; H. Chen ; J. A. Frenje ; M. Gatu-Johnson ; V. Yu. Glebov ; R. J. Leeper ; A. J. Mackinnon ; S. P. Regan ; J. S. Ross ; J. I. Weaver 



*Rev Sci Instrum* 94, 081101 (2023)  
<https://doi.org/10.1063/5.0128650>



CrossMark

## Articles You May Be Interested In

Semi-intuitive computations and artificial intelligence: Dimensional analysis as a case study

*Computers in Physics and IEEE Computational Science & Engineering* (March 1989)

Phonological processes of consonants from orthographic to pronounced words in the Buckeye Corpus

*J Acoust Soc Am* (October 2020)

# National Diagnostic Working Group (NDWG) for inertial confinement fusion (ICF)/high-energy density (HED) science: The whole exceeds the sum of its parts

Cite as: Rev. Sci. Instrum. 94, 081101 (2023); doi: 10.1063/5.0128650

Submitted: 29 September 2022 • Accepted: 3 July 2023 •

Published Online: 22 August 2023



View Online



Export Citation



CrossMark

J. D. Kilkenney,<sup>1,a)</sup> W. W. Hsing,<sup>2</sup> S. H. Batha,<sup>3</sup> G. A. Rochau,<sup>4</sup> T. C. Sangster,<sup>5</sup> P. M. Bell,<sup>2</sup>   
D. K. Bradley,<sup>2</sup> H. Chen,<sup>2</sup> J. A. Frenje,<sup>6</sup> M. Gatu-Johnson,<sup>6</sup> V. Yu. Glebov,<sup>5</sup> R. J. Leeper,<sup>3</sup>   
A. J. Mackinnon,<sup>2</sup> S. P. Regan,<sup>5</sup> J. S. Ross,<sup>2</sup> and J. I. Weaver<sup>7</sup>

## AFFILIATIONS

<sup>1</sup>General Atomics, San Diego, California 92186, USA

<sup>2</sup>Lawrence Livermore National Laboratory, Livermore, California 94551-0808, USA

<sup>3</sup>Los Alamos National Laboratory, Los Alamos, New Mexico 87545, USA

<sup>4</sup>Sandia National Laboratory, Livermore, California 94551, USA

<sup>5</sup>Laboratory for Laser Energetics, University of Rochester, Rochester, New York 14623, USA

<sup>6</sup>Plasma Science and Fusion Center, Massachusetts Institute of Technology, Cambridge, Massachusetts 02139, USA

<sup>7</sup>Naval Research Laboratory, 4555 Overlook Ave. SW, Washington, DC 20375, USA

**Note:** Paper published as part of the Special Topic on Diagnostics for inertial confinement fusion.

<sup>a)</sup>Author to whom correspondence should be addressed: [kilkenny1@llnl.gov](mailto:kilkenny1@llnl.gov)

## ABSTRACT

The National Diagnostic Working Group (NDWG) has led the effort to fully exploit the major inertial confinement fusion/high-energy density facilities in the US with the best available diagnostics. These diagnostics provide key data used to falsify early theories for ignition and suggest new theories, recently leading to an experiment that exceeds the Lawson condition required for ignition. The factors contributing to the success of the NDWG, collaboration and scope evolution, and the methods of accomplishment of the NDWG are discussed in this Review. Examples of collaborations in neutron and gamma spectroscopy, x-ray and neutron imaging, x-ray spectroscopy, and deep-ultraviolet Thomson scattering are given. An abbreviated history of the multi-decade collaborations and the present semiformal management framework is given together with the latest National Diagnostic Plan.

Published under an exclusive license by AIP Publishing. <https://doi.org/10.1063/5.0128650>

## NOMENCLATURE

ARIANE	active readout in a neutron environment	DSR	down scatter ratio
CBI	x-ray crystal backlit imager	EHXI	equatorial hard x-ray imager
CDR	conceptual design review	EMP	electromagnetic power
CNXI	combined neutron and x-ray imager	ERASER	early radiation artifact suppression electrode rig gated MCP
DANTE	broad band, time-resolved x-ray spectrometer	EXAFS	extended x-ray absorption fine structure
dHIRES	DIM HIgh-RESolution Spectrometer	FABS	full aperture backscatter station
DIM	diagnostic insertion manipulator	FFLEX	filter flourescer
DISC	DIM insertable (x-ray) streak camera	Flange-NADS	flange neutron activation diagnostic
DIXI	dilation x-ray imager	FPA	focal plane array of detectors, usually hCMOS
		GCD	gamma Cerenkov detector

GLEH	gated laser entrance hole x-ray pinhole imager	SPBT	south pole bang time
GRH	gamma reaction history	SPIDER	streaked polar instrumentation for detection of energetic radiation
GXD	time-gated x-ray detector		
GXI	time-gated x-ray imagers	SPIE	formerly Society of Photographic Instrumentation Engineers
hCMOS	hybridized complementary metal-oxide sensor		
hDISC	hardened DIM insertable (x-ray) streak camera	SRC	solid radiochemical collection diagnostic
HED	high-energy density	SSC	streaked slit camera
hGXI	hardened (gated) x-ray imager	SSI/SSII	supernovae I/II. Multi-wavelength x-ray spectrometer
hSLOS	hardened SLOS	SXI	static x-ray imager
HSXRS	hotspot x-ray spectrometer	SXRI	soft x-ray imager
HTPD	high-temperature plasma diagnostic conference	SXSS	soft x-ray streak spectrometer
KB	Kirkpatrick–Baez x-ray microscope	TARDIS	target diffraction <i>in situ</i>
L/D	length to diameter ratio of pores in an MCP	TIM	ten-inch manipulators
LaNSA	large area neutron scintillator array on Nova	TRXI	time-resolved x-ray imager (OMEGA)
LEH	laser entrance hole	VISAR	velocity interferometer system for any reflector
LOS	line of sight	WRF	wedged range filter
MCP	microchannel plate	XRFC	x-ray framing camera
MRS	magnetic recoil spectrometer		
MRSt	time-resolved magnetic recoil spectrometer		
NAD Well-Zr	neutron activation detector in a well using zirconium		
NAD–Cu	neutron activation detector using copper		
NAD—Snout	neutron activation detector DIM-mounted snout		
NBI	near backscatter imager		
NDP	National Diagnostic Plan		
NDWG	National Diagnostic Working Group		
NIS	neutron imaging system		
NITOF	neutron imaging time of flight		
NSTec	national securities technology		
NTOF20 SPEC-A	neutron time-of-flight spectrally resolving detector in the alcove		
NTOF20 SPEC-E	neutron time-of-flight spectrally resolving detector on the equator		
NTOF20IgHi	neutron time of flight at 20 m for ignition		
NTof4	neutron time of flight at 4 m (NTof4)		
NTOF4BT	neutron time-of-flight bang time at 4 m		
NXS	NIF x-ray spectrometer		
OPSPEC	opacity x-ray spectrometer–time-gated		
OTS	optical Thomson scattering		
PD	pulse dilation of the time history of a signal for detection by a slower detector		
pDIXI	polar dilation x-ray imager		
PMT	photo multiplier		
pToF	proton (particle) time-of-flight detector (pToF)		
RadChem	radio chemistry		
RAGS	radiochemical analysis of gaseous samples diagnostic		
RIC	radiation induced conductivity		
ROIC	readout integrated circuit		
RTNADS	real time neutron activation detectors		
SFX	Sydor x-ray framing camera		
SID	system for insertable diagnostics		
SIM	six-inch manipulators		
SLOS	single-line-of-sight x-ray imager usually with pulse dilation (PD)		
SOP	streaked optical pyrometer		

## I. INTRODUCTION: COLLABORATION ON DIAGNOSTICS FOR HED SCIENCE

The National Nuclear Security Administration (NNSA) has made significant investments in major facilities and high-performance computing to successfully execute NNSA's Stockpile Stewardship Program (SSP) and exceed the Lawson criterion required for ignition.<sup>1</sup> Sophisticated diagnostics provide the connection between the experiments done on the facilities and the simulations done on the supercomputers. It is essential to continuously advance these diagnostic capabilities to improve the detail and accuracy of data, to not only reveal new, previously unknown information about complex systems but also provide information needed to truly advance learning through the falsification of hypotheses.<sup>2</sup> Indeed, data acquired from continuous improvement of diagnostics on the National Ignition Facility (NIF) falsified early theories for ignition and aided in the development of new theories.

High-energy density (HED) diagnostics on the three major US inertial confinement fusion (ICF) facilities—NIF, OMEGA, and Z—have benefited from multi-decade interlaboratory collaborations, enhanced by numerous publications mainly in this journal. Apart from meeting at the high-temperature plasma diagnostic (HTPD) conference, the genesis of these collaborations came in 1993, when the so-called Joint Central Diagnostic Team (JCdT) took responsibility for the initial diagnostics plan in the NIF conceptual design report<sup>3</sup> (CDR). A decade and a half later, a limited and clearly inadequate set of diagnostics, approximating those in the CDR, was in use when NIF started full operations in 2009.

To respond to the increasing sophistication of ICF and HED experiments on the NIF, the expert scientific community undertook national cooperative diagnostics, with major significant assignments agreed to by an interlaboratory team calling itself the NIF Diagnostic Working Group. In 2015, to formalize the collaboration and expand the scope of this work to other major ICF facilities in the US, the NNSA directed the formation and scope of the National Diagnostics Working Group for HED Science (NDWG). The NDWG is a patently successful, multi-institutional alignment of

**TABLE I.** Factors and attributes for the NDWG success.

Factor	Attribute
Collaborations: NNSA labs, industry, university, Europe	Best facility for the job Agreed diagnostic responsibilities Coordination of R & D Attracts outside experts Coordination of engineering schedules Spin-offs
Scope expands with time	Falsifiability–upgrade, new diagnostics Copious publications
Methods of accomplishing a living National Diagnostic Plan	Targeted NDWG parallel sessions Large NDWG plenary meeting Commitment of resources NDWG management group

the HED diagnostic development effort of over a dozen institutions, including three in Europe and involving well over 100 diagnostic experts. The group has met at least annually from 2009 to 2021; a leadership team with the authority to make institutional commitments meets multiple times per year to plan and track progress. The purpose of the NDWG is to encourage interlaboratory cooperation and innovation and develop and steward a coordinated National Diagnostic Plan (NDP). The NDP defines diagnostic development

activities across the major ICF facilities, identifies technical challenges and opportunities, and schedules developments. The NDP is endorsed and funded by NNSA through the ICF and assessment-science program elements within the Office of Experimental Sciences and is reassessed annually to adjust to technical progress and the evolving needs of the national HED program. Version releases are published online.

The NDWG is a remarkable achievement in cooperation, showing that the whole is more than the sum of its parts. A summary of the main factors and resulting attributes of the NDWG is shown in Table I, expanded in this Review, and summarized at the end. An example is the history of gated MCP detector development discussed in Sec. II A. An early LLE/LANL spectacular result demonstrated to the international HED diagnostic community the value of gated x-ray imaging, the value of collaborations, and the value of industrial partners. As a result of further meetings at the HTPD and early NDWG meetings, LLNL, LLE, LANL, SNL, CEA, and industry all played a role in developing MCP gating, summarized in Table II. A discussion of the implosion issues falsified by gated x-ray imaging is presented in Sec. II A.

This Review comments on the NDWG and its predecessor, the Joint Central Diagnostic Team (JCdT).

Section II lists some NDWG achievements, commenting on success factors, as shown in Table I and enlarged upon in Table XX. The first and foremost success factor is collaboration. This includes reaching agreement on diagnostic responsibilities, coordinating diagnostic schedules, and attracting and expanding collaborations

**TABLE II.** The three-decade development effort on gated microchannel plates by LLNL, LANL, LLE, SNL, and industry. Acronyms are defined in the text.

Year	Technology	Instruments	
		Nova/NIF	OMEGA/Z
1983	MCP coating		
1985	Microstrip on MCP Auston switch Solid state pulser Pulse forming module 6 Ω pulser	4 open strips 4 strips	
1990	MCP temporal model Long pulse theory	MAX module	Serpentine MCP 30 ps MCP
1995	UV laser calibration CCD readout	Flexible gated MCP	MCP on Kirkpatrick–Baez (KB)
2000	Airbox technology Monte Carlo modeling	2× engineered GXD	Gated MCP spectrometer
2005	Microprobe/modeling Long pulse validation	4× engineered GXD	4× XRFC
2010	NIF calibration Microstrip crosstalk	4× engineered hGXI	4× Sydor framing camera
2015	ERASER		



with external institutions including industry. The second success factor is having a flexible scope, especially as ideas and theory are falsified and new/better diagnostics are invented. The third success factor is copious publications to document and share progress and allow criticism. Sometimes up to three different groups, over more than a decade have worked on these HED diagnostics and copious publications help continuity.

Section III summarizes diagnostic collaborations from 1993 to 2008.

Section IV describes activities of the NDWG years from 2009 to 2021, covering the formalization of the NDWG and its NDP. The methods of accomplishment in the generation of a living National Diagnostic Plan are described as indicated in Table I.

Section V summarizes the National Diagnostic Plan for HED science as of September 2021.

Section VI summarizes and concludes the Review.

## II. TECHNICAL EXAMPLES OF SUCCESSES OF THE NDWG

This section provides examples of highly successful collaborations on HED diagnostic development, several instances of falsification of theories, and cases of unanticipated science leading to further development of diagnostics.

### A. Gated x-ray imaging with microchannel plates (MCPs)

Because a picture is worth a thousand words, gated microchannel plate (MCP) x-ray imaging is now used at nearly every HED facility worldwide.<sup>4-6</sup>

The history of this technology, which arose from the HTPD, is an excellent example of collaboration, especially with industry. The origins of this story precede the NDWG but set the model for NDWG collaboration. Notably, MCP development has continued for three decades by LLNL, LANL, LLE, SNL, and industry as can be seen in Table II. Faster x-ray gating can now be done by pulse

dilation (PD) technology (Sec. II C 4), but gated MCP technology is adequate for most HED experiments and is used more for HED measurements than any other diagnostic.

Gated MCPs were investigated in the early 1980s to record soft x-ray spectra.<sup>7</sup> The technology for coating the surface of MCPs to form electrical microstrips was critical.<sup>8,9</sup> With this technology push, the experimentalists on Nova fielded, in SIMs (Sec. III D), gated MCPs to record pinhole images of HED plasmas.<sup>8</sup> This was made possible by a company<sup>10</sup> supplying a high power, jitter-free, compact, and reliable pulse generator for the MCP.<sup>11</sup> A subsequent series of papers in the late 1980s demonstrated this capability.<sup>12</sup>

LLNL benefited greatly from collaborating with LLE and OMEGA's much higher shot rate<sup>13</sup> and was able to demonstrate a seminal result in Fig. 1 where an implosion on OMEGA was followed in time as the voltage pulse swept along the length of the meander microstrip coated on a microchannel.<sup>14</sup> These data are so spectacular that a senior HED experimentalist asked if it were a simulation upon seeing them. An elegant feature of this design is that although the stagnation of the implosion is much brighter than early emission from the laser as it lights up the glass capsule in x rays, the attenuation of the voltage pulse (and gain) as it propagates along the microstrip compensates. For most applications, however, this droop in gain is a drawback requiring careful calibration.

Another notable outcome of LLNL/LLE collaboration was the demonstration of 30 ps gating by scaling the L/D micropore length/diameter ratio with the thickness of the MCP, taking advantage of the high shot rate on OMEGA for testing.<sup>15,16</sup> Further reductions in gate time by going to an even thinner MCP are impractical due to fragility, x-ray straight-through, and lower gain, but they are achieved by pulse dilation (Sec. II C 4).

A well-engineered version of gated MCP, the so-called MAX modules, was made to be fitted on chamber-mounted diagnostics on Nova.<sup>14</sup>

In the early 1990s, LLNL developed the gated x-ray pinhole cameras detectors (GXD) to operate in the SIMs (Sec. III D) on Nova and potentially the TIMs at OMEGA. Initially, the recording of

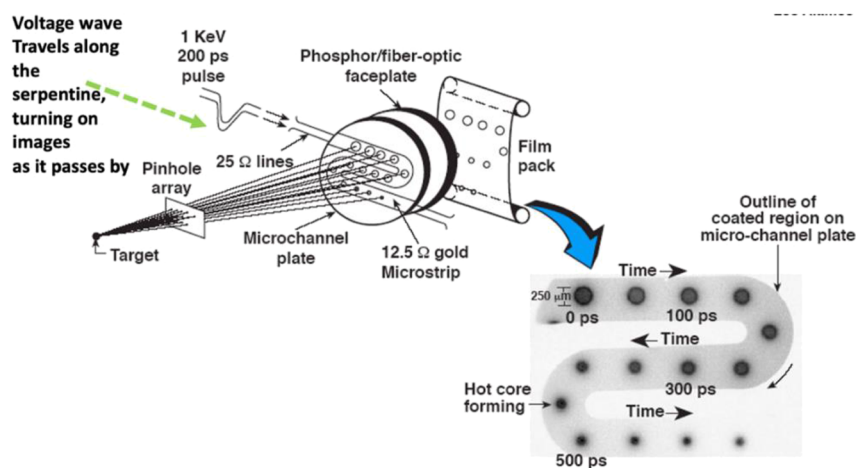


FIG. 1. The cartoon shows how the traveling voltage wave along a transmission line coated onto a MCP forms an x-ray movie of an implosion on OMEGA. The data shown are real.<sup>13</sup> Reproduced with permission from Bradley *et al.*, *Rev. Sci. Instrum.* **63**, 4813 (1992). Copyright 1992 AIP Publishing LLC.

the gated MCPs was onto film. A major improvement was to couple a CCD to the output.<sup>17</sup> Moreover, some users needed a flexible gate pulse 100–500 ps and so LLNL worked with industry for a suitable voltage pulse generator.<sup>18</sup>

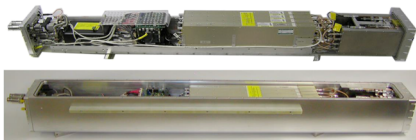
In a good example of interlaboratory collaboration, LANL took over major responsibilities for the gated MCPs on Nova, OMEGA, and initial NIF. LANL also built a dual MCP system for LLE to use on a Kirkpatrick–Baez x-ray optic on OMEGA.<sup>19</sup>

An innovation for the NIF was to field the GXD and its electronics in an “airbox” as shown in Fig. 2. The airbox keeps the electronics of the GXD near atmospheric pressure to protect it from high-voltage breakdown at chamber vacuum and provides thermal cooling of components and protection from system generated EMP. In use, the airboxes are inserted by manipulators to be near and aligned to the target during a shot. The airboxes were engineered to great effect to move around to any manipulator on NIF. Well-engineered versions of the GXD were constructed by LANL for early NIF.<sup>20</sup>

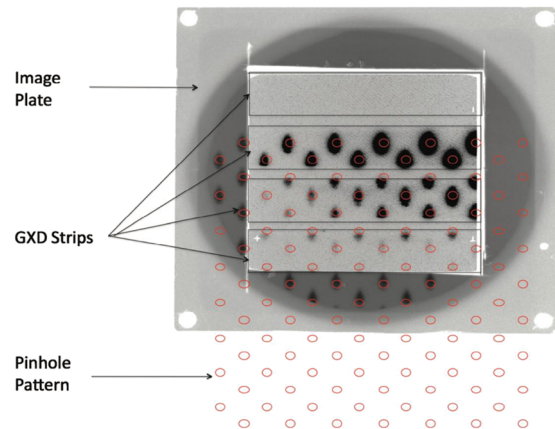
NIF now has eight airbox gated MCP detectors operable in any DIM location. There are four gated x-ray detectors (GXDs) with CCD readouts and four hardened GXDs (hGXDs) with film readout. Imagers or spectrometers are normally in front of the detector. LLE now has eight gated x-ray framing cameras. Four are called XRFC, which were assembled by LLNL, two have 30 ps gates and two have 100 ps gates. The LLNL–LLE developed technology was transferred to US industry and as a result OMEGA has four single-frame cameras (SFCs) built by Sydor Technologies, Inc.<sup>22</sup> They provide 2D spatially time-resolved frames or 1D spectrally resolved images of target features. Their systems can be configured with fast or slow detection heads for frames ranging from 40 to 1000 ps in duration. OMEGA’s GMXI gated camera came from LANL.

To improve ease of operation, an array of pinholes is used to make alignment easier and to also allow a time-integrated detector, image plate to be placed around the gated detector as shown in Fig. 3 and described by a LANL led paper.<sup>21</sup> Modern pinhole arrays have diamond looking signature pattern on the center to quantify mispointing of the snout.

The longer time scales on Z relaxed their need for ~100 ps gating, and several instruments with ns gating of MCPs were in place on Z by the late 1990s.<sup>23</sup> SNL accurately modeled the time



**FIG. 2.** The gated x-ray detector pulled outside the airbox (top) and within (bottom).<sup>20</sup> Various types of imaging and spectrometer nosecones can be placed in front of the detector when the instrument is in the NIF vacuum chamber. These gated x-ray detectors are each designed to fit within an aluminum airbox and are fitted with an array of environmental housekeeping sensors. These instruments are significantly different from earlier generations of gated x-ray images due, in part, to an innovative impedance matching scheme, advanced phosphor screens, pulsed phosphor circuits, precision assembly fixturing, unique system monitoring, and complete remote computer control.<sup>21</sup> Reproduced with permission from Oertel *et al.*, *Rev. Sci. Instrum.* **77**, 10E308 (2006). Copyright 2006 AIP Publishing LLC.



**FIG. 3.** Time-integrated image plate records the implosion images surrounding GXD images, with an overlay of the pin hole array.<sup>21</sup> Reproduced with permission from Kryala *et al.*, *Rev. Sci. Instrum.* **81**, 10E316 (2010). Copyright 2010 AIP Publishing LLC.

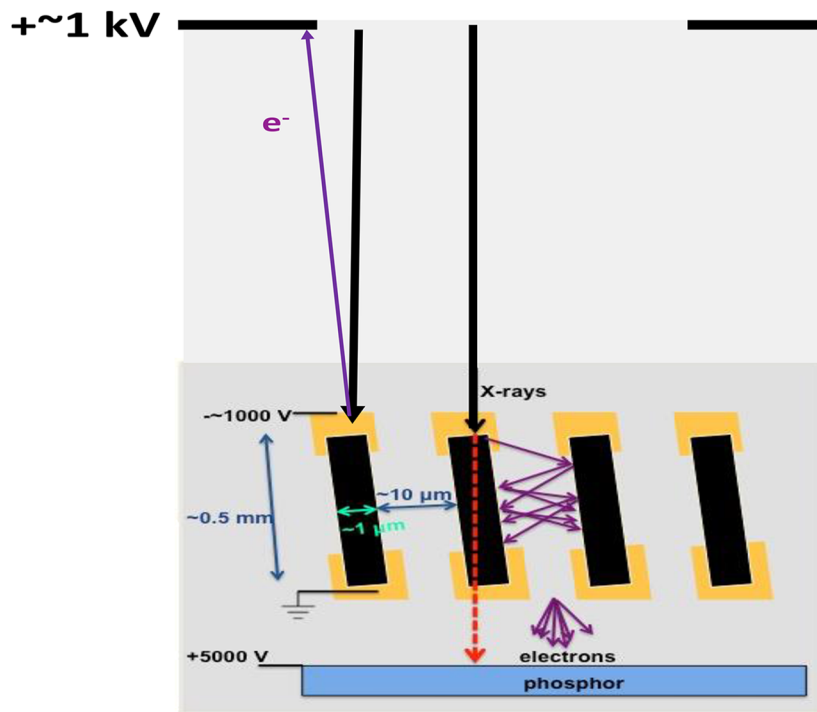
response of MCP gain introducing the new technology of electrical microprobe.<sup>24,25</sup>

Extensive use of MCP detectors on NIF unearthed nuances. Each conducting microstrip coated onto the MCP, together with the dielectric MCP and its rear-surface ground plane, acts as a transmission line: Voltage is transmitted along the strip as a traveling electromagnetic wave. Because of the strong dependence of MCP gain on voltage, small variations in voltage along the microstrip can lead to substantial variations in gain. When more than one microstrip is used, the multiple propagating waves may interact, inducing currents and voltages on neighboring strips. Any induced signal also travels along the microstrip and, as a result, the effective pulse voltage and propagation velocity may be altered. LLNL collaborated with SNL, which used slower gating of MCP cameras,<sup>25</sup> to understand and develop mitigation of the effects of cross-timing by careful relative strip timing.<sup>26</sup>

An even more subtle effect is that a MCP is slightly responsive to x-ray signals arriving before a gate pulse. Although gated MCPs had been used for decades, increasingly sophisticated HED experiments revealed this kind of artifact. These x rays liberate one or more electrons. While one might have expected early electrons to dissipate by either leaving the MCP surface or being reabsorbed, it appears that some are trapped at the surface of the MCP. As a result, when the voltage pulse passes at a later time, those trapped electrons are amplified, producing an additional background signal. Mitigation can be by a small eraser DC field (Fig. 4) applied to pull photoelectrons that are formed before a gate pulse is applied, away from the MCP.<sup>27</sup>

There is significant attenuation of the MCP gain from a small drop in voltage and the corresponding large drop in gain as the voltage pulse propagates along the strip. This effect requires a gain calibration against position along a strip. LLNL and CEA collaborated on complementary methods of calibration of the “droop” in MCP gain along the necessarily resistive microstrip.<sup>5,28</sup>

Gated MCP imagers are widely used: One of their many uses is to tune the symmetry of hohlraum drive. Importantly, they have



**FIG. 4.** Schematic diagram of Early Radiation Artifact Suppression Electrode Rig (ERASER).<sup>27</sup> Background electrons liberated by early x rays are attracted upward to the electrodes held at  $+ \sim 1$  kV as shown. Signal photoelectrons in purple are amplified as shown in the central channel of the MCP when a pulsed  $\sim 1000$  V is applied across the MCP in black. Reproduced with permission from Benedetti *et al.* *Rev. Sci. Instrum.* **87**, 023511 (2016). Copyright 2016 AIP Publishing LLC.

been used to quantitatively improve the physics model. For example, to match the measured implosion symmetry, models for heat transport<sup>29,30</sup> and the cross-beam-energy-transfer<sup>31</sup> are added. The images also reveal critical aspects that were previously underestimated in modeling. For example, gated imaging has shown that the capsule support structure<sup>32,33</sup> and the capsule fill tube<sup>34,35</sup> have detrimental effects on implosions underestimated by simulations. Similarly, imaging shows the effects of underpredicted mix.

In summary, gated MCP detectors are remarkably useful in HED applications. They do have limitations arising from relatively low saturation of gain and low detective quantum efficiency, but their use at almost all HED facilities is testament to their utility. Notably, the present status is due to shared ideas and resources from LLNL, LLE, industry, SNL, CEA, and LANL over the last 30 years. Although the development of gated MCP instruments started before the NDWG, the multilab, industry, and international collaboration was a marvelously productive collaboration and set a model for the NDWG.

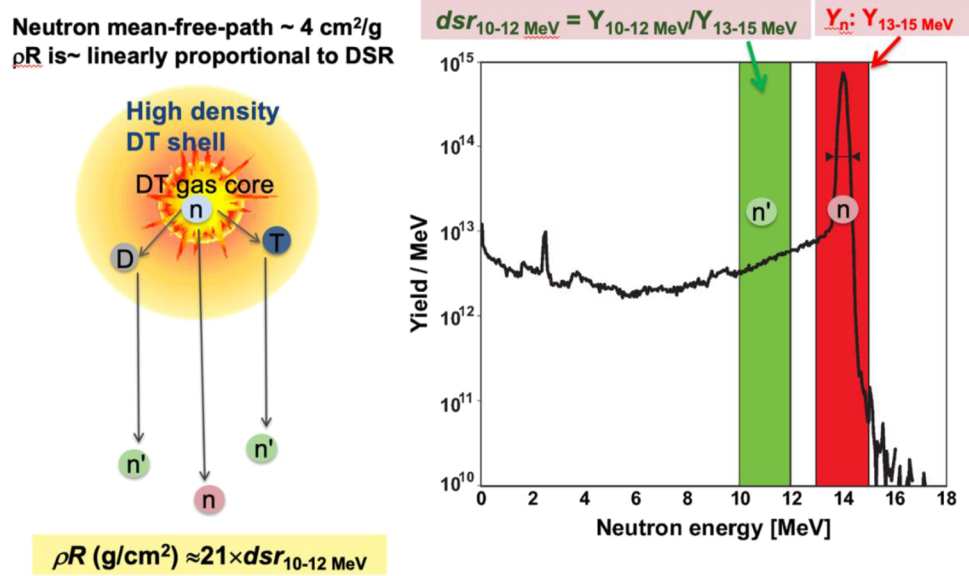
## B. Neutron spectroscopy

Nuclear diagnostics for inertial confinement fusion (ICF) plasmas have been comprehensively reviewed by Frenje.<sup>36</sup> Behind Frenje's opus, there is an interesting history that drove the nuclear diagnostics installed on the major HED facilities. In a burning plasma, early simulations/theory predicted isotropic yield and areal

density and a primary neutron spectral width  $\sim T_{\text{ion}}^{1/2}$ .<sup>37</sup> Brysk's paper<sup>37</sup> suggests measuring  $T_{\text{ion}}$  from the spectral width of primary neutrons: The conceptual simplicity of measuring  $T_{\text{ion}}$  with neutron-times-of-flight (nToF) drove their installation on the early HED facilities as well in the NIF CDR.

Areal density can also be obtained from neutron spectroscopy. The areal density of DD implosions can be measured by secondary DT neutrons<sup>38</sup> but only for imploded areal density less than  $\sim 0.1$  g/cm<sup>2</sup> and fusion of deuterium fuel. This means secondary neutron spectroscopy for areal density measurements was suitable for Nova, Z, and OMEGA but not for NIF ignition scale implosions because the compressed DT areal density is too high. Consequently, effort in the 1990s concentrated on single-hit LaNSA at Nova for tertiary scattered neutrons.<sup>39,40</sup> The sensitive neutron spectrometer (SNS) was developed in the waning days of the Nova laser and is conceptually similar to that of the LaNSA. It was transferred to the OMEGA laser soon after Nova was shut down in 1999 and operated continuously as the MEDUSA array on all of the neutron producing experiments of OMEGA until it was decommissioned for the construction of the OMEGA EP laser beginning in 2006.

Measuring higher DT areal density required development. The use of down-scattered neutrons for areal density was proposed by Azechi,<sup>41</sup> but as Azechi says it is "a formidable task to measure the lower energy scattered neutrons in the presence of and importantly *after* a large numbers of un-scattered neutrons." Quantitatively, it is hard because even a large areal density of, say, 1 gm/cm<sup>2</sup> of

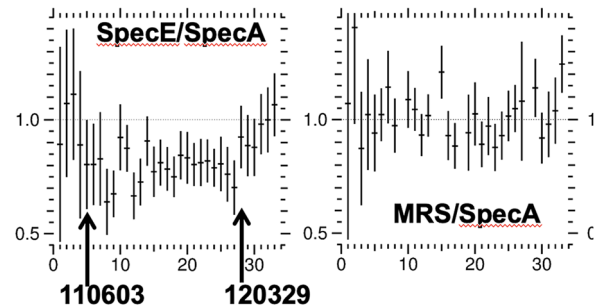


**FIG. 5.** The physics of down-scattered neutrons. The number of primary 14 MeV neutrons scattering off surrounding DT, as shown in Fig. 2, is a measure of the areal density of the surrounding D & T. The  $DSR_{10-12\text{ MeV}}$  defined as  $Y_{10-12\text{ MeV}}/Y_{13-15\text{ MeV}}$ , the fraction of neutrons scattered between 10 and 12 MeV is less than the total down-scattered neutrons ratio but is used because in this spectral region other sources of neutrons are insignificant. Adapted with permission from Frenje *et al.* Rev. Sci. Instrum. **79**, 10E502 (2008). Copyright 2008 AIP Publishing LLC.

compressed DT only scatters ~20% of the 14 MeV primary neutrons and over a 12.5 MeV neutron spectral width, down to the deuterium backscatter edge at 1.5 MeV. However, it is only the 10–12 MeV range that is not polluted by other sources of neutrons.

The physics of using down-scattered neutrons to measure the areal density of DT<sup>33</sup> is shown in Fig. 5. In the calculated neutron spectrum in Fig. 5, the spectral region between 10 and 12 MeV is dominated by down scattering and not thermal broadening of primary neutrons nor tritium–tritium thermonuclear neutrons. This is true even for igniting plasmas with  $T_{\text{ion}} \sim 12$  keV. Although the down scatter ratio into 10–12 MeV range is less than the total down-scattered ratio, it is a clean measurement of areal density given by the formula on the left in Fig. 5.<sup>36</sup>

MIT and LLE scientists started Azechi’s “formidable task” on OMEGA and NIF using a magnetic recoil spectrometer (MRS) and one spectrally resolving nToF as detailed in Secs. II B 2 and II B 1, respectively. NIF management scrutinized the reason for complementary measurement techniques. Popper’s reasoning<sup>2</sup> about falsifiability eventually held sway because measuring an observable in two different ways could falsify the measurements. Moreover, two nToFs were sanctioned. NIF management asked why two nToFs were needed, but as the first years of NIF cryogenic implosions were disappointing, the need for more diagnostics was becoming apparent. It is very interesting that initially the two nToFs systematically gave different results as shown in Fig. 6 (the date code for the NIF shot number shown is yy/mm/dd) although MRS generally agreed with Spec-A, which is the ~20 m distance nToF in the neutron alcove. It was initially suspected that there was a difference in calibration and so the detectors were interchanged but to no avail,

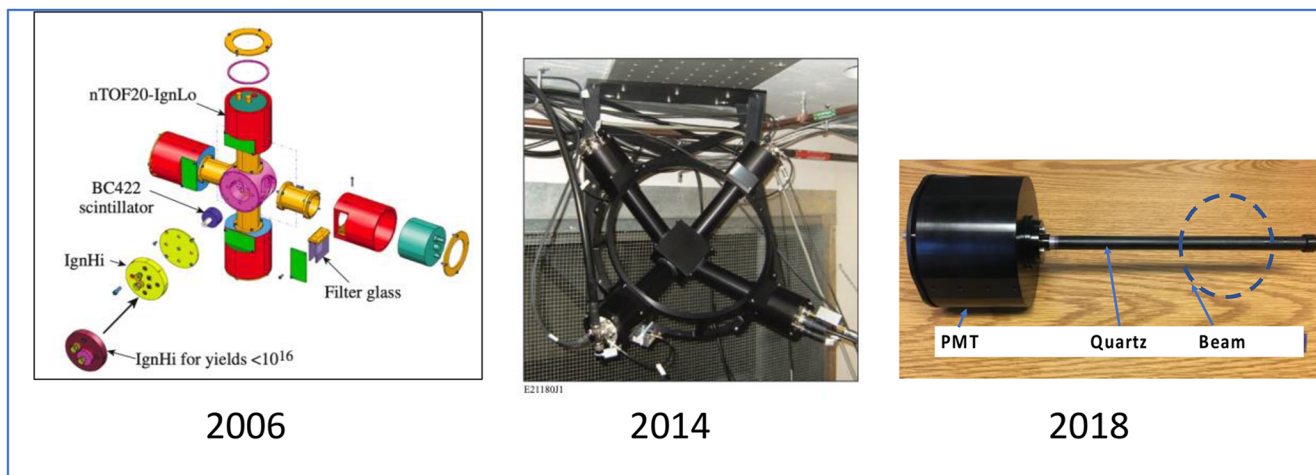


**FIG. 6.** Ratios of the down-scattered ratios  $DSR_{10-12\text{ MeV}}$  from three diagnostics Spec-A, Spec-E, and the MRS, plotted against NIF shot number from June 2011 (110603) to March 2012 (120329). At the time it was thought, incorrectly, that the calibration of Spec-E might have been systematically low. Courtesy Munro.

proving that the areal density was anisotropic. The assumption of areal density isotropy had been falsified.

Even the unscattered yield at 14 MeV was shown to be anisotropic because the areal density the neutrons scatter from is anisotropic. Initially, the unscattered yield on NIF was measured by one Zr and one Cu threshold neutron activation detector (NAD). However, an areal density anisotropy was measured by a related diagnostic, the flange-NADs, measuring the unscattered yield in 18 different directions<sup>42</sup> and later in 48 different directions with RTNADS.<sup>43</sup> Falsification of the theory of symmetry led to two more generations of nToF diagnostics as shown on Fig. 7. This expansion of scope took well over a decade to implement.





**FIG. 7.** The three generations of neutron time-of-flight (nToF) detectors used on NIF. Shown on the left, PMTs (red) are close to the BC422 scintillator. Shown in the center, the PMTs view the bibenzyl scintillator (center) through radial light pipes. Shown on the right, the neutron beam (dashed circle) is incident on one end of the quartz rod, and the other end goes to the PMT. Adapted with AIP Publishing LLC permission from Refs. 57–59.

With the wisdom of hindsight, it is clear a poor implosion will have a lower areal density at the position of say the capsule fill tube, causing a drift motion of the burning plasma and a consequent lower areal density in that direction. Such drift motion was first observed as shifts in neutron spectrum mean peak energy,<sup>44</sup> initiating an effort to understand the seeds for and effects of directional motion on NIF implosions.

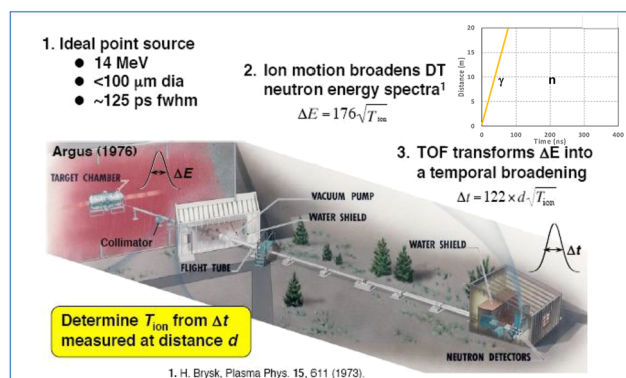
There is an interesting story about  $T_{ion}$  as measured using Brysk’s formula for spectral width. A LANL scientist<sup>45</sup> and LLNL theoretician<sup>46</sup> realized that a spatial variance of the drift velocity along the line of sight of a burning plasma adds to the Brysk neutron spectral broadening. Experimentalists<sup>47</sup> compared the spectral broadening of the DD to the DT neutrons verifying this theory. Moreover, in a series of beautiful experiments a deliberate drive asymmetry was imposed on a series of implosions showing that the Brysk derived  $T_{ion}$  varied with direction of observation.<sup>48</sup> So much for a scalar  $T_{ion}$ !

Again, with the wisdom of hindsight, the reliance on theory for complicated, unstable implosions was too optimistic but careful neutron spectroscopic measurements with input from LLE (and well-diagnosed DD and DT implosions on OMEGA), LANL, MIT as well as LLNL eventually improved our understanding. Central to the use of neutron spectroscopy to advancing our understanding of implosions was the diagnostic collaborations between LLNL, LLE, MIT, and LANL. The nToF story below also emphasizes this.

### 1. Neutron time-of-flight diagnostic for OMEGA, NIF (and Z)

This is the story of the collaborations over two decades, producing three generations of nTOFs for NIF as illustrated in Fig. 7.

For transitory HED experiments, nToF measurements are readily interpreted as a neutron spectrum as shown from a 1976 LLNL viewgraph (Fig. 8). It is interesting that the detector building

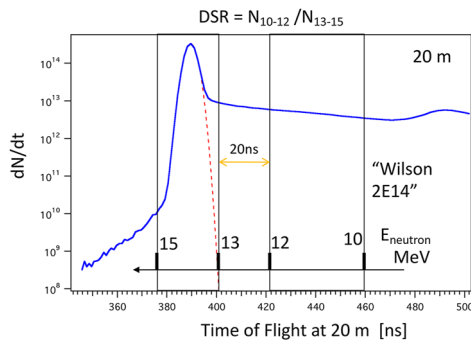


**FIG. 8.** Cartoon from 1976 illustrating the simple yet incomplete physics argument for determining ion temperature from the broadening of neutron arrival times at a distant neutron detector. In 1976, the Argus laser in B381 at LLNL was producing neutrons, but slow detectors required a long flight path. Reprinted with permission from H. G. Ahlstrom, Report No. UCID-18707 (1980). Copyright 1980 Lawrence Livermore Laboratory.<sup>207</sup>

shown is far ~80 m, from Argus, one of the earliest implosion lasers, because of the slow detection (PMT and scopes) technology available in 1976. It was because of the simple yet incomplete argument in Fig. 8 that nTOFs were included in the NIF CDR.

Nowadays, nTOFs are vital to measure areal density. Azechi, Cable, and Staf<sup>41</sup> had shown that areal density could be measured by down-scattered ratio (DSR). Hatchett<sup>49</sup> carefully defined  $DSR = Yield_{12-10 MeV} / Yield_{15-13 MeV}$  as shown and explained in Fig. 9 (Courtesy Wilson, LANL). Hatchett realized that 10 MeV stays above the TT neutrons and 12 MeV is below Brysk broadening.

However, it is a “formidable task,” to quote Azechi, to make a tiny arrival rate measurement after a much larger signal because of PMT saturation, scintillator slow decay, cables, etc. Another



**FIG. 9.** Calculated neutron spectrum vs arrival time at ~20 m, showing the 15 to 13 MeV region and the 12 to 10 MeV region used to calculate the down scatter ratio (DSR). The TT edge is visible ~9 MeV, and the broadened 14 MeV primaries extend down to 13 MeV. Courtesy Munro and Wilson.

formidable task is to make measurements over neutron yields from  $10^{11}$  to  $10^{18}$ . This is the amazing story of how the NDWG achieved this and much more. For the NIF CDR, this was thought to be too hard for the technology at that time and tertiary neutrons were to be used for areal density.

A standard nTOF has a scintillator with neutron induced glow detected by a PMT outputting current to a “scope.” This current mode type nTOF detector was used on Nova with poor accuracy.<sup>50</sup> One nTOF was included in the initial CDR planning on NIF but for  $T_{ion}$  not areal density. A much faster neutron detector than that used for Nova had to be designed, tested, and calibrated. LLE staff led the nTOF effort on NIF through the beginning of the NDWG.

LLE first worked on speeding up and increasing the dynamic range of the PMT. For DD neutrons from DT implosions, they worked with UK industry and AWE to enable gating out the earlier and larger (100×) DT neutron signal (or for DT neutrons, the earlier gamma signals). This mitigated the important charge depletion of the PMTs.<sup>51,52</sup> This collaboration on next-generation PMTs was also central and key to the gamma spectroscopy work of the NDWG.

The PMT also needs to be linear. The onset of PMT nonlinearity for a MCP PMT occurs as the “reservoir” of charge at the end of each channel becomes depleted after about a nano-Coulomb of extracted charge. Nonlinearity develops into detector saturation. Nonlinear effects in the photocathode have been observed by coauthors in other detectors but have not been examined or observed in this work. Studies of the saturation and speed of MCP PMTs were carried out for several years by the collaboration,<sup>52,53</sup> including SNL. Speeds of ~100 ps FWHM but with ringing were achieved for 10 mm diameter photocathodes. This was a great example of LLE collaboration with AWE and industry. Much of this was discussed at early NDWG meetings circa 2012.

Another part of the “formidable task” was identifying a scintillator without long decay, as the glow from slower, down-scattered 14 MeV neutrons would be contaminated by glow decaying from the much larger scintillation from the earlier, 14 MeV neutrons. Standard scintillators can be as fast as 4 ns but with a much longer-lived residual decay. More work was done on this over the

next 5 years by LLE and Lauck.<sup>54</sup> LLNL also found an alternative scintillator with less afterglow than standard scintillators.<sup>55</sup>

Both labs began to realize that a well-collimated line of sight minimized contributions from room re-scattering of neutrons was essential for making these measurements.<sup>56</sup>

OMEGA was routinely producing DT and DD neutron yields calibrated against activation or CR39 counting. As a result, LLE undertook responsibility for building, calibrating on OMEGA, and then transporting to NIF the first 4.5 m distance nTOFs (nTOF4.5) on NIF.<sup>57,58</sup> The calibration and linearity of the first-generation (2006) nTOFs were tested on OMEGA as shown in Fig. 10. This was a good example of interlaboratory task assignment and utilizing the appropriate facility for the job.

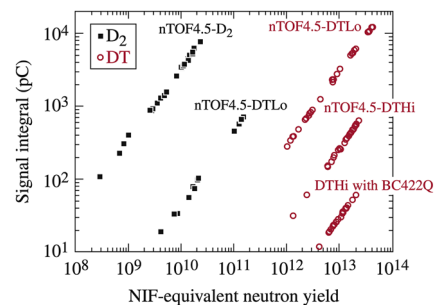
A second-generation nTOF detector for NIF was designed by LLNL and tested by LLE, incorporating features to reduce background signals from neutrons in the collimated beam scattered off the scintillator toward the four PMTs as shown in Fig. 7 (middle).<sup>58</sup> An important change shown in Fig. 7 (middle) was to distance the PMT from the scintillator and out of the neutron beam.

So, after two generations of nTOFs, with intense LLE-LLNL collaboration and using OMEGA as the best facility for the job of calibration, the nTOFs were installed on NIF.

Even though we had made the nTOFs faster, the response time of the detector was still about 4 ns FWHM. This is about the same at 20 m as the “Brysk” broadening at a  $T_{ion} \sim 5$  keV. An instrument response time similar to the width being measured is workable but not ideal. However, an important and arguably the most important physics that was coming out of the nTOFs was a measurement of the drift velocity of burning plasma from the neutron Doppler shift  $dE/E_n = -2 v_{drift}/v_n$ . To measure drift velocities, four or five nTOFs are needed as there are four free parameters in the shift: three directions plus the “Gamow” shift due to incident thermal energies of the triton and the deuteron. Moreover, for drift velocities ~10 km/s, arrival time accuracies of ~50 ps are needed.

Drift velocity measurements up to 100 km/s falsified the expectation that the stagnating and burning plasma was “stationary.” This was rediscovered on both OMEGA and NIF and shared at a meeting of the NDWG.

Then, in a stunning development a third-generation nTOF was invented. Replacing the scintillator with a quartz Cerenkov, neutron to light transducer.<sup>59</sup> Neutrons can produce Cerenkov light



**FIG. 10.** Summary of the nTOF4.5-K2, nTOF4.5-DTLo, and nTOF4.5-DTHi calibration on OMEGA.<sup>57</sup> Reproduced with permission from Glebov *et al.*, Rev. Sci. Instrum. **81**, 10D325 (2010). Copyright 2010 AIP Publishing LLC.

in quartz by exciting a nucleus, which then beta decays. Unlike the atomic decay from a scintillator, there is no long-lived glow: The speed of this neutron diagnostic is limited by the PMT, cabling, and “scope.” Although the use of quartz had been investigated decades earlier,<sup>60</sup> it was not until the availability of high purity quartz that the concept became viable. Notably, a stimulus for LLNL to reengage this concept came from LLE via a National Diagnostic Workshop with the CEA. This is another example of new or old ideas arising from collaborations.

In the end, as illustrated in Fig. 7 three generations of scientists produced three versions of the NIF nTOFs [LLE original, LLNL JAC Black (middle), and quartz Cerenkov (QCD)], taking a decade and a half.

The success of the nTOFs on NIF as discussed at many NDWG meetings led to LLNL/LLE agreeing to provide systems to Z. A good example of shared responsibility.

The nTOF story is another great example of success from the NDWG. There was significant input from LLE, LLNL, AWE, SNL, and industry. Experts were attracted to work on diagnostics. Diagnostic assignments were agreed. A new product was spun off by industry. At most of the fifteen large NDWG meetings, and at six specialized nTOF workshops, nTOFs were discussed. This was another marvelous story of collaborative research based on technology push arising from a NDWG meeting. Moreover, the original motivation for one nTOF measuring  $T_{\text{ion}}$  was found to be false or incomplete, but that led to measuring areal density and large drift velocities that very significantly impacted the approach to ignition. Because many nTOFs give a direction of any drift velocity, similar to a coarse picture, they suggest a direction to fix the drive asymmetry, which causes a drift velocity. Advances in nTOF have clearly helped discover new implosion physics. The NIF CDR only had one nTOF. We originally asked ourselves “Why do we need two nTOFs?” The whimsical response, “Because we cannot afford ten” is not quite right; it was to quantify implosion asymmetries. NIF has five nTOFs at the moment.

## 2. Neutron spectroscopy with magnetic recoil spectrometer and time resolution

A complementary instrument to the nTOF for neutron spectroscopy on OMEGA and NIF is the magnetic recoil spectrometer (MRS),<sup>61</sup> first used on JET.<sup>62</sup> Neutron energy dispersion is achieved by “knocking-on” deuterons from a nearby foil and then magnetically analyzing their energy. MIT staff who implemented this technology on JET first installed an MRS on OMEGA<sup>63</sup> as at the time it seemed the only way to measure the low DSR on OMEGA. Installation of MRS on OMEGA was a critical learning experience for the NIF MRS. The detector is CR39, a plastic that when carefully etched can detect single deuterons. A critical nuance on the etching is the phased etching development of the coincidence counting.<sup>64</sup> Without it, MRS would not have worked at OMEGA.

The MRS on OMEGA first recorded DSR in 2008<sup>65</sup> a major ICF milestone. At the time, MRS was the only proven technique for measuring DSR. Subsequently, LLE and MIT took on responsibility for the design, installation, and operation of another MRS on NIF. This recorded the first DSR data on NIF, as the nTOFs were at the time not capable of measuring down-scattered neutrons. The MRS worked beautifully on the second shot and played a critical role in the development of the nTOFs.

With an MRS on each laser, it was possible to develop nTOFs on OMEGA and bring them to the NIF with the cross-calibration of the spectral sensitivity provided by the MRS.

The NIF MRS also provided critical guidance to the ignition program as it provided robust data quickly. Complementary diagnostics with different weaknesses and strengths are incredibly important for any science as measurements cannot be proven to be right but they can be falsified by a different instrument. MRS complements nTOFs for DSR and “ $T_{\text{ion}}$ ,” and complements NAD for yield, as unlike nTOF, MRS is an absolute-yield diagnostic. It is also incredibly important to use functioning diagnostics to validate diagnostics being implemented for similar measurements.<sup>66</sup> MRS also provided the first measurements of peak shifts, identifying them as signatures of drift velocity,<sup>44</sup> spurring the efforts to resolve these measurements in 3D using an upgraded high-precision quartz nTOF suite.

With higher yields on NIF, MRS provides better data including  $T_{\text{ion}}$  and peak shifts.<sup>67</sup> With adequate shielding, the MRS will continue to provide better data as we go along.<sup>68</sup> As yields get higher, it is critical to move the MRS behind the shield wall. Out there, the MRS performance will be an order of magnitude better in terms of S/N. Energy resolution will be better as well. MRS is still important for coverage, DSR asymmetry, and 4PI DSR, especially when it is behind the shield wall for high yields and nTOFs are struggling.

This is another marvelous story of collaborations, bringing in new ideas and people and resource commitment by LLE and MIT to NIF diagnostics. Moreover, there is a great triple story on the complementarity of measurements.

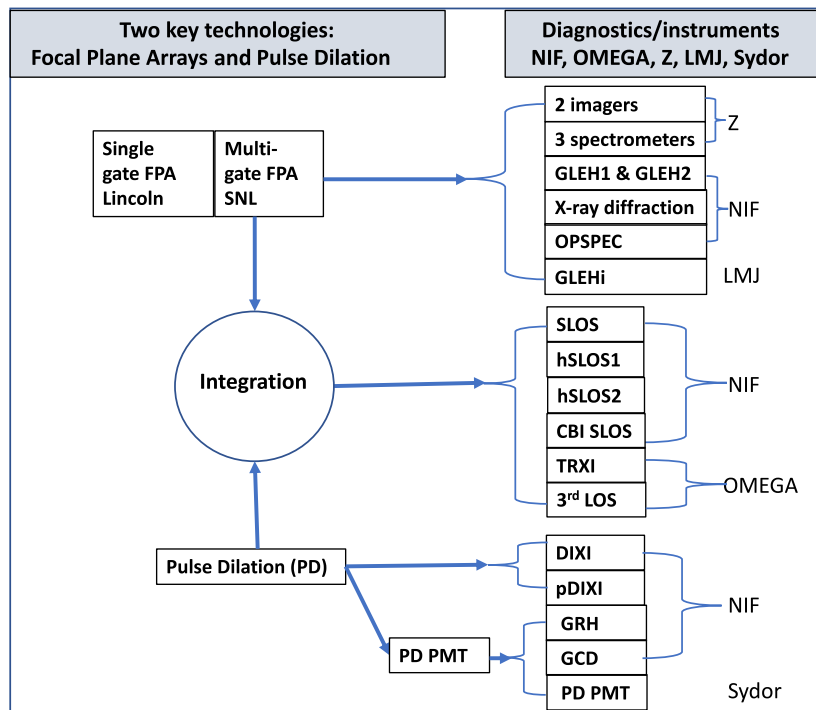
It is important but very difficult to time-resolve the neutron spectrum from an implosion. Some concepts to use an ultrafast nTOF are being developed but are a long way from implementation. Conceptually, a time-dependent spectrum can be obtained from MRS by a time-resolving detector at the dispersion and focal plane of the magnetic spectrometer.<sup>69–73</sup> The trouble is a large time skew at the focal plane that needs to be corrected for by the pulse dilation (PD) technique described in Sec. II C 4.<sup>74</sup> Smaller streak cameras can look at subsections of the focal plane and provide the same data as the PD but at a worse quality.<sup>75</sup> Research continues.

## C. The “SLOS/hCMOS” work of the NDWG

The outstanding achievement of the NDWG is the imprecisely named work called single-line-of-sight (SLOS) hybridized complementary metal-oxide sensor (hCMOS) diagnostics/detectors. Figure 11 clarifies our terminology. There are two basic technologies: (i) time-gated pixel arrays at the focal plane (FPA) and (ii) diagnostic-signal pulse dilation (PD). On the right of Fig. 11 are the diagnostics that use the two technologies, sometimes separately (top and bottom) and sometimes together (middle).

In this section, we start with time-gated focal plane arrays (FPAs) using the hCMOS technology. SNL has named these FPAs Furi, Icarus, and Daedalus (Sec. II C 1). This nanosecond gating is fast enough for the many diagnostics shown on the top right of Fig. 11. Details are provided in Secs. II C 1–II C 3. Pulse dilation (PD) stretches diagnostic signals, allowing recording of 10 ps or less. The diagnostics that just use this technology alone are shown on the bottom right of Fig. 11. Moreover, in another tour de force the





**FIG. 11.** The two technologies—(left upper) time-gated focal plane arrays and (left lower) pulse dilation—and the diagnostics that use either of the technologies alone (top and bottom right) or both technologies (middle right).

diagnostics that use both the FPAs and PD are shown in the middle on the right of Fig. 11. This is all a marvelous collaboration between, SNL, LLNL, GA, LANL, industry, and CEA for HED diagnostic development, and every part of it is all well documented in the Review of Scientific Instruments.

### 1. Multiple time-gated hybridized CMOS arrays

Many HED diagnostics need an array of gated light or x-ray detectors at their focal plane (FPA). Around 2005, MIT Lincoln Lab, LLNL, and LANL started work on gated FPAs. Gated MCP technology (Sec. II A) had demonstrated the need for  $\sim 100$  ps gating, guiding requirements for FPA gating times of  $\sim 100$  ps (PD had not been invented then). A  $256 \times 256$ , 250 ps, single-frame, readout integrated circuit (ROIC) was built with limited success,<sup>76–78</sup> but resource limitation and bump-bonding issues caused this effort to be abandoned (bump-bonding is the process that attaches an array of photodiodes to a ROIC).

At SNL on Z, the time gating requirement was more relaxed at  $\sim 2$  ns,<sup>79</sup> and so an in-house foundry located at the Microsystems Engineering, Science and Applications (MESA) complex at SNL was used to develop a  $\sim 2$  ns-gated hybridized CMOS sensor array<sup>80</sup> as part of the NDWG. In contrast to the Lincoln Lab work, this was a multi-time gate ROIC but with a propagating wave pixel switch. Four gate times for each pixel is achieved by sequentially switching its photocurrent to four small capacitors behind each pixel whose charge is read out later. The FPA hybridized a silicon photodiode detector array, directly “bump”-bonded to a CMOS ROIC. Several

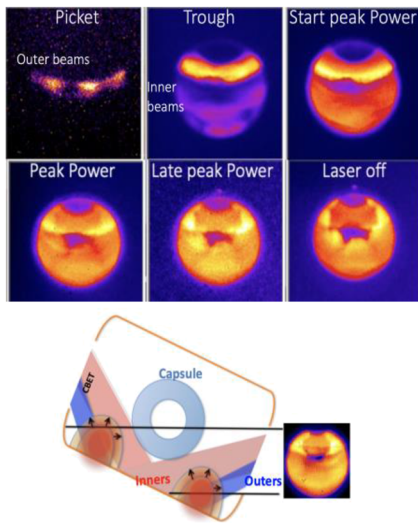
generations of these so-called hybridized CMOS (hCMOS) were and are being developed by SNL (see Table III).

The external hCMOS drive electronics were eventually supplied by LLNL as was the calibration.<sup>81</sup> The third-generation FPA, Icarus-2, is the most utilized so far, with a total of fifty-two Icarus-2 FPAs eventually delivered to Z, NIF, and OMEGA.<sup>82</sup> A fourth-generation FPA, Daedalus, has been completed. Testing of Daedalus V2 has been through review, fabrication has started, and it is planned to be used on the NIF gated opacity spectrometer OPSPEC discussed in Sec. II C 3.

The first key issue of hCMOS arrays<sup>80</sup> is the trade-off between decreasing x-ray efficiency of the photodiode array as  $h\nu$  increases and longer photoelectron collection delay at the gated readout electronics,<sup>80</sup> with increasing thickness of the array. A second

**TABLE III.** Several generations of hybridized CMOS FPAs built at the MESA facility at SNL.

FPA	Gate (ns)	No. Frames	No. Pixels
Furi	2	2	$448 \times 1024$
Hippogriff	2	2	$448 \times 1024$
Icarus-2	$\sim 1.5$	4	$512 \times 1024$
Daedalus	1	3(6)	$512 \times 1024$
$dx \mu\text{m}$		25	



**FIG. 12.** GLEH-2 images on NIF throughout the picket, trough, and peak power of the laser. The geometry is shown in the lower cartoon.

issue is the reduced dynamic range for harder x rays because one x-ray photon produces thousands of photoelectrons. Currently, the photodiodes are Si with a hCMOS gate time 1–2 ns—adequate for many applications (Fig. 11, top right). High-energy photodiode array development has started with the design, fabrication, and testing of discrete pixelated arrays of GaAs photodiodes at SNL and design, fabrication, and testing of discrete Ge diodes at LLNL. A spin-off from the gated FPA work at SNL is a startup company called Advanced hCMOS Systems, Inc.

## 2. Gated Laser Entrance Hole imager application of hCMOS FPA on NIF and LMJ

The 1–2 ns time gating of the SNL hCMOS FPAs is adequate for multi-ns phenomena such as measuring the morphology of the interior of hohlraums being irradiated by ~5 ns and highly shaped laser pulses.<sup>83</sup>

This was first demonstrated successfully on NIF using a first-generation hCMOS sensor Furi behind an x-ray pinhole imager looking through a laser entrance hole (GLEH-1) to capture the three-dimensional plasma dynamic evolution from the hohlraum interior walls.<sup>84</sup> 3D modeling is in progress.

An upgrade (GLEH-2) was implemented<sup>80</sup> using two ICARUS hCMOS sensors, providing much improved spectral, temporal, and spatial response.<sup>85</sup>

In addition, an ICARUS hCMOS camera system was loaned to the CEA in 2019 for use on the Laser Mega Joule (LMJ) facility in Bordeaux, France, as part of the CEA/NNSA collaboration. It has been fitted to the LMJ DMX line of sight. This camera was implemented on LMJ as GLEHi in a similar setup as that of NIF GLEH to capture the hohlraum data and has provided valuable data to the CEA ICF physics study group.

These diagnostics are shown on the upper right of Fig. 11; data are shown in Fig. 12.

## 3. Time-resolved x-ray diffraction, GLEH in France, and opacity diagnostics using hCMOS FPAs

X-ray diffraction diagnostics for HED identify phases of compressed materials. The technique has been used on NIF and OMEGA, limited to using the TARget Diffraction In Situ (TARDIS) diagnostic to obtain one or two snapshots per laser shot.<sup>86</sup> X-ray diffraction is being developed for Z.<sup>87</sup>

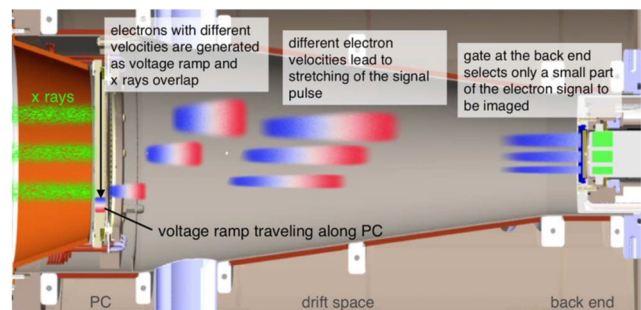
Time-resolved x-ray diffraction using gated hCMOS arrays provides significant enhancement to the HED materials-diffraction program with the capability of making many diffraction measurements/shots with a multi-gate FPA such as Icarus. Recently, a couple of four-frame hCMOS FPAs have been used to measure the transition in laser shocked lead from the hcp phase to the bcc phase at about 6 ns, with higher signal-to-noise ratio than achievable with TARDIS.<sup>88</sup>

In addition, a time-gated spectrometer, OPSPEC, is being fabricated for NIF opacity experiments. This will use Daedalus, the next-generation SNL FPA, to reduce background emission recorded from a backlit test material in a NIF hohlraum.

## 4. Pulse dilation technology: Application to dilation x-ray imager (DIXI)

Although MCP detectors can record as fast as 30 ps, an alternative approach to faster time gating is to decouple the photoelectron production from the gain in the electron image. With a separated transmission photocathode, the resulting electron image can be manipulated by electromagnetic fields in a drift region before its arrival at an MCP or hCMOS for time-gated gain. Importantly, the brief electron image at the photocathode can be stretched or dilated in time by ramping down an accelerating field, by factors of tens, allowing a relatively slow, say 200 ps, MCP gate to be used as shown in Fig. 13.

Pulse dilation is not a new idea,<sup>89,90</sup> but it was revised by Kentech personnel and tested using a short pulse UV laser by General Atomics, Kentech and LLNL—a result of NDWG meeting No. 2 (see Sec. IV B).<sup>91</sup>



**FIG. 13.** Cartoon showing how pulse dilation works for DIXI on NIF. A pinhole array forms many x-ray and photoelectron images. A traveling wave voltage on the photocathode accelerates electron images to different velocities. A drift tube dilates the photoelectron images by ~50 in time before a fraction of each image is recorded by a gated MCP. In contrast, SLOS uses a multi-gate FPA for recording.<sup>92</sup> Reproduced with permission from Nagel *et al.*, *Rev. Sci. Instrum.* **85**, 11E504 (2014). Copyright 2014 AIP Publishing LLC.

The PD concept was rapidly conceptualized by the NDWG and used in a diagnostic called the dilation x-ray imager (DIXI) for NIF.<sup>93,94</sup> DIXI records a time-sequence from many x-ray images. An array of pinholes casts multiple x-ray images onto a large, transmission photocathode with a traveling voltage that is ramped down. The electron images are transported to a 400 ps MCP single gate readout after the image temporal dilation resulting from the ramp, giving sub-10 ps gating at the photocathode. By using an array of pinholes, an x-ray movie of an implosion results as the ramped pulse sweeps along an electrical microstrip(s). Results from the NIF pulse dilation x-ray camera (DIXI) were reported in the work of Nagel *et al.*<sup>95</sup>

This rapid implementation of DIXI on NIF was helped by the use of test facilities at GA and a brilliant re-tread of an idea from an industrial partner deeply involved in the HED program through HTPD and NDWG meetings.

### 5. Pulse dilation technology: Application to World's fastest photomultiplier

One stunning development of PD that came from the NDWG meetings was the invention of the fastest (~20 ps) photomultiplier (PMT) in the world, the PD-PMT. It is currently used by LANL in the NDWG for gamma spectroscopy on the gamma Cerenkov detector (GCD)<sup>96</sup> and the gamma reaction history (GRH) diagnostic. This arose from an “aha” moment at the 16th NDWG meeting and is reported in the work of Dymoke-Bradshaw *et al.*<sup>97</sup> Importantly, the pulse dilation PMT instrument is now sold by a US vendor, Sydor Technologies, Inc.<sup>17</sup>

### 6. Pulse dilation and hCMOS applied to a SLOS detector

DIXI works by sweeping a time gate across many x-ray images formed by an array of many pinholes. The angular separation of the pinholes is normally small; nevertheless, each image is along a different line of sight. However, this concept does not easily work for more complex imaging systems, such as curved crystal imagers or Kirkpatrick-Baez (KB) microscopes, as there is not enough space for many imaging systems, except as reported by Marshall.<sup>98</sup> For more complex imaging systems, an x-ray “framing camera” recording many time-gated images along a single-line-of-sight SLOS could replace DIXI.

The integration of the pulse dilation technology with a multi-gated FPA for NIF and OMEGA diagnostics gave rise to the world's fastest x-ray framing cameras used on NIF and OMEGA.<sup>92,99,100</sup>

Technical details and the many issues of SLOS are covered elsewhere in this volume,<sup>101,102</sup> but SLOS is a supreme example of the benefits of collaboration within the NDWG: For the LLE instrument (middle right Fig. 11), GA was the integrator, SNL supplied the FPA (a.k.a. hCMOS), LLNL provided the readout electronics, and industry<sup>17</sup> supplied the fast electronics.

SLOS as defined above uses a pinhole to image x rays. The NIF curved Crystal (Backlit) Imager (CBI) instrument (middle right on Fig. 11) images x rays using a near normal incidence curved Bragg crystal imager.<sup>103</sup> This crystal imaging onto a SLOS (without the pinholes) is another supreme example of the benefit of NDWG collaborations (Sec. II D 2).

## D. X-ray spectroscopy

Precision measurements of HED plasma conditions such as density and temperature of, for example, an implosion target at stagnation is of great importance. HED plasmas usually evolve rapidly, and so direct spectroscopic measurements with time resolution of these parameters can provide robust constraints on theory.

### 1. Collaborations in x-ray spectroscopy: Early days

Four generations of x-ray spectrometers were designed, fabricated, calibrated, and fielded on NIF with an LLE lead. They were used to diagnose implosion hydrodynamics,<sup>104–106</sup> hohlraum plasmas and coronal plasmas,<sup>107</sup> x-ray source development for x-ray diffraction experiments, and national security applications.<sup>108,109</sup> All the spectrometers used Bragg reflection and were positioned in the NIF target chamber using a DIM (Sec. III D). Three of the spectrometers combine a slit with a Bragg crystal to achieve one-dimensional spatial imaging in the direction perpendicular to the plane of dispersion. These spectrometers are housed in snouts for the x-ray framing cameras called gated x-ray detector (GXD) and the hardened gated x-ray imager (hGXD) (Sec. II A). One of them recorded spatially resolved, time-resolved spectral images on the strips of the x-ray framing camera. The other two spectrometers recorded spatially resolved, time-integrated spectral images on calibrated image plates (IPs). The fourth spectrometer is coupled to a streak camera called the diagnostic insertion manipulator imaging streak camera (DISC) to achieve temporal resolution of a spatially integrated spectrum. Two used flat Bragg crystals, two used singly curved, elliptical Bragg crystals. The spectrometers are summarized in Table IV.

The first-generation instrument, called the hotspot x-ray spectrometer<sup>100</sup> (HSXRS), formed four temporally resolved spectral images covering the 10–10.9 keV photon energy range and four more covering the 11.7–12.8 keV range on a GXD. Slits provided 12× spatial magnification of the implosion hotspot plasma, measuring a ~0.1 mm diameter and indicating Ge doped ablator material being hydrodynamically mixed into the hotspot (i.e., hotspot mix). This is consistent with two-dimensional (2-D), radiation-hydrodynamics implosion simulations that indicated hotspot mix was possible.<sup>110</sup>

The limited diagnostic lines of sight to the target motivated the second-generation spectrometer using flat Bragg crystals, called SSI (Supersnout I), which combined four time-integrated spectral channels covering the 9.75–13.1 keV range with gated- and time-integrated, filtered x-ray imaging using pinhole arrays, and particle detectors. SSI increased the number of diagnostic lines of sight in a DIM from one to eight, increasing the data collection on a single laser shot on NIF. Systematic hotspot mix implosion experiments were performed with SSI using a Ge dopant in the ablator. An example of a Ge K-shell spectrum recorded with the SS I of a NIF symmetry capsule implosion can be found<sup>105</sup> that is consistent with 2D radiation-hydrodynamics implosion simulations.

A need for broader spectral range and mm-scale x-ray sources motivated the third-generation spectrometer, called SSII (Supersnout II), which combines time-integrated, elliptical Bragg crystal x-ray spectrometers for the 6–16 keV photon energy range, a broadband x-ray gated GXD, and time-integrated, filtered x-ray pinhole imager and particle detectors in a single snout to maximize the diagnostic access on the NIF. Hotspot mix implosion experiments were

**TABLE IV.** The spectral range, time resolution, and spatial resolution of the four generations of x-ray spectrometers designed, fabricated, calibrated, and fielded on the NIF by a LLE lead.

Generation (year)	Acronym	DIM-based detectors	Spectral range (keV)	Time resolution for x-ray spectrum	Spatial resolution for x-ray spectrum ( $\mu\text{m}$ )
First (2009)	HSXRS	GXD, hGXI, IP	10.0–10.9, 11.7–12.8 keV (simultaneous)	$\geq 100$ ps	10 or 100
Second (2010)	SSI	GXD, hGXI, IP, CR39	9.75–11.2, 11.4–13.1 (simultaneous)	Time-integrated	10 and 100
Third (2012)	SSII	GXD, hGXI, IP, CR39	5.8–10.1, 6.4–11.2, 7.2–12.7, 9.3–16.5 (simultaneous)	Time-integrated	30 or 100
Fourth (2014)	NXS	DISC, IP	1.9–2.4, 2.2–2.9, 2.6–3.7, 3.0–4.5, 3.6–6.0, 5.9–7.4, 6.7–8.9, 7.9–11.2, 9.0–13.7, 10.8–18.2 (one interval per NIF shot)	$\geq 10$ ps	Space integrated

performed with SSII using Ge and Cu dopants placed at different radial locations in the ablator to study the origin of hotspot mix. An example of a Ge K-shell spectrum recorded with the SS II on a NIF DT cryogenic implosion can be found,<sup>106</sup> which again was consistent with 2D radiation-hydrodynamics implosion simulations. The wide spectral range in SSII was exploited to characterize laser-driven x-ray sources for x-ray diffraction source experiments and national security applications.

Time-resolved measurements of mm-scale x-ray sources in the 2.0–18 keV photon energy range motivated the fourth-generation x-ray spectrometer, called the NIF x-ray spectrometer (NXS), utilizing an x-ray streak camera and a time-integrated channel to provide an *in situ* calibration of the streaked spectrum, with some work on OMEGA.<sup>111</sup> NXS has a spectral resolving power of  $\sim 100$  and a temporal resolution  $\geq 10$  ps. NXS does not cover the entire 2.0–18 keV range with a single snout, rather it divides the overall spectral range into ten spectral regions. Each spectral region is covered using a dedicated snout housing a singly curved, elliptical Bragg crystal. One of the ten possible snouts is chosen for a NIF experiment to record the spectral range of interest. Examples of spectra recorded with NXS on NIF can be found in the literature.<sup>105,106</sup>

HSXRS and Supersnout I had flat Bragg crystals. They achieved a spectral resolving power ( $E/dE$ ) in the range of 500–1000 for implosion hotspot scale sources ( $\sim 100 \mu\text{m}$ ). Larger sources would cause source broadening. Supersnout II and NXS utilized an elliptical Bragg reflection geometry. Moderate spectral resolving power ( $100 < E/dE < 500$ ) and spatial resolution of  $100 \mu\text{m}$  are achieved with elliptical geometry for mm-scale x-ray sources.

The development of these four generations of x-ray spectrometers, their calibration on the OMEGA laser facility, and their use as primary diagnostics in NIF high-energy density physics experiments during the 2009–2014 time frame were realized with strong multi-institutional collaborations. The leadership and grassroots efforts of the Ignition Diagnostics Working Group, which later became the National Diagnostics Working Group, helped form these collaborations. The research funded by the NNSA and DTRA greatly benefited from the national perspective that the collaborations provided.

In addition to this LLE collaboration, x-ray spectroscopy experts from the Naval Research Laboratory (NRL) collaborated with LLNL to increase the fidelity of the spectral reconstruction of the gold M-band spectrum from the NIF Dante system.<sup>112</sup> The NRL built Virgil spectrometer uses the central line of sight of Dante-1. It uses a pair of cylindrically bent crystals covering 1.5–3.0 and 3.0–6.0 keV, providing time-integrated, high-resolution spectra over Au M-band emission (1.5–6 keV). It allows Dante unfold techniques to more accurately account for gold M-band emission. Finally, CEA provided a band selecting x-ray mirror for one channel of Dante.

This set of spectrometers shows a marvelous collaboration between LLE and LLNL and LLNL, CEA, and NRL, taking advantage of the high shot rates on OMEGA and Nike at NRL for testing and calibrations. All the spectrometers were actively discussed at the NDWG meetings from 2009 to 2013. Institutional assignments were agreed upon and OMEGA or Nike was used as the appropriate facility for the task of testing and calibrating most of the instruments.

## 2. High-resolution x-ray spectroscopy: X-ray streak cameras, hCMOS, and SLOS

High-resolution x-ray spectroscopy is a powerful method to interpret local plasma conditions.<sup>113,114</sup> High-efficiency spectrometers with a resolving power  $\sim 1000$ – $2000$  beyond those described in Sec. II D 1 and an x-ray streak camera are needed. Such high-resolution spectrometers have now been built and fielded on each facility.

Figure 14 shows some surprising collaborations and interconnections between different technology disciplines and institutions that have arisen from highlighting x-ray spectroscopy in the meetings of the NDWG.

First, high-resolution time-resolved spectroscopic diagnoses of NIF implosions drove a need for better x-ray streak cameras that was met by a NDWG-CEA collaboration on streak cameras<sup>115</sup> and a connection with traditionally magnetic containment experts in x-ray spectroscopy. Second, the utility of x-ray imaging by curved crystals had been recognized for about 20 years in HED. To spectroscopically diagnose non-cryogenic implosion cores on NIF, a high-Z



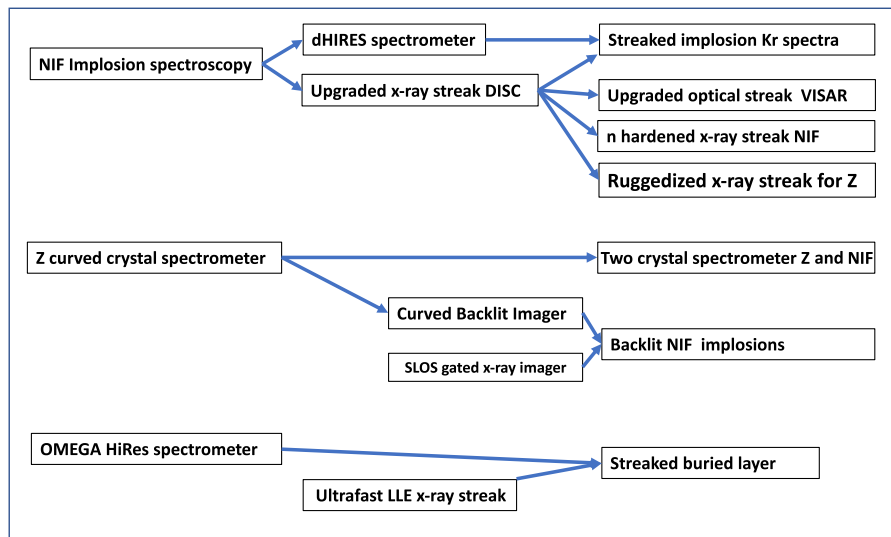


FIG. 14. The requirements of high-resolution spectroscopy on the three HED facilities (left) and the NDWG resulted in many new diagnostic capabilities (right).

dopant material is required such that its x-ray photons can propagate through the dense compressed shell without significant attenuation. To that end, a capsule with Kr-doped fuel was developed utilizing the 13–16 keV Kr K-emission lines from implosion cores.<sup>106,116</sup> A vital requirement of the design of the total instrument was that the NIF DIM-mounted x-ray streak cameras needed a x-ray focusing design for high throughput and spectrometer dispersion perpendicular to the target chamber radius. This unusual configuration had been invented by T Hall, from an earlier generation of HED scientists,<sup>117</sup> and was remembered at a NDWG meeting.

Using Hall's geometry, a three-channel, high-resolution, time-resolved x-ray spectrometer named dHIRES (*DIM High-RE Solution Spectrometer*) using two conical crystals for time-resolved channels and one cylindrical crystal for a time-integrated channel was designed and fielded. A high spectral resolution enabled detailed line-shape measurements and a comparison to Stark broadening calculations. Because of the NDWG meetings, the design, fabrication, and calibration of the spectrometer utilized a group of scientists formerly experienced in MFE spectroscopy.<sup>118</sup>

The need to time-resolve the NIF implosion spectra (also OMEGA, LMJ, and Z) also drove an ongoing collaboration on improved streak camera design. As usual, this was accomplished by engineering the streak camera inside the protection of an airbox. This design will soon be fielded in the extremely harsh environment of Z. Separately, there was an effort on improved electron optics. Here, LLE concentrated on ultrahigh-speed detection.<sup>119</sup> NIF concentrated on improving the spatial resolution of their DIM Insertable Streak Cameras (DISCs) to fully utilize the spectrometer dHIRES. As discussed by MacPhee,<sup>115</sup> the electron optics in streak cameras suffers from an optical aberration arising from the Petzval curvature of the focal plane of the electrons. LLNL and industry devised an aberration correction involving a grid that essentially flattened the field curvature at the detector plane doubling the spatial resolution. This breakthrough in electron optics is being applied to the manufacture by industry of an upgraded

optical streak camera for NIF VISAR. The space charge saturation effects are being modeled by CEA partners in the NDWG. Another direct outcome of the NDWG.

NIF implosions using the dHIRES in front of the upgraded DISC recorded data on a series of Kr-doped implosion shots, generating time-resolved (30 ps) spectra of the Kr He<sub>α</sub> and He<sub>β</sub> lines, with E/dE ~ 1300. The Stark broadened data were analyzed to provide time evolution of both temperature and density.<sup>120</sup>

Using DIMs to position instruments close to the target mitigates the 1/r<sup>2</sup> drop in fluence is mitigated, but at the expense of higher neutron fluxes which will “upset” the detectors. Recently, we have taken a small step toward operating a time-resolving spectrometer at higher yield.<sup>121</sup> By radiation-hardening, the streak tube control electronics, replacing the CCD with a hardened CMOS sensor and hardened electronics, better shielding, attention to time of flight, and precision timing, we have collected useful streaked spectroscopy data on an ICF implosions with over 40× the operational neutron yield of the previous unhardened diagnostic.

The NDWG benefited from the spherically bent crystal imaging work on Z, which included both x-ray radiography (i.e., backlighting) and self-emission imaging techniques.<sup>122–124</sup> As a result of this work and NDWG discussions, the CBI was built for the NIF.<sup>103</sup> The CBI produces a narrowband, x-ray radiograph with several micrometer resolution that is imaged onto a SLOS. This complex instrument represents a tour de force diagnostic with outstanding spatial (7 μm), temporal (~20 ps), and spectral (~1 eV) bandpass that diminishes the effect of the target emission, allowing very bright implosion plasmas to be imaged, almost at peak stagnation.

The NDWG also discussed the use of bent crystals for self-emission imaging, which ultimately was made more appealing and easier to implement due to the previous success of the backlighter configurations at both Z and NIF. Benefits of the narrowband nature of the Bragg reflection were first explored and used in the work of Aglitskiy *et al.*,<sup>125</sup> Harding *et al.*,<sup>124</sup> and Koch *et al.*<sup>126</sup> Of particular interest to the NDWG was the two-crystal,

differential-imaging technique developed in the work of Harding *et al.*<sup>124</sup> for magnetized liner inertial fusion (MagLIF) experiments on Z. This technique enables the visualization of wall mix by isolating spectral line emission from the background continuum emission. As a result of this work and further NDWG meetings, a similar multi-crystal instrument is being built for the NIF.

NDWG brought together disparate expertise on this superb x-ray imaging capability and added to it detector development (SLOS, Sec. II C 6) for backlight imaging of NIF implosions, despite high levels of stagnation emission.

Several gated FPA spectrometers and imagers have been used on Z including the following:

- i. gated x-ray backlighting using a spherical crystal optic (now 4-frame compatible),
- ii. gated x-ray spectroscopy with 1D imaging using a slit imaging optic and a convex crystal for opacity applications,
- iii. gated x-ray spectroscopy with 1D imaging using a spherical crystal optic,
- iv. gated x-ray imaging using a pinhole optic, and
- v. gated laser shadowgraphy.

A high-resolving-power, x-ray spectrometer for OMEGA EP based on two diagnostic channels, each with a spherical Bragg crystal, was installed.<sup>119</sup> The instrument's capabilities have been demonstrated by resolving the Cu  $K\alpha_{1,2}$  doublet on high power shots.

### E. VISAR (velocity interferometer system for any reflector)

The VISAR diagnostic is an interesting example of a diagnostic that was initially developed for equation-of-state experiments and not for ICF applications yet later became a core ICF diagnostic on NIF as an innovative and critical use was developed. It is used to time the sequence of ablatively driven shocks in an ICF implosion. The VISAR diagnostic has continued to expand its application

beyond what was initially conceived as new applications of the diagnostic have been developed. Table V lists some of the key advances in regard to the use of VISAR on HED facilities.

The VISAR system concept was developed by Barker and Hollenbach<sup>127</sup> to broaden the application of laser interferometry to surfaces that are imperfect, e.g., moderately reflective or roughened. The application for VISAR initially was for measuring velocity of free surfaces, particularly in shock wave research. Initially, it was not implemented as a core ICF diagnostic on Nova as the diagnostic was not mature and the applications had not yet been demonstrated.<sup>137</sup> Later, a VISAR system was installed on Nova for equation-of-state experiments. Instead of measurements from a free surface, which is the typical use of VISAR, the Nova VISAR was designed to image in 1D the shock propagation in transparent materials. When a shock passes through certain materials (i.e., deuterium, diamond, quartz), they transform into a metal and their optical reflectivity increases. Thus, an incident laser from a VISAR can reflect off the shock and the shock velocity measured.<sup>128</sup> This was the first use of VISAR in this manner. The success of this novel use of VISAR led to a proposal to use this to measure the shock timing in an ICF implosion on NIF.<sup>46,138</sup> The initial concept was to time the shocks in a planar sample attached to the side of the hohlraum; this evolved to measuring the shocks inside a capsule in perpendicular directions with the use of small turning mirrors. The successful use of VISAR on Nova resulted in the implementation of VISAR systems at other laser and Z-pinch facilities: Vulcan,<sup>139</sup> LULI,<sup>140</sup> LMJ,<sup>141</sup> Orion,<sup>142</sup> Z,<sup>143</sup> and others. This same basic VISAR design is now a core diagnostic at HED facilities worldwide.

While NIF was under construction, a VISAR was installed on OMEGA.<sup>130</sup> While similar in principle to the Nova VISAR, a number of improvements were made and tested. The high shot rate on OMEGA allowed rapid testing of design concepts. These improvements were then implemented in the design of VISAR on NIF.<sup>144</sup>

Several new applications were developed on OMEGA using the VISAR. Measurements of shock velocity were used in

**TABLE V.** Major advancements of VISAR on HED facilities.

VISAR advances	Date
Velocity interferometry system for any reflector (VISAR) developed <sup>127</sup>	1972
Line VISAR for diffuse reflecting surfaces, measurements of shock velocity in transparent materials <sup>128</sup>	1998
Application to ICF shock timing <sup>129</sup>	2001
Line VISAR on OMEGA and application to equation-of-state experiments and shock timing <sup>130</sup>	2004
Application to measurement of hohlraum temperature <sup>131</sup>	2006
Application to ICF shock timing inside an ICF capsule <sup>132</sup>	2009
Use of target-mounted turning mirror to redirect VISAR to an orthogonal line of sight on a half hohlraum <sup>133</sup>	2010
2D VISAR system demonstrated on OMEGA <sup>134</sup>	2010
Use of turning mirror inside an ICF capsule for dual axis VISAR shock timing <sup>135</sup>	2014
Understanding of streak camera nonlinearities <sup>115</sup>	2016
Effect of material structure on shock velocity nonuniformity measured on OMEGA <sup>136</sup>	2018

Richtmyer–Meshkov growth experiments.<sup>145</sup> Since a nonconstant shock velocity can result in Rayleigh–Taylor instability growth as well, precise and continuous measurements of the actual shock velocity enhance the accuracy of these hydrodynamic experiments. This was the first use of VISAR for hydrodynamic experiments on lasers. Another application was the use of VISAR to measure the hohlraum temperature.<sup>131</sup> Typically, there were two independent diagnostics used for the measurement of temperature inside a hohlraum: the Dante, a set of soft x-ray filtered diodes, and a SOP (Streaked Optical Pyrometer) that measured the breakout of a shock from an aluminum wedge installed on the side of a hohlraum.<sup>146</sup> By placing a transparent material, i.e., quartz on the side of the hohlraum, the shock velocity can be measured through the quartz and related to hohlraum temperature. There is a limit to the temperature that can be measured. Once it exceeds  $\sim 170$  eV, the quartz loses its optical transparency due to ionization in the unshocked material and the VISAR signal disappears.

The NIF VISAR was installed along an equatorial line of sight and used on the NIF Early Light Experiments. Original plans were to also install an additional polar line-of-sight VISAR for half-hohlraum and direct drive planar experiments. However, the use of a target-mounted mirror to relay the equatorial VISAR to the polar axis removed the need for a separate polar VISAR, a design that was even more complex than that of the equatorial VISAR due to the  $\sim 2\times$  longer optical relay path length.<sup>146</sup> To make the target-mounted turning mirror operate successfully, the mirror had to be shielded from unconverted light and electrons from the target. An entrance cone for the VISAR extended beyond the unconverted light footprint on NIF. The turning mirror was chosen to be made from fused silica to reduce the absorption and heating from x-ray preheat and remain reflective. The x-ray loading limits and impact on reflectivity of various candidate mirror materials were tested on OMEGA. Once demonstrated, the concept of an enclosed VISAR turning mirror is now used routinely on NIF. This is an example of where a relatively inexpensive target modification can reduce the need for a costly new diagnostic as well as the use of other complementary facilities to make rapid design decisions. The use of a turning mirror was used inside an ICF capsule to acquire 2-axis shock timing data with a single VISAR to measure the effect of radiation asymmetry on shock timing.<sup>135</sup>

The accuracy of determining the shock velocity hinges on the accuracy of determining the fractional fringe shift in time recorded on an optical streak camera.<sup>128,147</sup> The dominant source of uncertainty is from the spatial nonuniformities present in streak cameras and limits the accuracy of velocity determination to  $\sim 1\%$  at the center, increasing to 3% at the edges of the field of view. The spatial nonuniformity in a streak camera consists of spatial and temporal distortions, which can be calibrated out to some extent, and spatial resolution variations, which are more problematic.<sup>148</sup> There has recently been a fundamental improvement in the understanding of the source of streak camera nonlinearities (Sec. II D 2), which should lead to better accuracies in measurements using streak cameras, including VISAR.<sup>115</sup>

Electron optic aberrations in both x-ray and optical streak cameras are caused by Petzval field curvature and spherical aberrations, which result in reduced spatial resolution off axis. This can be corrected with electron optical components (mesh and cylinder) and demonstrated in an x-ray streak camera to have a near uniform

spatial resolution across the camera. The improvement should be possible in optical streak cameras as well, and work is under way to incorporate this in optical streak cameras on NIF. This highlights how sometimes deeper understanding of detectors can impact overall performance in a diagnostic system.

The NDWG played an important role in advocating for enhancements of the VISAR system, including calibrations and incorporation of streak camera improvements. It has planned a new high-resolution 2D-VISAR system for NIF.<sup>134</sup> The concept was again first demonstrated on a small system, the Jupiter laser system at LLNL, then implemented on OMEGA for further testing and development. It is also being implemented on other HED facilities, e.g., Nike.<sup>149</sup> This diagnostic has been used to measure the effect of material grain size on the shock front perturbation as a seed for instability growth on ICF capsules,<sup>136</sup> laser-imprint induced shock velocity nonuniformities,<sup>150</sup> and laser-driven metal ejecta.<sup>151</sup> On NIF, the effect of grain size on the actual first shock in a NIF capsule can be measured, since OMEGA cannot reach the first shock pressure and duration a capsule will experience on NIF. It is expected that as scientists become more familiar with this diagnostic capability, new applications will be developed.

In summary, the development of the line VISAR capability to directly measure shock velocity in transparent materials has opened up many applications in ICF, and HED science that were not initially envisioned, that have significantly impacted ICF and HED science. VISAR is routinely used to tune the shock timing and shock symmetry in ICF implosions.<sup>152</sup> Advances in fundamental streak camera understanding offer the potential of higher accuracy measurements. 2D VISAR is another new diagnostic capability in the early stages of development of applications. The evolution of this diagnostic progressed from a proof-of-principle on a small laser to OMEGA for testing and improvements and finally to NIF and other facilities. Thus, the time scale from concept to capability and development of new applications is  $\sim 10+$  years.

## F. Wolter x-ray imager for Z and NIF

There is a sister diagnostic review article in Review of Scientific Instruments on x-ray optics including the Wolter configurations by Kozioziemski.<sup>153</sup> A Wolter x-ray optic uses a full surface of revolution and so it provides orders of magnitude larger collecting solid angle than any other reflective x-ray optic.

The first use of a Wolter in HED was on Nova.<sup>154</sup> Time resolution was achieved using the first version of a production type module of a gated MCP detector. The optic was Ni coated optic and had a region that had good resolution but very bad scatter, which complicated its use compared to the ease of use of imaging pinholes.

However, the success of NASA's Chandra x-ray telescope,<sup>155</sup> recent replica technologies development, and our need to image in spectral bands caused us to form a collaboration for x-ray microscope imaging on NIF and Z. The NDWG collaborated with NASA Marshall Space Flight Center for optic production and the Harvard Smithsonian for multilayer mirror coating optimized for molybdenum characteristic x-ray lines. This group successfully delivered a multilayer coated Wolter for use on Z. Fein *et al.*<sup>156</sup> discuss the resolution and throughput of a Wolter compared to pinhole systems, as well as the recent achievement of  $5\ \mu\text{m}$  resolution on a NIF Wolter.<sup>157</sup> In the course of this work, some of the NIF



expertise in optical polishing was useful to NASA in improving their polishing techniques. Again, a fruitful internal collaboration within the NDWG but also a mutually beneficial collaboration with NASA space flight x-ray telescope experts.

### G. Neutron imaging

Some HED and ICF diagnostics have their origins in the underground nuclear test program of the national laboratories. One of these was neutron imaging, where a “neutron pinhole” creates an image of the neutron emitting region of a burning plasma. In the laboratory, a first proof-of-principle demonstration of neutron imaging was made on the Nova laser in the 1990s.<sup>158</sup> There is a sister diagnostic review article in the work of Fittinghof *et al.*<sup>159</sup> that details and references the major work on NIF to implement three quasi-orthogonal lines of sight for neutron imaging.

Starting in 2000, LANL began to develop new techniques, technology, and algorithms to make neutron imaging a standard diagnostic for ICF.<sup>160</sup> The project began by fielding a test bed at the OMEGA laser facility. Different methods of machining and fabricating complex pinhole arrays were tested, different types of scintillator material were used, and simple analysis algorithms tested. Most importantly, the demands of a reliable neutron imaging system (NIS) for the NIF were starting to be understood. Simultaneously, the CEA of France also tested alternative types of apertures and scintillators at OMEGA.

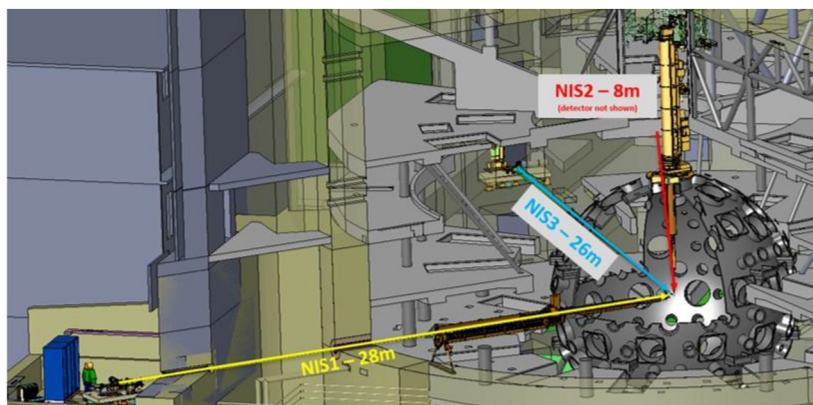
Many challenges needed to be overcome to achieve the desired  $10\ \mu\text{m}$  spatial resolution on the NIF. The neutron pinhole has to be 20 cm in length in order to fully suppress the 14 MeV neutrons that do not pass through the open pinhole. Because NIS measurements were required to be made over a large range of neutron yields with good signal-to-noise ratio (SNR), an array of pinholes and eventually penumbra are needed. In order to measure down-scattered neutrons, those scattered by the cold dense DT fuel, a long line of sight is needed to separate the different components of the neutron spectrum by their arrival times. The long line of sight (28 m) was achieved by constructing a two-story addition to the NIF building. Holes had to be drilled in the bio-shield wall and external wall

of the building and collimators had to be installed. This was another result of the collaboration between LANL and LLNL.

The neutron pinhole evolved from a single pinhole scribed in a 20 cm-long block of Au to an array of pinholes, now numbering 54 triangular pinholes and 16 penumbral apertures machined into 14 layers of Au, encased in a block of W, with 16 x-ray apertures in a foil mounted to the end of the block. This evolution occurred over 20 years and required the development of detailed molding of the pinhole imaging properties and improvements in micromachining techniques. Realization that high-resolution reconstructions of the burn region required exquisite characterization of each of the pinholes led to major improvements in characterizing each pinhole in the array and its location.

The relative shape of x-ray and neutron images was an ongoing question that led to the addition of x-ray apertures to the pinhole array and innovative image plate detectors in the line of sight (CNXI) again arising from discussions at the NDWG meetings. This allowed collection of both time-integrated x-ray and neutron images, on the same line of sight, proving that the x-ray and neutron images had significant differences. Early experiments at NIF showed the need for more three-dimensional information on the implosion shape. This spurred the addition of a second line of sight to the original one. A polar NIS was chosen to break the symmetry of the hohlraum shape. Eventually, a third line of sight was added to give three nearly orthogonal views of the implosion as shown in Fig. 15.

The extensive building modifications and subsequent integration of the instrument into the facility its software controls required very close collaboration between the diagnostic scientists, engineering team, and NIF engineers and facility operations. For example, the evolution of the alignment procedure for the NIS illustrates the close cooperation required. Recall that the pinholes are 20 cm long and less than  $20\ \mu\text{m}$  in extent. These pinholes must be placed along the axis of the NIS line of sight, not only in linear directions but also in pitch and yaw. The original concept involved using an optical telescope placed in an opposed target chamber port. The results were less reproducible than desired. Later iterations of the pinhole array took this into account and enlarged the volume at best focus



**FIG. 15.** The locations and lengths of throw of the three neutron imaging lines of sight on NIF. NIS1 and NIS3 image the primary and down-scattered neutrons. NIS1 can also image gammas. NIS2 only images primary neutrons. Courtesy Fetherley.

that is imaged onto the detector. When the polar NIS was added, an opposed port was not available. Using a newly developed laser positioning system, not only was the polar NIS able to be aligned but also more reproducible and faster alignment of the other two NISs was made possible.

The 2015 NDWG review, discussed later, led to the new requirement of also measuring the gamma-ray image from an implosion. Copious numbers of 4 MeV gamma rays are produced when neutrons collide with carbon atoms in the capsule ablator. The gamma rays arrive at the NIS recording system much sooner than do the neutrons, so time gating the measurement can isolate the gamma image from the neutron images. The addition of this measurement required a redesign of the detector and pinhole arrays of the NIS. These changes were incorporated into the construction of the third line-of-sight instrument and are included in the refurbishment of the original line-of-sight.

Early data from the NIS showed the true shape of the burning region was similar to the x-ray emitting region.<sup>161</sup> The images also confirmed that the compressed core was larger than simulated, indicating that the adiabat of the fuel was significantly higher than designed. Other measurements showed that the jet of material from the fuel fill tube was cooling the plasma and that the hotspot region could sometimes obtain unanticipated states such as a torus or as two separated burning regions.<sup>162</sup> More recently, addition of the gamma-ray imaging capability shows where the burning fuel shell, the cold fuel shell, and the ablator shells are providing stringent constraints for simulation codes.

## H. Ultraviolet Optical Thomson Scattering (UVTS)

Optical Thomson scattering (OTS) measures the spectrum of a probe laser scattered by a plasma, enabling time- and space-resolved measurements of nearly all of the plasma properties. It is the gold standard measurement technique used in tokomaks and at lower densities in ICF.

On NIF, Z, and OMEGA, a high-density plasma produces high pressures to drive shocks or to inhibit hohlraum wall motion for all SSP programs. There are no direct measurements of the high-density plasmas needed to capture the complex dynamics inside a hohlraum. Fundamental hohlraum environment parameters will be uniquely measured, at high densities ( $n_e$  is calculated to be  $>10^{21}$  e/cc in a NIF hohlraum), and this leads to the requirement for an ultraviolet Thomson scattering probe laser beam at the fifth harmonic,  $5\omega$ , in order to avoid significant absorption and refraction. Background plasma emission and other sources of non-Thomson scattered light indicate that to exceed a signal-to-noise of unity, the Thomson scattering probe laser must be 1–10 J in 1 ns at 210 nm, see the work of Ross *et al.*<sup>163</sup>

There are also less challenging experimental configurations that can benefit from  $3\omega$  UVTS on the NIF and are benefiting from  $4\omega$  OTS on OMEGA.<sup>164</sup> OTS has been implemented on Nova, Trident, JLF, and OMEGA although in less stressing conditions than an ignition hohlraum. UVTS on the NIF is therefore a transformative diagnostic because the uniquely short wavelength of the probe opens new windows in plasma density even after five decades of Thomson scattering from high-temperature plasmas.

For UVTS on the NIF, an ultraviolet probe beam is generated by fifth harmonic conversion of a 1.06  $\mu\text{m}$  glass laser beam. A

separate 100 J class laser beam line has been through the rigorous design review process and installed on the NIF including frequency conversion to 210 nm and delivery to target chamber center.

After discussion by the NDWG, work at LLE in FY16 measured conversion efficiencies from 1.06  $\mu\text{m}$  to 210 nm, albeit with smaller beams, of 10%–20%. The detector for the scattered light is a dual spectrometer multiplexing onto an ultraviolet sensitive streak camera. The detector was designed and built in FY16. The detector has been used to measure the background levels for NIF hohlraums and direct drive capsules. The detector has already been used for  $3\omega$  OTS on the NIF from relatively low-density plasma for planar laser plasma instability experiments.<sup>165</sup>

## III. EARLY DAYS: COLLABORATIVE HED DIAGNOSTICS 1993–2008

This is a synopsis of the collegially coordinated national diagnostic effort from the late 1980s, through the NIF Conceptual Design Report (CDR), to an implementation of diagnostics for the first phase of NIF program ~2009.

### A. The high-temperature plasma diagnostic conference and proceedings of SPIE

The NDWG originated at the high-temperature plasma diagnostic (HTPD) conference. This conference was started and has continued for decades because of the diagnostic commonality between hot HED and hot magnetically contained plasmas.

The biannual HTPD series started in Knoxville in 1976 and has been held continuously to the twenty-fourth HTPD in Rochester in 2022. Its longevity is testament to the utility of the conference. The community has voted with its feet and the conference has flourished. The committee is self-organizing: As members of the committee retire, new committee members are informally proposed and accepted and carry on the good work.

A valuable feature of the HTPD is that the proceedings have been published in the *Review of Scientific Instruments* since the early 1980s. A page limit makes the papers particularly readable. The proceedings are usually a special issue where scores of papers per volume archive the progress of diagnostics for HED plasmas. For example, since 2008, ~60 to 80 papers are published biennially on HED plasma diagnostics.

High-quality engineering is essential for diagnostics on large facilities. Starting 2012, a series of conferences, called “Target Diagnostics Physics and Engineering for Inertial Confinement Fusion” organized by SPIE, focused on engineering of the HED diagnostics. About 20 papers/year from these meetings were published in each *SPIE Proceedings* from 2012 to 2018. As befits SPIE, an organization that initially called itself the Society of Photographic Instrumentation Engineers, before the abovementioned conference, there were over the decades many high-speed imaging conferences and proceedings that were relevant to HED diagnostics. As with HTPD publishing in *Review of Scientific Instruments*, a valuable feature of these SPIE conferences was publication in the proceedings of SPIE of HED diagnostic engineering.

The HTPD and SPIE conferences generate a sense of community among diagnostic scientists and engineers and is a backdrop for the NDWG.

**TABLE VI.** The NIF CDR anticipated collaborations between LLL, LANL, and SNL on diagnostics nurtured by the HTPD and the SPIE Conferences. Boldface indicates the five different categories.

Measurement	Diagnostic	Acronym	Lab	Nova equivalent
<b>Laser characterization</b>				
Beam spot size, position, and smoothing	Static x-ray imager (ruggedized)	SXI	LLNL	
Beam synchronization	Streak x-ray cameras	SSC	LLNL	SSC
<b>Hohlraum characterization</b>				
Time history of hohlraum radiation temperature	Soft x-ray power diagnostic	SXSS	SNL/LLNL	SOP
	Shock breakout systems	SOP	LLNL/SNL	SOP
Absolute high-energy x-ray spectra	Filter fluorescent	FFLEX	LLNL	FFLEX
Time-dependent size of hohlraum diagnostic hole	Soft x-ray imaging system	SXRI	SNL	GSXRFC
<b>Spatial symmetry of hohlraum radiation drive</b>				
	Gated x-ray imaging system	GXI	LANL/SNL	GXI
<b>Implosion characterization</b>				
Capsule neutron yield	Total neutron yield system	YN	SNL	Yield
Fuel ion temperature	Neutron time of flight	NTOF	LANL	
Capsule imploded core image	Neutron imaging	NI	LLNL	NPAM
<b>Diagnostic vacuum inserter</b>				
	Twelve-inch manipulator	TIM	LLNL	SIM

## B. Diagnostics for the NIF Conceptual Design Review (CDR)

The US inertial confinement fusion program evolved in the 1980s and 1990s; it is a long and fascinating story. In the early 1990s, LLNL proposed the National Ignition Facility follow-on to Nova<sup>166</sup> and published a conceptual design report (CDR).<sup>3</sup> We now know NIF came to pass and achieved ignition<sup>1</sup> a quarter of a century after the CDR.

The team for the NIF CDR was based at Livermore but with major contributions from LANL, SNL, and LLE. Notably, there was a national team in diagnostics for the NIF, which called itself the Joint Central Diagnostic Team (JCdT)—with apologies to the ITER joint central teams. The group was experienced in operating diagnostics on relatively large facilities.<sup>50</sup> The JCdT met several times to discuss the diagnostics required for ignition and formulated the diagnostic section of the CDR document, which was also presented at the 1994 HTPD in Rochester.<sup>167</sup>

The functional requirements of the NIF<sup>168</sup> were driven by the implosion/ignition mission of NIF. In the CDR phase I, HED diagnostics were needed to verify achievement of these requirements. They were NIF versions of previous Nova diagnostics, as shown in Table VI. Much later, as described in Sec. IV C, the use of HED facilities for non-implosion HED missions evolved together with additional diagnostics.

At this time, some Phase II diagnostics were envisaged, with a large neutron scintillator array (like LaNSA on Nova) and neutron penumbral imaging.

## C. Post-CDR NIF diagnostic activities

Two years later in 1996, there was another invited talk on NIF diagnostics at the HTPD meeting in Monterey, where another national diagnostic leader, this time from SNL, reported the current planning status for NIF diagnostics<sup>169</sup> as shown in Table VI

followed by another summary paper in 2001.<sup>170</sup> Besides the three labs, there were coauthors from LLE and MIT. Institutional responsibility had been assigned for each diagnostic; see Table VII. This assignment was possible because the members of the JCdT were also the diagnostic managers at the sites participating in the NIF.

Unsurprisingly, there were several areas where eventual implementation of the diagnostics differed from the planning discussed by Leeper:

- The soft x-ray spectral diagnostic was determined to be the Dante system and not a transmission grating system.
- Tertiary neutron diagnosis was not used for areal density. Down-scattered neutrons were eventually used (Sec. II B 1).
- Although Cu activation is used for yield measurements, the main nuclear activation effort is with Zr.
- The soft x-ray imaging system was in the end simplified to a pinhole camera imaging system.
- A workhorse diagnostic on NIF is VISAR (Sec. II E), but it was absent from plans in the mid-90s, as its utility only became apparent in the late 1990s.

Newcomer institutions by 2001 were CEA, New York State University Geneseo and General Atomics.

A notable inclusion in Murphy's 2001 paper<sup>170</sup> was the gamma Cerenkov detector, variously called the GCD or, in a folded version, the gamma reaction history (GRH) detector.

## D. Diagnostic vacuum insertors and manipulators

The size of the Nova and the NIF target chambers and the concomitant pump down times drove the planning of how diagnostics were attached to the target chambers and aligned to targets. Although some diagnostics can be attached to the outside of the chamber, some need to be closer and need to be removed before unloading of a data recording media or refurbishment after a shot without venting the target chamber.

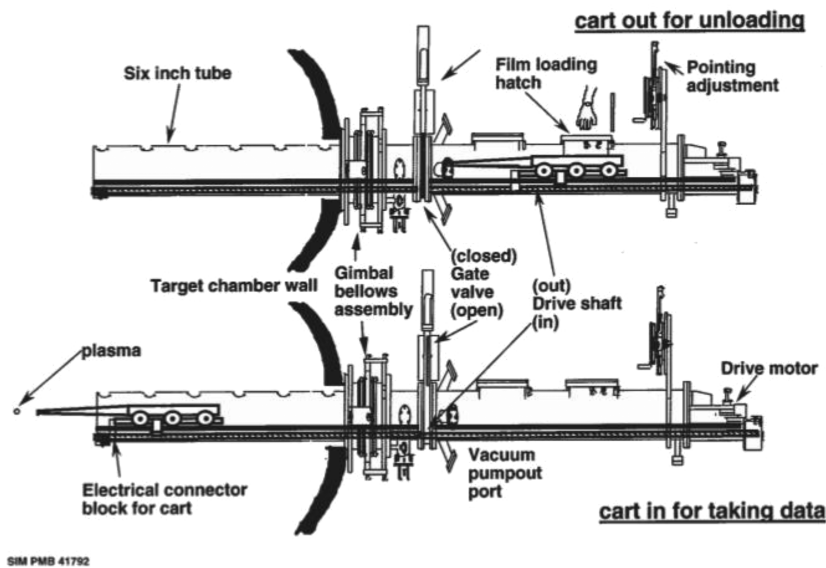
**TABLE VII.** Agreed diagnostic responsibilities for NIF between labs as of 1997. Bold face indicates the functions of the diagnostics. Shown in italics are the additional diagnostics added post-CDR.

Measurement	Diagnostic	Acronym	Responsible
<b>Laser characterization</b>			
Beam spot size, position, and smoothing	Static x-ray imaging system	SXI	LLNL
Beam synchronization	Streak x-ray camera system	SSC	LLNL
<i>Energy reflected from laser plasma</i>	<i>Optical backscattering system</i>	<i>FABS</i>	<i>LANL/LLNL</i>
<b>Hohlraum characterization</b>			
Time history of hohlraum radiation temperature	Soft x-ray power spectral	SXSS	SNL/LANL/LLNL
	Passive shock breakout system	SOP	LLNL
	<i>Active shock breakout system</i>	<i>ASBO</i>	<i>SNL/LLNL</i>
Absolute high-energy x-ray spectra	Filter fluorescer diagnostic	FFLEX	AWE/LLNL
Time-dependent size of hohlraum diagnostic hole	Soft x-ray imaging system	SXRI	SNL
<b>Spatial symmetry of hohlraum radiation drive</b>			
	Time-resolved x-ray imaging	TRXI	LANL/LLNL/LLE
<b>Implosion characterization</b>			
Capsule neutron yield	Total neutron yield system	YN	SNL/LANL
Fuel ion temperature	Neutron time-of-flight system	NTOF	LANL
Capsule imploded core image	Neutron imaging system	NI	LLNL
<i>Bang time and fuel burn history</i>	<i>Reaction history system</i>	<i>RHS</i>	<i>LLNL/LANL</i>
<i>Fuel areal density</i>	<i>Tertiary neutrons or protons</i>	<i>TN or TP</i>	<i>LLNL/LLE/MIT</i>
<i>Time-resolved fuel ion temperature</i>	<i>n-p recoil technique</i>	<i>TRIT</i>	<i>LANL/SNL</i>
<b>Diagnostic vacuum inserter</b>			
	Twelve-inch manipulator	TIM	LLNL

One advantage of laser facilities is that the laser beams can be repointed, thus allowing flexible target geometries. The diagnostics lines of sight need also to be flexible to take advantage of the different target geometries. By using vacuum load lock manipulators

arranged around the target chamber, the same diagnostic can rapidly be loaded into a manipulator on a different lines of sight. This allows moving instruments between facilities with similar manipulators. Instruments built for the Nova laser were fielded on OMEGA,

**The main components of a SIM ( Six-Inch Manipulator )**



**FIG. 16.** Main characteristics of three US and one French (LMJ) diagnostic inserters/manipulators.

23 August 2023 21:50:46



**TABLE VIII.** Main characteristics of three US and one French (LMJ) diagnostic inserters/manipulators.

Attribute	SIM -Nova	TIM (OMEGA)	SID (LMJ)	DIM (NIF)
Chamber diam.	4.4	3.25	10	10
Diagnostic length m	1.7	1.5	5.5	3
Diagnostic diam. M	0.11	0.18 × 0.23	0.2	0.3
Diagnostic Mass lb	23	45	20	195
Positioning x/y, z micron	50,50	30,10	10,100	25,250
Port size m	0.2	0.6 × 0.45	0.5	0.48
Diagnostic loading	End/top	Top	Top	End, became side

for example. Interchangeability of diagnostics between manipulators of various facility was accommodated to some extent but the detailed specifications of the manipulator had to fit the existing target chambers protocols.

Nova used 6 in. diameter vacuum load lock manipulators called SIMs, illustrated in the cartoon in Fig. 16 and detailed in Table VIII. It presents the main characteristics of three US and one French (LMJ) diagnostic inserters/manipulators. Diagnostics could be loaded onto a cart from the load lock, which was then evacuated, allowing the gate valve to be opened. The cart was then driven forward close to the target. Sideways alignment of the diagnostic was possible because of the gimbals shown around a large bellows. The bellows allows a small angular but relatively large positional motion of a diagnostic on the end of the long SIM. Similarly, NIF planned DIMs (diagnostic insertion manipulators), OMEGA built TIMs (ten-inch), and LMJ planned SIDs (Diagnostic Insertion Systems).

This was planned 25 years ago and as of 2021, NIF has five DIM-like manipulators, OMEGA has seven ten-inch manipulators (TIMs), and LMJ has six Diagnostic Insertion Systems (SIDs). A good example of a diagnostic that was designed to operate in the OMEGA TIM is described by Oertel.<sup>171</sup>

#### IV. THE NIF DIAGNOSTIC WORKING GROUP, 2009–2021

##### A. Diagnostic status at start of NIF operations: A need to evolve

When NIF started operating with all 192 beams in 2008, there were only eight diagnostics in operation, those used on an eight-beam version of NIF called NEL. Although there were another dozen diagnostics conceptually planned, it was realized that a more detailed and realistic plan needed to be formulated for the NIF diagnostics. Moreover, these initial planned set of diagnostics were success oriented for  $10^{18}$  neutron yield and chosen to make a few key measurements on the performance of the hohlraums and implosions, based on prior experience from Nova and OMEGA. Measurement-accuracy requirements were created based on success philosophy. As it turned out, there was a lot of unknown science. As we now know, there can be large implosion anisotropies from fill tubes, support tents, capsule pits, and implosion drift velocities and hohlraum wall motion, but at the time these factors did not figure in describing the diagnostic accuracy requirements.

The plan needed to evolve due to diagnostics improvements and a need for failure diagnostics. As a result, starting in 2009 a set

of workshops was initiated that led to a far more formalized apportioning of responsibility for NIF diagnostics. This set of meetings gradually transformed itself into meetings of the National Diagnostic Working Group (NDWG) creating a living National Diagnostic Plan (NDP) for the three major US facilities.

##### B. National diagnostic meetings, 2009–2014

In this quinquennium, NIF diagnostics went from a handful of operational diagnostics with collegial interlab responsibilities to ~65 operational diagnostics with significant responsibility in the national program. The method of accomplishment used the factors laid out in the table at the end of Sec. I: first and foremost, detailed, transparent collaboration accomplished at nine large general workshops held between February 2009 and September 2014, twice a year during the first 3 years and once a year afterward. There were also many more, smaller workshops focused on specific diagnostics.

Participation at the large workshop started with 60 scientists and engineers from LLNL, LANL, SNL, State University of New York (SUNY), MIT, and LLE and grew to 117 by the ninth workshop in 2014 (see Table IX). Importantly, new participants with their own ideas and resources had been added.

The initial goals of the meetings were to develop NIF ignition diagnostics and plan scope, schedule, budget, and risk. The goals evolved and by the eighth workshop, NNSA had said that the NIF diagnostics working group had been so successful that its charter should be expanded to include the other large HED facilities: The NIF Diagnostic Workshop group morphed into a broader National Diagnostic Working Group (NDWG). The final workshop in this period focused on discussions of a new generation of diagnostics to more fully exploit NIF, OMEGA, and Z and to examine the failure modes in the attempts so far to achieve ignition. The Senate Energy and Water Appropriation Subcommittee directed NNSA to better coordinate diagnostic development across the national labs and universities for use at the major inertial confinement fusion facilities and to make sure that critical diagnostics are in place to take needed scientific measurement.

A national management group had identified 18 possible major new diagnostics and calibration facilities to be considered for the plan with associated multi-institutional teams, as discussed in Sec. IV E.

The method of accomplishment at the workshops was to have large (60–110 participants) plenary sessions interspersed with many targeted smaller (~25) group meetings. A management group suggested a set of questions pertinent to the small groups to answer.

**TABLE IX.** Attendee numbers and institutions at the 9th NDWG meeting (2014).

Institution	Attendees	Institution	Attendees	Institution.	Attendees
LLNL	55	Industry (US, UK)	8	MIT	3
SNL	11	LLE	8	PPL	2
LANL	10	CEA, AWE, IC	7	NNSA	1
NSTec	9	LBL	3	NRL	1
				U of N	1

An example of the questions posed to the small groups is shown in [Table X](#).

Besides the large group meetings with plenary and parallel small group breakout sessions, other small, targeted workshops were held during the year. For example, the fourth large workshop in 2010 was preceded during the year by eight mini-workshops on high-yield x-ray imaging, nToF PMT electrical recording, mix modeling, scanning/etching for MRS, wedge range filters, nuclear activation, nToF scintillators, and south pole bang time (SPBT).

Many new ideas arose during the workshops. For example, SPBT (south pole bang time) and SPIDER (streaked polar instrumentation for diagnosing energetic radiation) came directly from the workshops. A better measure of when stagnation of an implosion occurs was needed. At the second workshop, we realized there was a lot of access space below (south pole) and above the NIF hohlraums,

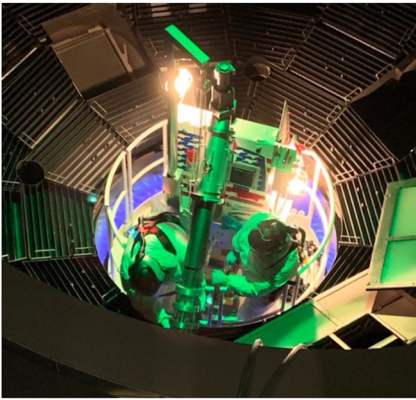
which have a vertical axis. A group at the workshop suggested a fixed position crystal spectrometer bang time diagnostic located below (south) the hohlraum as shown in [Fig. 17](#). LLE took responsibility and this SPBT diagnostic which was run for about a decade.<sup>172</sup>

Likewise, the need for a higher speed fixed x-ray detector, SPIDER, was satisfied by SNL mounting an x-ray streak camera on a port close (7°) to the north pole.<sup>173</sup>

As expected after robust discussions, some proposals were not pursued. For example, the need to time-resolve gamma emission in a complementary manner to GRH had been recognized. A gamma-to-electron magnetic spectrometer (GEMS) had been conceived. Knocked on Compton electrons would be magnetically energy analyzed. As this was explored, consensus on inadequate temporal performance coupled with a low level of technological development caused this concept to be abandoned.

**TABLE X.** Examples of directed questions posed to small parallel groups on successive days of a plenary NDWG meeting. A summary of the small group discussions was reported out to the plenary session at the end of the large workshop and a subsequent report was made to the NIF director and NNSA.

High-speed photo Diode/PMT	Is the pulse dilation PMT working? Are there incremental improvements of PMT and PD?
3D x-ray implosion imaging	Where next for each of the three facilities?
Optical diagnostic for n <sub>e</sub> L and B probing	With the deep UV optical probes available, can we use phase shifts/Faraday rotation to measure B?
Calibration of image plates	Should we regularize the calibration and readout procedures for NIF, OMEGA, and Z?
Where next for nToFs on NIF, Z, and OMEGA?	Do the new Cerenkov detectors change the way we field the next nToFs on the three facilities?
Coded aperture imaging: x rays and neutrons	Given progress with circular apertures on NIF, is there any benefit to other coded aperture schemes?
VISAR next step on NIF, OMEGA, and Z	Where next, both incremental and sudden for VISAR on NIF, OMEGA, and Z?
Hardened focal plane arrays (FPAs)	National plan for the best schemes, such as dump and read, to harden our FPAs?



**FIG. 17.** The south pole bang time diagnostic being removed from the NIF target chamber for decommissioning August 2022. Courtesy Van Wouterghem.

### C. Overview of non-ignition HED-based diagnostics

While the largest laser and pulse power facilities were initially built to pursue inertial confinement fusion, the high-energy density (HED) conditions achievable coupled with the broad suite of diagnostics led to strong interest in developing applications and diagnostics for HED experiments. The set of ICF diagnostics were used for these HED experiments, and new diagnostics were developed whose main purpose initially was to support these HED experiments. Many of these HED diagnostics also found important applications to ICF as well (i.e., 1D, 2D VISAR). The NDWG develops diagnostics that have broad application to both ICF and HED applications.

The HED applications can be broadly grouped into four categories with associated diagnostics:

- radiation transport and opacity,
- material properties at high pressure,
- hydrodynamics and radiation-hydrodynamics, and
- ignition applications and burn.

Each category benefits from a group of diagnostics that are often shared between them. Radiation transport and opacity experiments use calibrated broad band time-resolved and x-ray imaging spectrometers. High pressure material experiments utilize phase structure and kinetics diagnostics, such as time-resolved diffraction diagnostics, 1D and 2D VISAR for equation-of-state, and temperature diagnostics such as optical pyrometer and EXAFS spectrometers. High photon energy radiography is used for higher Z measurements to infer strength via Rayleigh–Taylor growth. Hydrodynamics and radiation-hydrodynamics measurements use high-resolution x-ray imaging diagnostics to measure instability growth and mix. Burn diagnostics use radiochemical diagnostics to measure isotopes from nuclear reactions and decay products. [Table XI](#) lists diagnostics that have been developed in these areas along with citations of their first publications.

Radiation transport diagnostics include the set of diagnostics developed on Nova, OMEGA, and NIF to measure subsonic and supersonic radiation driven Marshak waves in low-density materials and their interactions with materials.<sup>185</sup>

A 6 ns point backlighter was developed to radiograph material evolution<sup>174</sup> and detected with an x-ray streak camera in a DIM along a polar axis.<sup>186</sup>

A second Dante was developed in collaboration with AWE and installed on NIF to measure the radiation transported through material perturbations. As such, the second Dante was placed on

**TABLE XI.** HED non-implosion diagnostics developed on NNSA HED facilities.

Category	HED diagnostic	Date
Radiation transport and opacity	Long-duration point radiography <sup>174</sup>	2008
	Soft x-ray imaging spectrometer <sup>175,176</sup>	2012
	Second Dante on NIF <sup>177</sup>	2014
Material properties	1D VISAR; <sup>130</sup> turning mirror <sup>133</sup>	2004
	EXAFS spectroscopy to CID <sup>178</sup>	2005
	2D VISAR system demonstrated on OMEGA <sup>134</sup>	2010
	Powder x-ray diffraction image plate (PXRDIIP) <sup>179</sup>	2012
	TARDIS (x-ray sample diffraction) <sup>91</sup>	2013
	Time-resolved diffraction detector <sup>180</sup>	2018
	Multi-optic EXAFS spectrometer <sup>181</sup>	2021
Hydrodynamics and radiation-hydrodynamics	250 ps x-ray CMOS detector <sup>78</sup>	2012
Ignition applications and burn	Grating actuated transient optical recorder (GATOR) <sup>182</sup>	2012
	Gaseous collection radiochemistry <sup>183</sup>	2012
	Solid collection radiochemistry <sup>184</sup>	2012



the opposite hemisphere on NIF from the existing Dante. It was also placed closer to the target chamber center to measure lower temperatures than the existing Dante. The  $64^\circ$  angle from the polar axis is greater than the  $36^\circ$  original Dante angle and was chosen due to practical constraints.<sup>187</sup> To corroborate the drive on the half-hohlraum driven by laser beams from the lower hemisphere of NIF, an enclosed VISAR turning mirror was used to redirect the equatorial VISAR to the polar axis.<sup>133</sup> A transmission grating imaging spectrometer front end to an x-ray streak camera was developed to measure the burn-through of a Marshak wave.<sup>175</sup>

The NDWG community also developed diagnostics for OMEGA and Z. The Marshak wave diagnostic described earlier was developed and used on OMEGA experiments.<sup>185</sup> The Nova Dante was transferred and extended in accuracy on OMEGA. The analysis technique for nTOF was transferred to OMEGA for greater accuracy of OMEGA neutron spectroscopy. The need for a two-dimensional measurement of shock break out was discussed by the whole NDWG community and developed and used on OMEGA. The line VISAR from OMEGA and NIF was developed by a SNL/LLNL team and installed for use on Z. In progress is a team development of an x-ray streak camera and nToF's for Z.

Most of these diagnostics are now used by all programs on NIF. X-ray streak cameras and other instruments are routinely run in the polar DIM. The second Dante is used by other programs, including ICF to measure the x-ray flux on the upper hemisphere on NIF. The enclosed VISAR turning mirror technique is routinely used by many experiments. Opacity experiments use specialized calibrated spectrometers, either variable spaced gratings coupled to an x-ray framing camera or crystal spectrometers coupled to film or an image plate. Work is ongoing to replace the film/image plate with a CMOS detector.

Capabilities that HED facilities provide are the ability to compress materials quasi-isentropically to high pressure (tens of Mbars) and shock compress materials to extremely high pressure ( $\sim$ Gbar). Material property experiments use 1D line VISAR and 2D VISAR systems for equation-of-state measurements. VISAR diagnostics are covered in more detail elsewhere in this Review. Temperature measurements are made by an optical pyrometer diagnostic system as part of the 1D VISAR system and with spectrometers using the EXAFS technique.<sup>188</sup> The EXAFS measurement technique is routinely used on synchrotrons to measure temperature in materials; it is being actively developed on laser-driven high pressure experiments as well. The first demonstration at OMEGA used an implosion to create a continuum source of x rays and a flat crystal spectrometer to measure the extended x-ray absorption fine structure for Ti and Fe K-edges.<sup>178,189</sup>

The HED program on NIF wants to move to increasingly higher Z materials, requiring higher photon energy x-ray sources generated by laser illumination onto foils and measurements at the K- and L-edges of elements. The spectrometer design uses a toroidal crystal that has high collection efficiency and minimizes the effect of source size broadening on the spectral resolution. Different crystals are used to match the K- and L-edges of particular materials.<sup>181</sup> These are particularly challenging measurements due to the need for high spectral resolution and collection efficiency, which places very high demands on the crystal surface and uniformity. Another important measurement in materials at high pressure is the structure and phase. The material structure can be measured by using diffracting

x rays from the compressed material. Typically, the detector is film or an image plate. The time resolution comes from the impulse of x rays created; typically, one data point at compression is collected on a single experiment. The diagnostic detector is usually integrated with the target holder, which is a unique feature among the diagnostics. Because of the close proximity of the target with the detector, debris and background signal mitigation are issues that must be mitigated. To increase the data from a single experiment and also be able to study the kinetics of phase transitions, work is ongoing to replace the film or image plate detector with a gated hCMOS detector.<sup>180</sup> Because the active detector is  $10\times$  closer to the target than any other diagnostic, much work is required to mitigate debris and background signal. The approach is promising, and data have been acquired on a prototype instrument.

Hydrodynamic and radiation-hydrodynamic experiments measure the instability growth in planar and convergent geometry. Typically, they use x-ray radiography as the primary measurement. Key attributes of the measurement are high spatial resolution and temporal gating to reduce motion blurring. The typical configuration uses an area x-ray source of a few keV and a pinhole onto a gated microchannel plate detector.<sup>190,191</sup> This provides about  $10\text{--}20\ \mu\text{m}$  spatial resolution at the target and 100 ps of temporal resolution. However, as the opacity of the experiment increases due to the larger target sizes, higher density materials and/or higher compression, higher photon energy is required. This in turn requires point backlighters to create the necessary fluence of higher photon energy x rays and a single-line-of sight gated detector. As described in Sec. II C, early attempts were made to create a fast CMOS direct x-ray detector for this purpose. A  $512 \times 512$  segmented detector was designed by MIT Lincoln Labs, the CMOS fabricated at Taiwan Semiconductor Manufacturing Company (TSMC), and a detector constructed and tested at LLNL.<sup>78</sup>

The temporal gate width was measured to be 250 ps. The work was discontinued due to the high costs to iterate on the design and fabrication of prototype CMOS chips and the year-long lead time at a commercial foundry. The current work on CMOS detectors takes advantage of the existing CMOS fabrication facility at Sandia National Laboratories, which is more suited to R & D as well as the invention of time-dilation front end, which eliminated the need for short gate times.<sup>192</sup> Work is also currently under way to improve the spatial resolution for hydrodynamics experiments to  $\sim 3$  to  $5\ \mu\text{m}$  using collection optics such as a curved crystal<sup>103</sup> or zone plates<sup>193</sup> and to reduce temporal blurring by using a shorter pulse x-ray source.

Two classes of diagnostics were developed to study burning plasmas. Radiochemistry is a measurement technique that was developed to study reactions in a burning plasma.<sup>194</sup>

By selectively doping portions of a capsule, the resultant nuclear reaction products can provide information on mix, reaction chains, and branching ratios that are not possible elsewhere due to the high n fluences from a burning DT plasma. Hardware to collect the reaction products, gaseous<sup>183</sup> and solids,<sup>184</sup> and rapid analysis of the decays have been developed and installed. Selective capsule doping has been a challenge to develop and has limited the application of these diagnostics. Another diagnostic was developed to provide an x-ray image in the presence of high yield. It utilizes x-ray absorption induced index of refraction changes in a semiconductor, which has a response time of  $\sim 30$  fs.<sup>195</sup> A binary grating on the surface

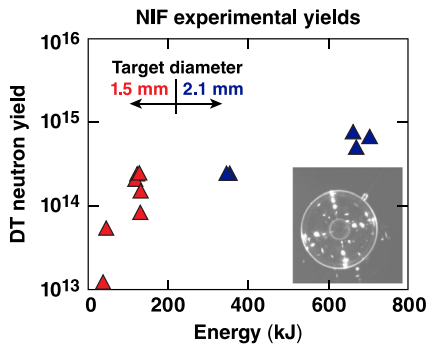


FIG. 18. DT neutron yields from NIF direct drive capsules.

of the semiconductor encodes the x-ray image onto the semiconductor. An interference pattern results, which can be encoded onto an incident laser beam, transported a distance away, and the image optically reconstructed. The technique has been demonstrated in the laboratory recording two static frames. While promising, it still requires demonstration on an implosion at a smaller scale before being considered as a viable diagnostic.

Since most HED experiments are used to compare with simulations, careful instrumental calibrations are required. There has been a long-standing collaboration with the Livermore Operations run currently by the Nevada National Security Site (NNSS) organization in this area. Instruments characterization and calibrations include optical and x-ray cameras, gated imagers, CCDs, and diodes.<sup>148,196</sup>

In summary, a number of diagnostics have been developed for non-implosion HED applications. Some have been broadly applicable to many other areas as people have discovered new applications for these diagnostics, such as VISAR, second DANTE, polar DIM. Most of the other diagnostics have highly specialized applications and have also been used for discovery science in the same physics area. The NDWG has played a major role in the development of these broad use diagnostics and also the most important specialized diagnostics.

#### D. Commissioning the set of NIF diagnostics installed by 2014

By 2014, a first set of 65, mainly implosion, diagnostics was operational on NIF.<sup>197</sup> The implosion diagnostic suite for NIF had to be commissioned and calibrated. Initially, direct drive gas-filled capsule implosions were used<sup>198</sup> in a collaboration between LLNL, LANL, LLE, and GA. However, indirectly driven capsules in near-vacuum hohlraums turned out to be better sources.<sup>199</sup> By using relatively low implosion convergences, good agreement with simulations was obtained, thus providing a well-characterized source of x rays, gamma rays, and nuclear particles to ensure all diagnostics were performing well.

##### 1. Directly driven capsules: “Exploding pushers”

Thin glass shells filled with DD, DHe,<sup>3</sup> or DT gas mixtures were used to provide sources of neutrons, protons, and x rays on the NIF utilizing polar direct drive geometry.<sup>200</sup> In this design, the thin glass outer wall of the capsule wall is heated by keV electrons produced by the laser illumination. This causes the wall to

“explode” into the interior gas, driving a strong shock, which heats the gas rapidly to high temperatures ( $\sim 10$  keV) in a low convergence implosion. This produces a short burst of fusion neutrons and/or protons with negligible areal density at stagnation.<sup>201</sup> These implosions provide a good source of nuclear particles without the complication of scattered neutrons. They allow cross-calibration of neutron time-of-flight diagnostics against absolute techniques such as nuclear activation.

The 1.5–2.1 mm diameter, 4–10  $\mu\text{m}$  thick glass shells were fabricated at General Atomics. These “Hoppe” shells were then filled with DT, DD, or DHe<sup>3</sup> gas mixtures at LLE and used for calibration experiments on both OMEGA and NIF. This is another example of the strong national collaboration that pooled expertise and resources at multiple institutions to develop these diagnostics. Interestingly, the experimental design for the NIF polar direct drive geometry was put together by a summer high school intern at LLE; this work was published in 2008.<sup>200</sup> Figure 18 shows how the DT neutron yield varied as function of NIF laser energy. These low mass targets produced yields in the range of  $10^{13}$  to  $7 \times 10^{14}$ , areal densities  $< 20$  mg/cc, and ion temperatures around 10 keV, which were ideal for commissioning NIF’s nuclear diagnostics.

Unfortunately, the bulk velocity of the neutron emitting hotspot on directly driven exploding pushers were too high (on average  $> 100$  km/s) to commission the unscattered neutron diagnostics FNADS/RTNADS. A new platform utilizing indirectly driven single shock implosions was used to fill this gap.

X-ray instrument timing is routinely verified by direct illumination of gold spheres.<sup>202</sup>

##### 2. Indirectly driven single shock implosions

A new commissioning platform that provided DT neutron yields about  $5 \times 10^{14}$  with negligible stagnation DT fuel areal density ( $< 20$  mg/cm<sup>2</sup>) and minimal hotspot bulk velocity ( $< 50$  km/s) was developed using near-vacuum hohlraum and a thin (120  $\mu\text{m}$ ) plastic capsule driven by a simple one-shock pulse shape.<sup>199</sup> When driven by low power 325 TW, total energy of 933 kJ in a 4.5 ns laser pulse, this experiment resulted in a low convergence (5 $\times$ ) implosion with measured stagnation parameters (e.g., DD/DT neutron yield, ion temperature, fuel areal density, time of peak x-ray emission, and fwhm of both x-ray and neutron emitting hotspot) that agreed with 1D HYDRA simulations within experimental errors as shown in Table XII.<sup>199</sup>

This platform has become a workhorse that is used to provide a reproducible and well-behaved quiescent source to both commission new diagnostics and recalibrate existing diagnostics following component changes and upgrades. In addition, the 1D behavior and good agreement with HYDRA simulations helped to spur new interest in low gas-filled hohlraums as an experimental platform using high-density carbon (HDC) ablaters.<sup>203,204</sup> Developments of these platforms in turn led to the near ignition result on the NIF.<sup>1</sup>

##### 3. List of diagnostics operational by $\sim 2014$

Tables XIII–XVI describe the NIF implosion diagnostics operational by about 2014. In addition, for the convenience of the reader the left-hand column also cites developments relevant to that cell and the sections of this Review where they are discussed.

**TABLE XII.** Summary of the performance of the DD implosion (N131203) and the DT implosion (N130503) with uncertainties(unc.) compared to the corresponding integrated HYDRA simulations.<sup>200</sup>

Observable	N130312	Uncertainty	N130503	Uncertainty	HYDRA post shot
DD n yield $10^{-12}$	5.1	0.2			4.3
DT n yield $10^{-14}$			5.12	0.09	5
DD $T_{\text{ion}}$ (keV)	3.5	0.2			3.5
DT $T_{\text{ion}}$ (keV)			4.6	0.2	4.6
Bang time ns	4.8	0.1	4.8	0.1	4.7
Radius mm	197	6	197	6	200
$T_{\text{rad}}$ (eV)	293	5	293	5	290
Fuel $\rho r$ mg/cm <sup>2</sup>	16	2	16	2	15.5
Total $\rho r$ mg/cm <sup>2</sup>	52	8	52	8	44

**TABLE XIII.** Diagnostics of laser absorption and hohlraum condition.

Diagnostic	Acronym	Responsible lab
Full aperture backscatter station	FABS31 FABS36	LLNL
Near backscatter imager	NBI23.5 NBI31 NBI36	LLNL
Broadband, time-resolved x-ray spectrometer	Dante1 Dante2	LLNL
Filter fluorescer (time-resolved)	FFLEX FFLEX TR	LLNL/AWE
Static x-ray imager, lower, upper <sup>82,85</sup> (Sec. II C 2)	SXI-L SXI-U	LLNL
Equatorial hard x-ray imager	EHXI	LLNL
Electromagnetic power	EMP	LLNL

**TABLE XIV.** Target response/implosion diagnostics.

Diagnostic	Acronym	Responsible lab
Streaked optical pyrometer	SOP	LLNL
Velocity int. system for any reflector <sup>115,134–136,149</sup> (Sec. II E)	VISAR	LLNL/LLE
DIM insertable (x-ray) streak camera <sup>115</sup> (Sec. II D 2)	DISC (3 <sup>a</sup> )	LLNL/LLE
Time-gated x-ray detector <sup>26–28</sup> (Sec. II A)	GXD (2 <sup>a</sup> )	LLNL/LANL
Hardened (gated) x-ray imager <sup>121</sup> (Sec. II D 2)	hGXI (2 <sup>a</sup> )	LLNL/LLE
Neutron time-of-flight bang time at 4 m	nToF4BT	LLE/LLNL
Proton (particle) time-of-flight detector	pToF	MIT/LLNL/LLE
South pole bang time	SPBT	LLE/LLNL
Streaked polar instrument for detecting energetic radiation	SPIDER	SNL/LLNL
Time-resolved gamma reaction history <sup>96,97</sup> (Sec. II C 5)	GRH	LANL/LLNL

<sup>a</sup>Number in parentheses is the number of units.

**TABLE XV.** Diagnostics of the hotspot.

Diagnostic	Acronym	Responsible lab
Neutron activation detector using Cu	NAD—Cu	SNL
Well-mounted neutron activation detector, Zr	Well NAD	LLNL
Neutron activation detector using indium	NAD—Snout	LLNL
Active readout neutron environment GXD	ARIANE	LLNL
Dilation imager for x rays at ignition <sup>92,100</sup> (Sec. II C 4)	DIXI	GA/LLNL
Neutron Imaging System <sup>159,160</sup> (Sec. II G)	NIS	LANL/LLNL
Neutron imaging time of flight	NITOF	LANL
Neutron time of flight <sup>52,59</sup> (Sec. II B 1)	IgnHi	LLE/LLNL
Neutron time of flight 4m	NTOF4 (3 <sup>a</sup> )	LLE/LLNL

<sup>a</sup>Number in parentheses is the number of units.

**TABLE XVI.** Diagnostics of areal density.

Diagnostic	Acronym	Responsible lab
Compton radiography	CR	LLNL
Magnetic Recoil Spectrometer <sup>73</sup> (Sec. II B 2)	MRS	MIT/LLE/LLNL
Neutron activation detector (flange mounted) <sup>42,43</sup> (Sec. II B 2)	FINAD(17)	LLNL
Neutron time-of-flight spectrometer <sup>59,60</sup> (Sec. II B 1)	SPEC-A, SPEC-E	LLNL/LLE
Radiochemical analysis of gaseous samples	RAGS	LLNL
Solid radiochemical collection diagnostic	SRC (many)	LLNL/LANL
Wedged range filter	WRF (many)	MIT/LLNL

### E. The National Diagnostic Plan (NDP): 2015

With input from the broad diagnostic program described in Section IV B, a National Diagnostic Plan (NDP) was developed in 2014 by a diagnostic management group of scientists and engineers. A very important increase in the scope work was to include diagnostics for all HED stockpile-stewardship experiments and not just ignition related diagnostics.

The NDP is a long document that is revised annually. The 2015 version was published by NNSA.<sup>205</sup> Since 2015, the NDP has evolved: The 2021 version is discussed in Sec. VI and accessible in full online.<sup>206</sup>

The NDP is described as follows: “Recognizing the need for enhanced coordination to develop advanced ICF diagnostics, the ICF/HED community formed the National Diagnostic Working Group (NDWG) of technical experts to formulate and execute a National Diagnostic Plan (NDP). Seventeen institutions participate in the NDP including LLNL, LANL, SNL, GA, NRL, MIT and other organizations such as PPPL and industry. International involvement from AWE and Commissariat Energie Atomique (CEA) also contributes to the depth and breadth of the NDP.”

The NDWG identified eight transformational diagnostics in the NDP. These were single LOS imaging (SLOS or DIXI-SLOS), ultraviolet Thomson scattering (UVTS), 3D n/gamma imaging, (NIS), gamma spectroscopy (GCD), time-resolved neutron spectrum (MRS-time), hard x-ray imaging (Wolter), time-resolved

diffraction (XRDt), and high-resolution x-ray spectroscopy. These eight evolved to ten by 2021, see Table XVIII.

These will provide unprecedented information on the implosion physics in fusion relevant regimes, determine the plasma conditions created by both laser and pulse power drivers, and enable dynamic measurements of a range of relevant conditions on the properties of materials utilized in nuclear weapons.

### F. Expert review of the NDP 2015

In 2014, NNSA contracted a group of subject matter experts to review the work and the plans of the NDWG described in this Review to prepare for its own internal planning and also to prepare a report requested by the Senate. In January 2015, a seven-person external group of diagnostic experts and a Federal Official reviewed the National Diagnostic Plan. The full report is available from the lead author and is excerpted below.

Overall, the comments from the individual reviewers were highly positive on the feasibility, practicability, and transformative nature of each of the eight diagnostics proposed. Each was considered highly worthy of continued development with the potential to improve experimental measurements vital to and tied to key mission requirements, and reviewers were favorably impressed at the breadth of discussions across the community that had revitalized this area by bringing to bear several new capabilities in development elsewhere. The efforts highlight the value of the Federally Funded Research and Development Center construct.

Some reviewers expressed concern at the outset that the proposed list only contained “winners” and that therefore some other diagnostics worthy of consideration were excluded prematurely. These concerns were allayed when “also rans” were discussed and it became clear that these were proposals where technical risk was very much higher or the scope and reach was much smaller, in both cases, therefore, more suitable for a smaller development effort within the discretion and budget of a specific facility.

A second common concern is that no overall sense of priorities among the proposals was presented to guide development in the event that there is a shortfall in available resources. Two key technologies did rise to the forefront as seminal developments that had a crosscutting impact, the pulse dilation technology being developed at General Atomics, and already employed as a first step in the LLNL DIXI detector, and the fast gated CMOS framing camera technology, which is an unanticipated spin-off from years of investment in fabrication capabilities at the MESA facility at SNL.

There was some concern that even tighter integration was needed between the diagnostics development effort and the experimental and design communities to ensure that diagnostic capabilities continue to meet needs and expectations as progress is made on all fronts.

Overall, however, the considered review of each reviewer was that each of the eight proposed diagnostics was transformative, had a reasonable probability of success, would have substantial payoff to the mission requirements, and should proceed if resources can be made available.

### G. NDWG meetings 2015–2021

Following the 2015 review of the NDP, NNSA agreed to a charter for the NDWG and its relationship to the NNSA HED plan. In summary, large meetings of the NDWG were held annually to review the NDP and provide recommendations to a NDP management review group to increment or decrement the NDP. A summary

TABLE XVII. Summary of large meetings of the NDWG.

NDWG series	When	Where	No. of attendees	Major highlights
10	Oct-15	LANL	133	<ul style="list-style-type: none"> <li>• NDP, UGT diagnostics and MARIE diagnostics presented</li> <li>• Pulse dilation technology application to x-ray imaging and 10 ps Cerenkov detectors proposed</li> </ul>
11	Nov-16	LLNL	115	<ul style="list-style-type: none"> <li>• Engineering plans presented for optical Thomson scattering, hCMOS, neutron imaging, and high-resolution x-ray spectrometry</li> <li>• Recommended important areas of collaboration and investment to the NNSA and laboratory leaderships and modifications to NDP</li> </ul>
12	Dec-17	GA	~110	<ul style="list-style-type: none"> <li>• Suite of material diagnostics improvements to study material aging recommended; time-resolved x-ray diffraction initiated using hCMOS detectors</li> <li>• Diagnostic technologies discussed for 3D implosion imaging on NIF, Z, OMEGA, measurement of magnetic fields with optical probes, calibration of image plates, improvements for nToF, coded aperture imaging, VISAR improvements 2D and 3D, and hardened focal plane arrays</li> </ul>
13	Dec-18	LLE	127	<ul style="list-style-type: none"> <li>• Diagnostic needs for HED experiments presented</li> <li>• Next set of transformational diagnostics discussed</li> <li>• Diagnostic technologies discussed for hard x-ray detectors including structured photocathodes and hybrid CMOS, dual-slot streak cameras, major upgrade to NIF VISAR/SOP system</li> </ul>
14	Dec-19	LLNL	~120	<ul style="list-style-type: none"> <li>• Diagnostic technologies discussed for high-resolution x-ray imaging, passive detectors, hotspot drift velocity, 15 keV photon detection, burn widths, and magnetic-field diagnostics</li> </ul>
15	Dec-21	LANL/virtual	N/A	



of the large meetings of the NDWG is shown in [Table XVII](#), together with dates and locations.

With input from these large NDWG meetings, the management group readjusts the NDP including the expected diagnostic schedule and makes recommendation to the managers of the facilities and NNSA for changes to the diagnostics at the facilities.

The major change in the NDP during this period was a result of the NNSA directed broadening of the scope from NIF to include the major national HED facilities. This resulted, for example, in the addition of VISAR, nToF, and x-ray streak cameras on Z, and time-dilation imagers on OMEGA.

The NDP management group consists of one or two diagnostic leads from LLNL, LANL, SNL, LLE, MIT, GA, and NNSA. Cognizant of their home institution's budget, they can make work commitments to the NDWG that are usually honored by their home institution.

## V. THE NATIONAL DIAGNOSTIC PLAN (NDP) FOR HED SCIENCE, SEPTEMBER 2021

The NDP is updated annually, as described earlier in this Review. Section [IV E](#) is a summary of the NDP written in 2015. The

**TABLE XVIII.** The ten transformational diagnostics of the NDP with institutional involvement and capability.

Transformative diagnostic	Collaborating institutions	New capability
Single LOS imaging (SLOS or DIXI-SLOS)	SNL, GA, LLNL, LLE	Multidimensional shape and spectra with unprecedented time and space resolution for fusion, Pu strength, and radiation effects sources
Ultraviolet Thomson scattering (UVTS)	LLE, LLNL, LANL, NRL	Localized plasma conditions and turbulence in hohlraums and laser direct drive ablation plasma; additional uses include plasma conditions at low density for rad flow studies and many discovery science applications.
3D n/gamma imaging (NIS)	LANL, LLNL	3D shape and size of both burning and cold compressed fuel, as well as remaining carbon ablator
Gamma spectroscopy (GCD)	LANL, AWE, GA, LLNL, SNL, NNSS	Fusion burn history allowing inferred pressure with increased precision and measured truncation of burn from degradation mechanisms such as mix and loss of confinement
Time-resolved neutron spectrum (MRS-time)	MIT, LLNL, GA, LLE	Time evolution of the fusion burn temperature and areal density
Hard x-ray imaging (Wolter)	SNL, LLNL, NASA, Harvard	High-energy source distribution and space-resolved plasma conditions in the hot plasma; also enables high spatial and temporal resolution for radiography to infer material strength
Time-resolved diffraction (XRDT)	SNL, LLNL, LLE	Time evolution of material structure (including weapon materials) and compression at high pressure; also enables more efficient facility use through multiple measurements on a single shot
High-resolution velocimeter (HRV)	LLNL, LLE, SNL	Higher accuracy (<1%) time evolution of material EOS at high pressure; also enables more efficient facility use through multiple high-fidelity measurements on a single shot
>15 keV X-ray detection (DHEX)	LLNL, LLE, SNL	Multiple-frame time-resolved detection of high-energy (>15 keV) x rays with high detection efficiency
hCMOS	SNL, LLNL	Multi-frame, burst mode imaging sensor capable of capturing images on the nanosecond time scale

**TABLE XIX.** How the missions of the SSP will be enhanced by new observables measured by the ten transformational diagnostics being developed under the guidance of the NDWG.

Mission	New observable	Technique	Acronym
Materials	Strength vs time of compressed Pu	>4 images/costly target	SLOS, hCMOS
	Phase change of compressed Pu—rates	Time-resolved x-ray diffraction	XRDt
	EOS of compressed Pu	High-resolution velocimeter	HRV
Hydro and properties	3D structure at ~50 keV	X-ray bands imager + SLOS	Wolter, hMCOS
	High-energy x-ray images of structure	Detection of high-energy x rays	DHEX
	$T_e$ of Marshak wave	Deep UV Thomson scattering	UVTS
Outputs and survivability	Hard spectrum vs space and time	X-ray bands imager + SLOS	Wolter, hCMOS
TN burn and pursuit of high yield	Time history of burn	Ultrafast Cerenkov detector	GCD
	3D $T_e$ and density vs time	Dilation tube + SLOS + Wolter	SLOS, hCMOS
	3D burn, 3D mix vs time	3D neutron/imaging	NIS
	$T_{ion}$ and areal density vs time	Neutron spectrum vs time	MRS-time
All	Hohlraum density and T vs space and time	Deep U.V. Thomson scattering	UVTS

latest (2021) version of the NDP is a 44-page document accessible online.<sup>206</sup>

This section is a summary of the latest version of the NDP.

The national diagnostics development effort is divided into three groups:

- Transformational diagnostics: diagnostics requiring a major national effort with the potential to transform experimental capability for the most critical science needs across the complex.
- Broad diagnostics: diagnostic efforts and techniques requiring significant national efforts that will enable new or more precise measurements across the complex.
- Local diagnostics: important diagnostics that implement known technology for a local need and are identified by facility management responding to the needs of the local user community.

The NDWG has identified ten transformational diagnostics, shown in Table XVIII, that will provide unprecedented information from experiments in support of the SSP at NIF, Z, and OMEGA.

Table XIX shows how the missions of the SSP experiments, including materials, complex hydrodynamics, radiation flow and effects, and thermonuclear burn and boost, will produce new observables, which need to be measured using a variety of the largely new diagnostic technologies used in the ten transformational diagnostics. The data provided by these diagnostics will validate and improve the physics contained within the SSP's simulations and both uncover and quantify important phenomena that lie beyond our present understanding.

In addition to these transformational diagnostics there are

- a set of broad diagnostics coordinated across the ICF sites,
- a large number of local diagnostics associated with the three large facilities: NIF, Z, and OMEGA.

## VI. CONCLUSION

The National Diagnostic Working Group has been highly successful in coordinating and implementing the HED diagnostics on NIF, OMEGA, and Z. It is the work of well over 100 scientists and engineers over more than a decade. This Review summarizes the achievements of the NDWG and analyzes the reasons for its success.

First and foremost are the collaborations of the NDWG. Besides the NNSA Labs, participants include universities, European institutions, and, importantly, industry. Collaborations attract external experts. Examples of the benefits of involving experts from industry as well as other institutions are referenced in Table XX. Industry also benefits by spin-off marketable products, as seen in Table XX. Collaborations also lead to the use of non-home facilities for testing and calibrations. The high shot rate of OMEGA has been particularly useful as discussed in Secs. II A and II B 2. A final benefit of collaboration is the agreed diagnostic responsibility and usually some financial responsibility at other institution.

A second factor is the accommodations of change of scope of diagnostics. As theories and ideas are falsified or improved, more diagnostics are needed with a concomitant scope and schedule change. Examples are referenced in Table XX. Likewise, as better experiments are developed a need for improved accuracy arises as referenced in Table XIX. Improved accuracy requirements leads to many generations of diagnostics, such as three generations of nToF's and four generations at least of spectrometers as well as schedule expansion. Staff benefit greatly from publications. The HTPD and SPIE conferences and the associated publications have been a forcing factor in motivating copious diagnostic papers over the years.

A third factor is the methods of accomplishment of the NDWG. A moderately large (to cover personnel changes) management group is responsible for keeping a national diagnostic schedule updated. As the schedule is often paced by resources, the members of this group have significant budget responsibility at their home institutions and respect from NNSA. The members of the group get



**TABLE XX.** The success factors of the NDWG, some attributes of the success factors with examples discussed in this Review.

Factor	Attribute	Examples			
		Institution	Diagnostic	Sections	
Collaborations	Attract external experts	Industry	Gated MCP	II A	
		Industry	Pulse dilation	II C 4	
		Industry	Gated PMT	II B 1	
		Industry	Electron optics	II D 2	
		MIT	MRS	II B 2	
		PPPL	DHIRES	II D 2	
		NRL	Virgil	II D 1	
		CEA	Dante mirror	II D 1	
		Spin-offs	Photek/Sydor	PD-PMT	II C 5
			Sydor	XRFC	II A
	SNL		Advanced hCMOS systems	II C 1	
	NASA Marshall		X-ray optics polishing	II F	
	Best facility for the job	OMEGA	nToF calibration	II B 1	
		OMEGA	NXS calibration	II D 1	
		Nike	Virgil calibration	II D 1	
	Agreed diagnostic responsibility	OMEGA	OMEGA gated MCP, serpentine	II A	
		NNSS Livermore Office	Calibration	IV C	
		LLNL	nToF calibration OMEGA	II B 1	
		LLNL	XRFC for OMEGA	II A	
		SNL	hCMOS	II C 1	
LANL		NIS, GRH, and GCD	II G		
LLNL		Wolter for Z	II F		
Scope expansion in time	Falsifiability/accuracy— new/upgraded diagnostics	Reason	Diagnostic		
		Falsifiability: anisotropy	Many nTOFs, many NADS	II B 1	
		Falsifiability: burn drift velocity	Faster nTOFs	II B 1	
		Falsifiability: fill tube, mix	X-ray gating	II A	
		Accuracy	VISAR	II E	
	Copious publications	Accuracy	Spectrometers, streak cameras	II D 2	
		Review of scientific instruments		III A	
		Proceedings of the SPIE		III A	
		Methods of accomplishment	NDWG management group with engineers	Updated National Diagnostic Plan (NDP) with schedules	IV E, V
				Resource recommendations to facilities/NNSA	IV B, IV E
Targeted NDWG parallel sessions	New ideas from broad community		IV B, IV G		
Large NDWG plenary meeting	Review updated NDP Review output parallel session updated NDP Changes in programs		IV F IV G		

23 August 2023 21:50:46

information about diagnostic from the large annual NDWG meetings; see [Table XVII](#). These large meetings alone cannot engender detailed discussion and so typically several parallel small group discussions with discussion topics set by the management meeting occur. Importantly, the small groups report out at the plenary session and thus the management group at the end of the meetings.

A hybrid meeting process leads to many scientists and engineers feeling ownership of the NDP. Clearly, this method works.

The entire ICF and NNSA community supported the development of very difficult, expensive instruments that took a long time to germinate and develop. The success of the NDWG is a credit to the whole community as shown in [Fig. 19](#).



FIG. 19. Participants of the ninth meeting of the NDWG held in September 2014 with ~117 attendees. Photograph by Jason Laurie LLNL with permission.

## ACKNOWLEDGMENTS

The NDWG is a collegial association of greater than 100 scientists and engineers who have all contributed to the work of the NDWG.

This work was performed under the auspices of the U.S. Department of Energy by General Atomics under Contract Grant No. 89233119CNA000063, by Lawrence Livermore National Laboratory under Contract Grant No. DE-AC52-07NA27344, by Los Alamos National Laboratory under Contract Grant No. 89233218CNA, by Sandia National Laboratory under Contract Grant No. DE-NA000352, by the Laboratory for Laser Energetics under Award Grant No. DE-NA0003856, the University of Rochester, and the New York State Energy Research and Development Authority, and the U.S. Department of Energy, National Nuclear Security Administration and U.S. Naval Research Laboratory.

## AUTHOR DECLARATIONS

### Conflict of Interest

The authors have no conflicts of interest to disclose.

## Author Contributions

**J. D. Kilkenny:** Conceptualization (lead); Methodology (lead); Writing – original draft (lead). **W. W. Hsing:** Conceptualization (supporting); Writing – original draft (supporting); Writing – review & editing (equal). **S. Batha:** Conceptualization (supporting); Writing – original draft (supporting). **G. A. Rochau:** Conceptualization (supporting); Writing – original draft (supporting). **T. C. Sangster:** Conceptualization (supporting). **P. M. Bell:** Conceptualization (supporting). **D. K. Bradley:** Conceptualization (supporting); Writing – original draft (supporting). **H. Chen:** Conceptualization (equal). **J. A. Frenje:** Conceptualization (equal); Writing – original draft (equal). **M. Gatu-Johnson:** Writing – original draft (equal). **V. Yu. Glebov:** Writing – original draft (equal). **R. J. Leeper:** Conceptualization (equal). **A. J. Mackinnon:** Writing – original draft (equal). **S. P. Regan:** Writing – original draft (equal). **J. S. Ross:** Writing – original draft (equal). **J. I. Weaver:** Writing – review & editing (equal).

## DATA AVAILABILITY

This is a review article and so there were no new data. Reasonable requests for details of meetings discussed in this article will be answered.

## REFERENCES

- Indirect Drive ICF Collaboration, *Phys. Rev. Lett.* **129**, 075001 (2022).
- K. R. Popper, *The Logic of Scientific Discovery* (Hutchinson, 1974).
- “National ignition facility conceptual design report,” Report UCRL-PROP-117093 ES (Lawrence Livermore National Laboratory, 1994).
- M. Koga, T. Fujiwara, T. Sakaiya, M. Lee, K. Shigemori, H. Shiraga, and H. Azechi, *Rev. Sci. Instrum.* **79**, 10E909 (2008).
- C. Trosseille, D. Aubert, L. Auger, S. Bazzoli, T. Beck, P. Brunel, M. Burillo, C. Chollet, J. Gazave, S. Jasmin, P. Maruenda, I. Moreau, G. Oudot, J. Raimbourg, G. Soullie, P. Stemmler, and C. Zuber, *Rev. Sci. Instrum.* **85**, 11D620 (2014).
- H. Cai, J. Liu, X. Peng, W. Li, Y. Ye, J. Wu, T. Zhang, Q. Deng, L. Niu, H. Niu, S. Liu, and G. Yang, *Chin. J. Lasers* **39**, 0117001 (2012).
- G. Power and P. Bell, *Proc. SPIE* **981**, 166 (1989).
- M. J. Eckart, R. L. Hanks, J. D. Kilkenny, R. Pasha, J. D. Wiedwald, and J. D. Hares, *Rev. Sci. Instrum.* **57**, 2046 (1986).
- G. Power, “Gain variation with gold coating thickness in pulsed microchannel plate striplines,” Lawrence Livermore National Laboratory Report UCID-21321, 1988 (unpublished).
- A. K. L. Dymoke-Bradshaw, *Proc. SPIE* **1757** (1992).
- D. K. Bradley, J. Delettrez, P. A. Jaanimagi, F. J. Marshall, C. P. Verdon, J. D. Kilkenny, and P. Bell, *Proc. SPIE* **0981**, 176 (1989).
- P. M. Bell, J. D. Kilkenny, G. Power, R. Bonner, and D. K. Bradley, *Proc. SPIE* **1155**, 430 (1989).
- D. K. Bradley, P. M. Bell, J. D. Kilkenny, R. Hanks, O. Landen, P. A. Jaanimagi, P. W. Mckenty, and C. P. Verdon, *Rev. Sci. Instrum.* **63**, 4813 (1992).
- J. D. Wiedwald, R. L. Hanks, G. L. Tietbohl, D. O. Bishop, G. D. Power, F. R. Kelly, and P. M. Bell, *Proc. SPIE* **1155**, 53 (1989).
- O. L. Landen, P. M. Bell, J. A. Oertel, J. J. Satariano, and D. K. Bradley, *Proc. SPIE* **2002**, 2 (1994).
- D. K. Bradley, P. M. Bell, O. L. Landen, J. D. Kilkenny, and J. Oertel, *Rev. Sci. Instrum.* **66**, 716 (1995).
- L. M. Logory, D. R. Farley, A. D. Conder, E. A. Belli, P. M. Bell, and P. L. Miller, *Rev. Sci. Instrum.* **69**, 4054 (1998).
- K. S. Budil, T. S. Perry, P. M. Bell, J. D. Hares, P. L. Miller, T. A. Peyser, R. Wallace, H. Louis, and D. E. Smith, *Rev. Sci. Instrum.* **67**, 485 (1996).
- J. A. Oertel, T. Archuleta, C. G. Peterson, and F. J. Marshall, *Proc. SPIE* **2869**, 709 (1997).
- J. A. Oertel, R. Aragonz, T. Archuleta, C. Barnes, L. Casper, V. Fatherley, T. Heinrichs, R. King, D. Landers, F. Lopez, P. Sanchez, G. Sandoval, L. Schrank, P. Walsh, P. Bell, M. Brown, R. Costa, J. Holder, S. Montelongo, and N. Pederson, *Rev. Sci. Instrum.* **77**, 10E308 (2006).

- <sup>21</sup>G. A. Kyrala, S. Dixit, S. Glenzer, D. Kalantar, D. Bradley, N. Izumi, N. Meezan, O. L. Landen, D. Callahan, S. V. Weber, J. P. Holder, S. Glenn, M. J. Edwards, P. Bell, J. Kimbrough, J. Koch, R. Prasad, L. Suter, J. L. Kline, and J. Kilkenny, *Rev. Sci. Instrum.* **81**, 10E316 (2010).
- <sup>22</sup>Sydor Technologies, 78 Schuyler Baldwin Dr, Fairport, NY 14450, USA.
- <sup>23</sup>T. Nash, M. Derzon, R. Leeper, D. Jobe, M. Hurst, and J. Seamen, *Rev. Sci. Instrum.* **70**, 302 (1999).
- <sup>24</sup>C. A. Kruschwitz, M. Wu, and G. A. Rochau, *Rev. Sci. Instrum.* **82**, 023102 (2011).
- <sup>25</sup>G. A. Rochau, M. Wu, C. Kruschwitz, N. Joseph, K. Moy, J. Bailey, M. Krane, R. Thomas, D. Nielsen, and A. Tibbitts, *Rev. Sci. Instrum.* **79**, 10E902 (2008).
- <sup>26</sup>L. R. Benedetti, P. M. Bell, D. K. Bradley, C. G. Brown, S. M. Glenn, R. Heeter, J. P. Holder, N. Izumi, S. F. Khan, G. Lacaillie, N. Simanovskaia, V. A. Smalyuk, and R. Thomas, *Rev. Sci. Instrum.* **83**, 10E135 (2012).
- <sup>27</sup>L. R. Benedetti, J. P. Holder, M. Perkins, C. G. Brown, C. S. Anderson, F. V. Allen, R. B. Petre, D. Hargrove, S. M. Glenn, N. Simanovskaia, D. K. Bradley, and P. Bell, *Rev. Sci. Instrum.* **87**, 23511 (2016).
- <sup>28</sup>L. R. Benedetti, C. Trosseille, J. P. Holder, K. Piston, D. Hargrove, D. K. Bradley, P. Bell, J. Raimbourg, M. Prat, L. A. Pickworth, and S. F. Khan, *Rev. Sci. Instrum.* **87**, 11D622 (2016).
- <sup>29</sup>N. B. Meezan, D. T. Woods, N. Izumi, H. Chen, H. A. Scott, M. B. Schneider, D. A. Liedahl, O. S. Jones, G. B. Zimmerman, J. D. Moody, O. L. Landen, and W. W. Hsing, *Phys. Plasmas* **27**, 102704 (2020).
- <sup>30</sup>O. S. Jones, L. J. Suter, H. A. Scott, M. A. Barrios, W. A. Farmer, S. B. Hansen, D. A. Liedahl, C. W. Mauche, A. S. Moore, M. D. Rosen, J. D. Salmonson, D. J. Strozzi, C. A. Thomas, and D. P. Turnbull, *Phys. Plasmas* **24**, 056312 (2017).
- <sup>31</sup>D. A. Callahan, O. A. Hurricane, J. E. Ralph, C. A. Thomas, K. L. Baker, L. R. Benedetti, L. F. B. Hopkins, D. T. Casey, T. Chapman, C. E. Czajka, E. L. Dewald, L. Divol, T. Doppner, D. E. Hinkel, M. Hohenberger, L. C. Jarrott, S. F. Khan, A. L. Kritcher, O. L. Landen, S. LePape, S. A. MacLaren, L. P. Masse, N. B. Meezan, A. E. Pak, J. D. Salmonson, D. T. Woods, N. Izumi, T. Ma, D. A. Mariscal, S. R. Nagel, J. L. Kline, G. A. Kyrala, E. N. Loomis, S. A. Yi, A. B. Zylstra, and S. H. Batha, *Phys. Plasmas* **25**, 056305 (2018).
- <sup>32</sup>R. Tommasini, J. E. Field, B. A. Hammel, O. L. Landen, S. W. Haan, C. Aracne-Ruddle, L. R. Benedetti, D. K. Bradley, D. A. Callahan, E. L. Dewald, T. Doepfner, M. J. Edwards, O. A. Hurricane, N. Izumi, O. A. Jones, T. Ma, N. B. Meezan, S. R. Nagel, J. R. Rygg, K. S. Segraves, M. Stadermann, R. J. Strauser, and R. P. J. Town, *Phys. Plasmas* **22**, 056315 (2015).
- <sup>33</sup>S. R. Nagel, S. W. Haan, J. R. Rygg, M. Barrios, L. R. Benedetti, D. K. Bradley, J. E. Field, B. A. Hammel, N. Izumi, O. S. Jones, S. F. Khan, T. Ma, A. E. Pak, R. Tommasini, and R. P. J. Town, *Phys. Plasmas* **22**, 022704 (2015).
- <sup>34</sup>A. Pak, L. Divol, C. R. Weber, L. F. B. Hopkins, D. S. Clark, E. L. Dewald, D. N. Fittinghoff, V. Geppert-Kleinrath, M. Hohenberger, S. Le Pape, T. Ma, A. G. MacPhee, D. A. Mariscal, E. Marley, A. S. Moore, L. A. Pickworth, P. L. Volegov, C. Wilde, O. A. Hurricane, and P. K. Patel, *Phys. Rev. Lett.* **124**, 145001 (2020).
- <sup>35</sup>A. G. MacPhee, V. A. Smalyuk, O. L. Landen, C. R. Weber, H. F. Robey, E. L. Alfonso, J. Biener, T. Bunn, J. W. Crippen, M. Farrell, S. Felker, J. E. Field, W. W. Hsing, C. Kong, J. Milovich, A. Moore, A. Nikroo, N. Rice, M. Stadermann, and C. Wild, *Phys. Plasmas* **25**, 054505 (2018).
- <sup>36</sup>J. A. Frenje, *Plasma Phys. Controlled Fusion* **62**, 023001 (2020).
- <sup>37</sup>H. Brysk, *Plasma Phys. Controlled Fusion* **15**, 611 (1973).
- <sup>38</sup>M. D. Cable and S. P. Hatchett, *J. Appl. Phys.* **62**, 2233 (1987).
- <sup>39</sup>M. D. Cable, S. P. Hatchett, and M. B. Nelson, *Rev. Sci. Instrum.* **63**, 4823 (1992).
- <sup>40</sup>R. G. Watt, R. E. Chrien, K. A. Klare, T. J. Murphy, D. C. Wilson, and S. Haan, *Rev. Sci. Instrum.* **72**, 846 (2001).
- <sup>41</sup>H. Azechi, M. D. Cable, and R. O. Stapf, *Laser Part. Beams* **9**, 119 (1991).
- <sup>42</sup>D. L. Bleuel, C. B. Yeamans, L. A. Bernstein, R. M. Bionta, J. A. Caggiano, D. T. Casey, G. W. Cooper, O. B. Drury, J. A. Frenje, C. A. Hagmann, R. Hatarik, J. P. Knauer, M. G. Johnson, K. M. Knittel, R. J. Leeper, J. M. McNaney, M. Moran, C. L. Ruiz, and D. H. G. Schneider, *Rev. Sci. Instrum.* **83**, 10D313 (2012).
- <sup>43</sup>R. M. Bionta, G. P. Grim, K. D. Hahn, E. P. Hartouni, E. A. Henry, H. Y. Khater, A. S. Moore, and D. J. Schlossberg, *Rev. Sci. Instrum.* **92**, 043527 (2021).
- <sup>44</sup>M. G. Johnson, D. T. Casey, J. A. Frenje, C.-K. Li, F. H. Séguin, R. D. Petrasso, R. Ashabranner, R. Bionta, S. LePape, M. McKernan, A. Mackinnon, J. D. Kilkenny, J. Knauer, and T. C. Sangster, *Phys. Plasmas* **20**, 042707 (2013).
- <sup>45</sup>T. J. Murphy, *Phys. Plasmas* **21**, 072701 (2014).
- <sup>46</sup>D. H. Munro, J. E. Field, R. Hatarik, J. L. Peterson, E. P. Hartouni, B. K. Spears, and J. D. Kilkenny, *Phys. Plasmas* **24**, 056301 (2017).
- <sup>47</sup>M. G. Johnson, J. P. Knauer, C. J. Cerjan, M. J. Eckart, G. P. Grim, E. P. Hartouni, R. Hatarik, J. D. Kilkenny, O. L. Landen, D. B. Sayre, B. K. Spears, R. M. Bionta, E. J. Bond, J. A. Caggiano, D. Callahan, D. T. Casey, T. Doppner, J. A. Frenje, V. Y. Glebov, O. Hurricane, A. Kritcher, S. LePape, T. Ma, A. Mackinnon, N. Meezan, P. Patel, R. D. Petrasso, J. E. Ralph, P. T. Springer, and C. B. Yeamans, *Phys. Rev. E* **94**, 021202 (2016).
- <sup>48</sup>D. J. Schlossberg, G. P. Grim, D. T. Casey, A. S. Moore, R. Nora, B. Bachmann, L. R. Benedetti, R. M. Bionta, M. J. Eckart, J. E. Field, D. N. Fittinghoff, M. G. Johnson, V. Geppert-Kleinrath, E. P. Hartouni, R. Hatarik, W. W. Hsing, L. C. Jarrott, S. F. Khan, J. D. Kilkenny, O. L. Landen, B. J. MacGowan, A. J. Mackinnon, K. D. Meaney, D. H. Munro, S. R. Nagel, A. Pak, P. K. Patel, B. K. Spears, P. L. Volegov, and C. V. Young, *Phys. Rev. Lett.* **127**, 125001 (2021).
- <sup>49</sup>S. P. Hatchett, private communication (2009).
- <sup>50</sup>J. D. Kilkenny, *Rev. Sci. Instrum.* **63**, 4688 (1992).
- <sup>51</sup>J. S. Milnes, C. J. Horsfield, M. S. Rubery, V. Y. Glebov, and H. W. Herrmann, *Rev. Sci. Instrum.* **83**, 10D301 (2012).
- <sup>52</sup>P. S. Datte, M. Eckart, A. S. Moore, W. Thompson, and G. V. de Dios, *Rev. Sci. Instrum.* **87**, 11D837 (2016).
- <sup>53</sup>J. S. Milnes, C. J. Horsfield, T. M. Conneely, and J. Howorth, *Rev. Sci. Instrum.* **85**, 11E601 (2014).
- <sup>54</sup>R. Lauck, M. Brandis, B. Bromberger, V. Dangendorf, M. B. Goldberg, I. Mor, K. Tittelmeier, and D. Vartsky, *IEEE Trans. Nucl. Sci.* **56**, 989 (2009).
- <sup>55</sup>R. Hatarik, L. A. Bernstein, J. A. Caggiano, M. L. Carman, D. H. G. Schneider, N. P. Zaitseva, and M. Wiedeking, *Rev. Sci. Instrum.* **83**, 10D911 (2012).
- <sup>56</sup>V. Y. Glebov, C. J. Forrest, K. L. Marshall, M. Romanofsky, T. C. Sangster, M. J. Shoup, and C. Stoeckl, *Rev. Sci. Instrum.* **85**, 11E102 (2014).
- <sup>57</sup>V. Y. Glebov, T. C. Sangster, C. Stoeckl, J. P. Knauer, W. Theobald, K. L. Marshall, M. J. Shoup, T. Buczek, M. Cruz, T. Duffy, M. Romanofsky, M. Fox, A. Pruyne, M. J. Moran, R. A. Lerche, J. McNaney, J. D. Kilkenny, M. J. Eckart, D. Schneider, D. Munro, W. Stoeckl, R. Zacharias, J. J. Haslam, T. Clancy, M. Yeoman, D. Warwas, C. J. Horsfield, J. L. Bourgade, O. Landoas, L. Disdier, G. A. Chandler, and R. J. Leeper, *Rev. Sci. Instrum.* **81**, 10D325 (2010).
- <sup>58</sup>V. Y. Glebov, C. Forrest, J. P. Knauer, A. Pruyne, M. Romanofsky, T. C. Sangster, M. J. Shoup, C. Stoeckl, J. A. Caggiano, M. L. Carman, T. J. Clancy, R. Hatarik, J. McNaney, and N. P. Zaitseva, *Rev. Sci. Instrum.* **83**, 10D309 (2012).
- <sup>59</sup>A. S. Moore, D. J. Schlossberg, E. P. Hartouni, D. Sayre, M. J. Eckart, R. Hatarik, F. Barbosa, J. Root, C. Waltz, B. Beeman, M. S. Rubery, and G. P. Grim, *Rev. Sci. Instrum.* **89**, 10I120 (2018).
- <sup>60</sup>J. E. Doyle and W. C. Dickenson, "The Cerenkov response of lucite and quartz to gamma and fast neutron radiation," Document No. UCRL-7032, 1962.
- <sup>61</sup>D. T. Casey, J. A. Frenje, M. G. Johnson, F. H. Seguin, C. K. Li, R. D. Petrasso, V. Y. Glebov, J. Katz, J. Magoon, D. D. Meyerhofer, T. C. Sangster, M. Shoup, J. Ulreich, R. C. Ashabranner, R. M. Bionta, A. C. Carpenter, B. Felker, H. Y. Khater, S. LePape, A. MacKinnon, M. A. McKernan, M. Moran, J. R. Rygg, M. F. Yeoman, R. Zacharias, R. J. Leeper, K. Fletcher, M. Farrell, D. Jasion, J. Kilkenny, and R. Paguio, *Rev. Sci. Instrum.* **84**, 043506 (2013).
- <sup>62</sup>E. A. Sundenn, H. Sjöstrand, S. Conroy, G. Ericsson, M. G. Johnson, L. Giacomelli, C. Hellesen, A. Hjalmarsson, E. Ronchi, M. Weiszflog, J. Källne, G. Gorini, M. Tardocchi, A. Combo, N. Cruz, A. Batista, R. Pereira, R. Fortuna, J. Sousa, and S. Popovichev, *Nucl. Instrum. Methods Phys. Res., Sect. A* **610**, 682 (2009).
- <sup>63</sup>J. A. Frenje, D. T. Casey, C. K. Li, J. R. Rygg, F. H. Seguin, R. D. Petrasso, V. Yu Glebov, D. D. Meyerhofer, T. C. Sangster, S. Hatchett, S. Haan, C. Cerjan, O. Landen, M. Moran, P. Song, D. C. Wilson, and R. J. Leeper, *Rev. Sci. Instrum.* **79**, 10E502 (2008).
- <sup>64</sup>D. T. Casey, J. A. Frenje, F. H. Seguin, C. K. Li, M. J. Rosenberg, H. Rinderknecht, M. J. E. Manuel, M. G. Johnson, J. C. Schaeffer, R. Frankel, N. Sinenian, R. A. Childs, R. D. Petrasso, V. Y. Glebov, T. C. Sangster, M. Burke, and S. Roberts, *Rev. Sci. Instrum.* **82**, 073502 (2011).
- <sup>65</sup>J. A. Frenje, D. T. Casey, C. K. Li, F. H. Séguin, R. D. Petrasso, V. Y. Glebov, P. B. Radha, T. C. Sangster, D. D. Meyerhofer, S. P. Hatchett, S. W. Haan, C. J. Cerjan, O. L. Landen, K. A. Fletcher, and R. J. Leeper, *Phys. Plasmas* **17**, 056311 (2010).



- <sup>66</sup>M. G. Johnson, J. A. Frenje, D. T. Casey, C. K. Li, F. H. Seguin, R. Petrasso, R. Ashbranner, R. M. Bionta, D. L. Bleuel, E. J. Bond, J. A. Caggiano, A. Carpenter, C. J. Cerjan, T. J. Clancy, T. Doepfner, M. J. Eckart, M. J. Edwards, S. Friedrich, S. H. Glenzer, S. W. Haan, E. P. Hartouni, R. Hatarik, S. P. Hatchett, O. S. Jones, G. Kyrala, S. Le Pape, R. A. Lerche, O. L. Landen, T. Ma, A. J. MacKinnon, M. A. McKernan, M. J. Moran, E. Moses, D. H. Munro, J. McNaney, H. S. Park, J. Ralph, B. Remington, J. R. Rygg, S. M. Sepke, V. Smalyuk, B. Spears, P. T. Springer, C. B. Yeamans, M. Farrell, D. Jasion, J. D. Kilkenny, A. Nikroo, R. Paguio, J. P. Knauer, V. Y. Glebov, T. C. Sangster, R. Betti, C. Stoeckl, J. Magoon, M. J. Shoup, G. P. Grim, J. Kline, G. L. Morgan, T. J. Murphy, R. J. Leeper, C. L. Ruiz, G. W. Cooper, and A. J. Nelson, *Rev. Sci. Instrum.* **83**, 10D308 (2012).
- <sup>67</sup>M. G. Johnson, J. A. Frenje, R. M. Bionta, D. T. Casey, M. J. Eckart, M. P. Farrell, G. P. Grim, E. P. Hartouni, R. Hatarik, M. Hoppe, J. D. Kilkenny, C. K. Li, R. D. Petrasso, H. G. Reynolds, D. B. Sayre, M. E. Schoff, F. H. Seguin, K. Skulina, and C. B. Yeamans, *Rev. Sci. Instrum.* **87**, 11D816 (2016).
- <sup>68</sup>M. G. Johnson, T. M. Johnson, B. J. Lahmann, F. H. Séguin, B. Sperry, N. Bhandarkar, R. M. Bionta, E. Casco, D. T. Casey, A. J. Mackinnon, N. Masters, A. Moore, A. Nikroo, M. Hoppe, R. Mohammed, W. Sweet, C. Freeman, V. Picciotto, J. Roumell, and J. A. Frenje, *Rev. Sci. Instrum.* **93**, 083513 (2022).
- <sup>69</sup>J. A. Frenje, T. J. Hilsabeck, C. W. Wink, P. Bell, R. Bionta, C. Cerjan, M. G. Johnson, J. D. Kilkenny, C. K. Li, F. H. Seguin, and R. D. Petrasso, *Rev. Sci. Instrum.* **87**, 11D806 (2016).
- <sup>70</sup>C. E. Parker, J. A. Frenje, M. G. Johnson, D. J. Schlossberg, H. G. Reynolds, L. B. Hopkins, R. Bionta, D. T. Casey, S. J. Felker, T. J. Hilsabeck, J. D. Kilkenny, C. K. Li, A. J. MacKinnon, H. Robey, M. E. Schoff, F. H. Seguin, C. W. Wink, and R. D. Petrasso, *Rev. Sci. Instrum.* **89**, 113508 (2018).
- <sup>71</sup>C. E. Parker, J. A. Frenje, O. H. W. Siegmund, C. J. Forrest, V. Y. Glebov, J. D. Kendrick, C. W. Wink, M. G. Johnson, T. J. Hilsabeck, S. T. Ivancic, J. Katz, J. D. Kilkenny, B. Lahmann, C. K. Li, F. H. Seguin, C. M. Sorce, C. Trosseille, and R. D. Petrasso, *Rev. Sci. Instrum.* **90**, 103306 (2019).
- <sup>72</sup>J. H. Kunimune, J. A. Frenje, G. P. A. Berg, C. A. Trosseille, R. C. Nora, C. S. Waltz, A. S. Moore, J. D. Kilkenny, and A. J. Mackinnon, *Rev. Sci. Instrum.* **92**, 033514 (2021).
- <sup>73</sup>G. P. A. Berg, J. A. Frenje, J. H. Kunimune, C. A. Trosseille, M. Couder, J. D. Kilkenny, A. J. Mackinnon, A. S. Moore, C. S. Waltz, and M. C. Wiescher, *Rev. Sci. Instrum.* **93**, 033505 (2022).
- <sup>74</sup>T. J. Hilsabeck, J. A. Frenje, J. D. Hares, and C. W. Wink, *Rev. Sci. Instrum.* **87**, 11D807 (2016).
- <sup>75</sup>J. H. Kunimune, M. G. Johnson, A. S. Moore, C. A. Trosseille, T. M. Johnson, G. P. A. Berg, A. J. Mackinnon, J. D. Kilkenny, and J. A. Frenje, *Rev. Sci. Instrum.* **93**, 083511 (2022).
- <sup>76</sup>R. Berger, D. D. Rathman, B. M. Tyrrell, E. J. Kohler, M. K. Rose, R. A. Murphy, T. S. Perry, H. F. Robey, F. A. Weber, D. M. Craig, A. M. Soares, S. P. Vernon, and R. K. Reich, *IEEE J. Solid-State Circuits* **43**, 1940 (2008).
- <sup>77</sup>R. K. Reich, D. D. Rathman, D. M. O'Mara, D. J. Young, A. H. Loomis, E. J. Kohler, R. M. Osgood, R. A. Murphy, M. Rose, R. Berger, S. A. Watson, M. D. Ulibarri, T. Perry, and B. B. Kosicki, *Rev. Sci. Instrum.* **74**, 2027 (2003).
- <sup>78</sup>A. T. Teruya, S. P. Vernon, J. D. Moody, W. W. Hsing, C. G. Brown, M. Griffin, A. S. Mead, and V. Tran, *Proc. SPIE* **8505**, 85050F (2012).
- <sup>79</sup>L. Claus, L. Fang, R. Kay, M. Kimmel, J. Long, G. Robertson, M. Sanchez, J. Stahoviak, D. Trotter, and J. L. Porter, *Proc. SPIE* **9591**, 9591OP (2017).
- <sup>80</sup>Q. Looker, A. P. Colombo, and J. L. Porter, *Rev. Sci. Instrum.* **92**, 053504 (2021).
- <sup>81</sup>L. R. Benedetti, N. E. Palmer, E. R. Hurd, C. E. Durand, A. C. Carpenter, M. S. Dayton, B. Golick, J. P. Holder, C. Trosseille, K. Werellapatha, and M. G. Gorman, *Rev. Sci. Instrum.* **92**, 044708 (2021).
- <sup>82</sup>Q. Looker, A. P. Colombo, M. Kimmel, and J. L. Porter, *Rev. Sci. Instrum.* **91**, 043502 (2020).
- <sup>83</sup>H. Chen, D. T. Woods, O. S. Jones, L. R. Benedetti, E. L. Dewald, N. Izumi, S. A. MacLaren, N. B. Meezan, J. D. Moody, N. E. Palmer, M. B. Schneider, and M. Vandenboomgaerde, *Phys. Plasmas* **27**, 022702 (2020).
- <sup>84</sup>H. Chen, N. Palmer, M. Dayton, A. Carpenter, M. B. Schneider, P. M. Bell, D. K. Bradley, L. D. Claus, L. Fang, T. Hilsabeck, M. Hohenberger, O. S. Jones, J. D. Kilkenny, M. W. Kimmel, G. Robertson, G. Rochau, M. O. Sanchez, J. W. Stahoviak, D. C. Trotter, and J. L. Porter, *Rev. Sci. Instrum.* **87**, 11E203 (2016).
- <sup>85</sup>H. Chen, B. Golick, N. Palmer, A. Carpenter, L. D. Claus, M. Dayton, J. Dean, C. Durand, B. Funsten, R. B. Petre, C. M. Hardy, J. Hill, J. Holder, E. Hurd, N. Izumi, J. Kehl, S. Khan, C. Macaraeg, M. O. Sanchez, T. Sarginson, M. B. Schneider, and C. Trosseille, *Rev. Sci. Instrum.* **92**, 033506 (2021).
- <sup>86</sup>J. R. Rygg, R. F. Smith, A. E. Lazicki, D. G. Braun, D. E. Fratanduono, R. G. Kraus, J. M. McNaney, D. C. Swift, C. E. Wehrenberg, F. Coppari, M. F. Ahmed, M. A. Barrios, K. J. M. Blobaum, G. W. Collins, A. L. Cook, P. Di Nicola, E. G. Dzenitis, S. Gonzales, B. F. Heidl, M. Hohenberger, A. House, N. Izumi, D. H. Kalantar, S. F. Khan, T. R. Kohut, C. Kumar, N. D. Masters, D. N. Polsin, S. P. Regan, C. A. Smith, R. M. Vignes, M. A. Wall, J. Ward, J. S. Wark, T. L. Zobrist, A. Arsenlis, and J. H. Eggert, *Rev. Sci. Instrum.* **91**, 043902 (2020).
- <sup>87</sup>T. Ao, D. V. Morgan, B. S. Stoltzfus, K. N. Austin, J. Usher, E. Breden, L. M. Pacheco, S. Dean, J. L. Brown, S. Duwal, H. Fan, P. Kalita, M. D. Knudson, M. A. Rodriguez, and J. M. D. Lane, *Rev. Sci. Instrum.* **93**, 053909 (2022).
- <sup>88</sup>L. R. Benedetti, private communication (2022).
- <sup>89</sup>R. D. Prosser, *J. Phys. E: Sci. Instrum.* **9**, 57 (1976).
- <sup>90</sup>J. D. Mcgee, J. Beesley, and A. D. Berg, *J. Sci. Instrum.* **43**, 153 (1966).
- <sup>91</sup>M. F. Ahmed, A. House, R. F. Smith, J. Ayers, Z. S. Lamb, and D. W. Swift, *Proc. SPIE* **8850**, 88500N (2013).
- <sup>92</sup>S. R. Nagel, A. C. Carpenter, J. Park, M. S. Dayton, P. M. Bell, D. K. Bradley, B. T. Funsten, B. W. Hatch, S. Heerey, J. M. Hill, J. P. Holder, E. R. Hurd, C. C. Macaraeg, P. B. Patel, R. B. Petre, K. Piston, C. A. Trosseille, K. Engelhorn, T. J. Hilsabeck, T. M. Chung, A. K. L. Dymoke-Bradshaw, J. D. Hares, L. D. Claus, T. D. England, B. B. Mitchell, J. L. Porter, G. Robertson, and M. O. Sanchez, *Rev. Sci. Instrum.* **89**, 10G125 (2018).
- <sup>93</sup>S. R. Nagel, T. J. Hilsabeck, P. M. Bell, D. K. Bradley, M. J. Ayers, M. A. Barrios, B. Felker, R. F. Smith, G. W. Collins, O. S. Jones, J. D. Kilkenny, T. Chung, K. Piston, K. S. Raman, B. Sammulu, J. D. Hares, and A. K. L. Dymoke-Bradshaw, *Rev. Sci. Instrum.* **83**, 10E116 (2012).
- <sup>94</sup>S. R. Nagel, T. J. Hilsabeck, P. M. Bell, D. K. Bradley, M. J. Ayers, K. Piston, B. Felker, J. D. Kilkenny, T. Chung, B. Sammulu, J. D. Hares, and A. K. L. Dymoke-Bradshaw, *Rev. Sci. Instrum.* **85**, 11E504 (2014).
- <sup>95</sup>S. R. Nagel, L. R. Benedetti, D. K. Bradley, T. J. Hilsabeck, N. Izumi, S. Khan, G. A. Kyrala, T. Ma, and A. Pak, *Rev. Sci. Instrum.* **87**, 11E311 (2016).
- <sup>96</sup>H. Geppert-Kleinrath, Y. Kim, K. D. Meaney, H. W. Herrmann, N. M. Hoffman, A. Kritcher, J. A. Carrera, and S. Gales, *High Energy Density Phys.* **37**, 100862 (2020).
- <sup>97</sup>A. K. L. Dymoke-Bradshaw, J. D. Hares, J. Milnes, H. W. Herrmann, C. J. Horsfield, S. G. Gales, A. Leatherland, T. Hilsabeck, and J. D. Kilkenny, *Rev. Sci. Instrum.* **89**, 10I137 (2018).
- <sup>98</sup>F. J. Marshall, R. E. Bahr, V. N. Goncharov, V. Y. Glebov, B. Peng, S. P. Regan, T. C. Sangster, and C. Stoeckl, *Rev. Sci. Instrum.* **88**, 093702 (2017).
- <sup>99</sup>K. Engelhorn, T. J. Hilsabeck, J. Kilkenny, D. Morris, T. M. Chung, A. Dymoke-Bradshaw, J. D. Hares, P. Bell, D. Bradley, A. C. Carpenter, M. Dayton, S. R. Nagel, L. Claus, J. Porter, G. Rochau, M. Sanchez, S. Ivancic, C. Sorce, and W. Theobald, *Rev. Sci. Instrum.* **89**, 10G123 (2018).
- <sup>100</sup>W. Theobald, C. Sorce, M. Bedzyk, S. T. Ivancic, F. J. Marshall, C. Stoeckl, R. C. Shah, M. Lawrie, S. P. Regan, T. C. Sangster, E. M. Campbell, T. J. Hilsabeck, K. Englehorn, J. D. Kilkenny, D. Morris, T. M. Chung, J. D. Hares, A. K. L. Dymoke-Bradshaw, P. Bell, J. Celeste, A. C. Carpenter, M. Dayton, D. K. Bradley, M. C. Jackson, L. Pickworth, S. R. Nagel, G. Rochau, J. Porter, M. Sanchez, L. Claus, G. Robertson, and Q. Looker, *Rev. Sci. Instrum.* **89**, 10G117 (2018).
- <sup>101</sup>C. Trosseille, C. E. Durand, E. R. Hurd, M. S. Dayton, K. Engelhorn, G. N. Hall, J. P. Holder, O. L. Landen, A. C. Carpenter, and S. R. Nagel, *Rev. Sci. Instrum.* **93**, 023505 (2022).
- <sup>102</sup>C. Trosseille, A. M. Garafalo, M. S. Dayton, C. E. Durand, B. T. Funsten, T. J. Hilsabeck, E. Imhoff, S. B. Morioka, K. W. Piston, A. E. Raymond, A. C. Welton, L. Claus, M. Sanchez, J. D. Hares, T. M. Chung, A. C. Carpenter, and S. R. Nagel, *Rev. Sci. Instrum.* **93**, 083516 (2022).
- <sup>103</sup>G. N. Hall, C. M. Krauland, M. S. Schollmeier, G. E. Kemp, J. G. Buscho, R. Hibbard, N. Thompson, E. R. Casco, M. J. Ayers, S. L. Ayers, N. B. Meezan, L. F. B. Hopkins, R. Nora, B. A. Hammel, L. Masse, J. E. Field, D. K. Bradley, P. Bell, O. L. Landen, J. D. Kilkenny, D. Mariscal, J. Park, T. J. McCarville, R. Lowe-Webb, D. Kalantar, T. Kohut, and K. Piston, *Rev. Sci. Instrum.* **90**, 013702 (2019).
- <sup>104</sup>S. P. Regan, R. Epstein, B. A. Hammel, L. J. Suter, J. Ralph, H. Scott, M. A. Barrios, D. K. Bradley, D. A. Callahan, C. Cerjan, G. W. Collins, S. N. Dixit, T. Doepfner, M. J. Edwards, D. R. Farley, S. Glenn, S. H. Glenzer, I. E. Golovkin, S. W. Haan, A. Hamza, D. G. Hicks, N. Izumi, J. D. Kilkenny, J. L. Kline, G. A.

- Kyrala, O. L. Landen, T. Ma, J. J. MacFarlane, R. C. Mancini, R. L. McCrory, N. B. Meezan, D. D. Meyerhofer, A. Nikroo, K. J. Peterson, T. C. Sangster, P. Springer, and R. P. J. Town, *Phys. Plasmas* **19**, 056307 (2012).
- <sup>105</sup>S. P. Regan, R. Epstein, B. A. Hammel, L. J. Suter, H. A. Scott, M. A. Barrios, D. K. Bradley, D. A. Callahan, C. Cerjan, G. W. Collins, S. N. Dixit, T. Doppner, M. J. Edwards, D. R. Farley, K. B. Fournier, S. Glenn, S. H. Glenzer, I. E. Golovkin, S. W. Haan, A. Hamza, D. G. Hicks, N. Izumi, O. S. Jones, J. D. Kilkenny, J. L. Kline, G. A. Kyrala, O. L. Landen, T. Ma, J. J. MacFarlane, A. J. MacKinnon, R. C. Mancini, R. L. McCrory, N. B. Meezan, D. D. Meyerhofer, A. Nikroo, H. S. Park, J. Ralph, B. A. Remington, T. C. Sangster, V. A. Smalyuk, P. T. Springer, and R. P. J. Town, *Phys. Rev. Lett.* **111**, 045001 (2013).
- <sup>106</sup>T. Ma, H. Chen, P. K. Patel, M. B. Schneider, M. A. Barrios, D. T. Casey, H. K. Chung, B. A. Hammel, L. F. B. Hopkins, L. C. Jarrott, S. F. Khan, B. Lahmann, R. Nora, M. J. Rosenberg, A. Pak, S. P. Regan, H. A. Scott, H. Sio, B. K. Spears, and C. R. Weber, *Rev. Sci. Instrum.* **87**, 11E327 (2016).
- <sup>107</sup>M. A. Barrios, D. A. Liedahl, M. B. Schneider, O. Jones, G. V. Brown, S. P. Regan, K. B. Fournier, A. S. Moore, J. S. Ross, O. Landen, R. L. Kauffman, A. Nikroo, J. Kroll, J. Jaquez, H. Huang, S. B. Hansen, D. A. Callahan, D. E. Hinkel, D. Bradley, and J. D. Moody, *Phys. Plasmas* **23**, 056307 (2016).
- <sup>108</sup>K. B. Fournier, M. J. May, J. D. Colvin, M. A. Barrios, J. R. Patterson, and S. P. Regan, *Phys. Rev. E* **88**, 033104 (2013).
- <sup>109</sup>M. A. Barrios, S. P. Regan, K. B. Fournier, R. Epstein, R. Smith, A. Lazicki, R. Rygg, D. E. Fratanduono, J. Eggert, H. S. Park, C. Huntington, D. K. Bradley, O. L. Landen, and G. W. Collins, *Rev. Sci. Instrum.* **85**, 11D502 (2014).
- <sup>110</sup>B. A. Hammel, H. A. Scott, S. P. Regan, C. Cerjan, D. S. Clark, M. J. Edwards, R. Epstein, S. H. Glenzer, S. W. Haan, N. Izumi, J. A. Koch, G. A. Kyrala, O. L. Landen, S. H. Langer, K. Peterson, V. A. Smalyuk, L. J. Suter, and D. C. Wilson, *Phys. Plasmas* **18**, 056310 (2011).
- <sup>111</sup>F. Perez, G. E. Kemp, S. P. Regan, M. A. Barrios, J. Pino, H. Scott, S. Ayers, H. Chen, J. Emig, J. D. Colvin, M. Bedzyk, M. J. Shoup, A. Agliata, B. Yaakobi, F. J. Marshall, R. A. Hamilton, J. Jaquez, M. Farrell, A. Nikroo, and K. B. Fournier, *Rev. Sci. Instrum.* **85**, 11D613 (2014).
- <sup>112</sup>M. J. May, J. Weaver, K. Widmann, G. E. Kemp, D. Thorn, J. D. Colvin, M. B. Schneider, A. Moore, and B. E. Blue, *Rev. Sci. Instrum.* **87**, 11E330 (2016).
- <sup>113</sup>J. D. Kilkenny, R. W. Lee, M. H. Key, and J. G. Lunney, *Phys. Rev. A* **22**, 2746 (1980).
- <sup>114</sup>C. J. Keane, B. A. Hammel, D. R. Kania, J. D. Kilkenny, R. W. Lee, A. L. Osterheld, L. J. Suter, R. C. Mancini, C. F. Hooper, and N. D. Delamater, *Phys. Fluids B* **5**, 3328 (1993).
- <sup>115</sup>A. G. MacPhee, A. K. L. Dymoke-Bradshaw, J. D. Hares, J. Hassett, B. W. Hatch, A. L. Meadowcroft, P. M. Bell, D. K. Bradley, P. S. Datte, O. L. Landen, N. E. Palmer, K. W. Piston, V. V. Rekow, T. J. Hilsabeck, and J. D. Kilkenny, *Rev. Sci. Instrum.* **87**, 11E202 (2016).
- <sup>116</sup>H. Chen, T. Ma, R. Nora, M. A. Barrios, H. A. Scott, M. B. Schneider, L. B. Hopkins, D. T. Casey, B. A. Hammel, L. C. Jarrott, O. L. Landen, P. K. Patel, M. J. Rosenberg, and B. K. Spears, *Phys. Plasmas* **24**, 072715 (2017).
- <sup>117</sup>T. A. Hall, *J. Phys. E: Sci. Instrum.* **17**, 110 (1984).
- <sup>118</sup>K. W. Hill, M. Bitter, L. Delgado-Aparicio, D. Johnson, R. Feder, P. Beiersdorfer, J. Dunn, K. Morris, E. Wang, M. Reinke, Y. Podpaly, J. E. Rice, R. Barnsley, M. O'Mullane, and S. G. Lee, *Rev. Sci. Instrum.* **81**, 10E322 (2010).
- <sup>119</sup>P. M. Nilson, F. Ehrne, C. Mileham, D. Mastro Simone, R. K. Jungquist, C. Taylor, C. R. Stillman, S. T. Ivancic, R. Boni, J. Hassett, D. J. Lonobile, R. W. Kidder, M. J. Shoup, A. A. Solodov, C. Stoeckl, W. Theobald, D. H. Froula, K. W. Hill, L. Gao, M. Bitter, P. Efthimion, and D. D. Meyerhofer, *Rev. Sci. Instrum.* **87**, 11D504 (2016).
- <sup>120</sup>L. Gao, B. F. Kraus, K. W. Hill, M. B. Schneider, A. Christopherson, B. Bachmann, M. Bitter, P. Efthimion, N. Pablant, R. Betti, C. Thomas, D. Thorn, A. G. MacPhee, S. Khan, R. Kauffman, D. Liedahl, H. Chen, D. Bradley, J. Kilkenny, B. Lahmann, E. Stambulchik, and Y. Maron, *Phys. Rev. Lett.* **128**, 185002 (2022).
- <sup>121</sup>A. G. MacPhee, P. M. Bell, D. Boyle, A. C. Carpenter, L. Claus, M. Dayton, J. Dean, A. K. L. Dymoke-Bradshaw, C. Durand, B. Funsten, A. Garafalo, B. P. Golick, J. D. Hares, J. Hill, J. M. Kehl, S. F. Khan, J. D. Kilkenny, M. J. MacDonald, D. Maheshwari, I. J. McCubbin, S. R. Nagel, P. R. Nyholm, N. E. Palmer, R. B. Petre, M. Sanchez, M. B. Schneider, M. O. Schoelmerich, S. Stoupin, and A. Welton, *Rev. Sci. Instrum.* **93**, 083519 (2022).
- <sup>122</sup>M. S. Schollmeier, M. Geissel, J. E. Shores, I. C. Smith, and J. L. Porter, *Appl. Opt.* **54**, 5147 (2015).
- <sup>123</sup>K. R. Carpenter, R. C. Mancini, E. C. Harding, A. J. Harvey-Thompson, M. Geissel, M. R. Weis, S. B. Hansen, K. J. Peterson, and G. A. Rochau, *Phys. Plasmas* **27**, 052704 (2020).
- <sup>124</sup>E. C. Harding, G. K. Robertson, M. S. Schollmeier, G. S. Dunham, M. R. Gomez, P. F. Knapp, J. R. Fein, C. S. Speas, and G. A. Rochau, "X-ray self-emission imaging with spherically bent Bragg crystals on the Z-machine" (unpublished, 2022).
- <sup>125</sup>Y. Aglitskiy, T. Lehecka, S. Obenschain, S. Bodner, C. Pawley, K. Gerber, J. Sethian, C. M. Brown, J. Seely, U. Feldman, and G. Holland, *Appl. Opt.* **37**, 5253 (1998).
- <sup>126</sup>J. A. Koch, J. E. Field, J. D. Kilkenny, E. Harding, G. A. Rochau, A. M. Covington, E. C. Dutra, R. R. Freeman, G. N. Hall, M. J. Haugh, and J. A. King, *High Energy Density Phys.* **23**, 184 (2017).
- <sup>127</sup>L. M. Barker and R. E. Hollenbach, *J. Appl. Phys.* **43**, 4669 (1972).
- <sup>128</sup>P. M. Celliers, G. W. Collins, L. B. Da Silva, D. M. Gold, and R. Cauble, *Appl. Phys. Lett.* **73**, 1320 (1998).
- <sup>129</sup>D. H. Munro, P. M. Celliers, G. W. Collins, D. M. Gold, L. B. Da Silva, S. W. Haan, R. C. Cauble, B. A. Hammel, and W. W. Hsing, *Phys. Plasmas* **8**, 2245 (2001).
- <sup>130</sup>P. M. Celliers, D. K. Bradley, G. W. Collins, D. G. Hicks, T. R. Boehly, and W. J. Armstrong, *Rev. Sci. Instrum.* **75**, 4916 (2004).
- <sup>131</sup>R. E. Olson, D. K. Bradley, G. A. Rochau, G. W. Collins, R. J. Leeper, and L. J. Suter, *Rev. Sci. Instrum.* **77**, 10e523 (2006).
- <sup>132</sup>T. R. Boehly, D. Munro, P. M. Celliers, R. E. Olson, D. G. Hicks, V. N. Goncharov, G. W. Collins, H. F. Robey, S. X. Hu, J. A. Morozas, T. C. Sangster, O. L. Landen, and D. D. Meyerhofer, *Phys. Plasmas* **16**, 056302 (2009).
- <sup>133</sup>S. A. MacLaren, H. S. Park, P. M. Celliers, A. R. Cooper, M. E. Foord, M. B. Schneider, R. M. Seugling, R. J. Wallace, P. E. Young, T. R. Boehly, and A. S. Moore, "Characterization of a halfraum x-ray drive using VISAR at the National Ignition Facility" (unpublished) (2012).
- <sup>134</sup>P. M. Celliers, D. J. Erskine, C. M. Sorce, D. G. Braun, O. L. Landen, and G. W. Collins, *Rev. Sci. Instrum.* **81**, 035101 (2010).
- <sup>135</sup>J. D. Moody, H. F. Robey, P. M. Celliers, D. H. Munro, D. A. Barker, K. L. Baker, T. Doppner, N. L. Hash, L. B. Hopkins, K. LaFortune, O. L. Landen, S. LePape, B. J. MacGowan, J. E. Ralph, J. S. Ross, C. Widmayer, A. Nikroo, E. Giraldez, and T. Boehly, *Phys. Plasmas* **21**, 092702 (2014).
- <sup>136</sup>S. J. Ali, P. M. Celliers, S. Haan, T. R. Boehly, N. Whiting, S. H. Baxamusa, H. Reynolds, M. A. Johnson, J. D. Hughes, B. Watson, H. Huang, J. Biener, K. Engelhorn, V. A. Smalyuk, and O. L. Landen, *Phys. Plasmas* **25**, 092708 (2018).
- <sup>137</sup>E. M. Campbell, J. T. Hunt, E. S. Bliss, D. R. Speck, and R. P. Drake, *Rev. Sci. Instrum.* **57**, 2101 (1986).
- <sup>138</sup>H. F. Robey, T. R. Boehly, R. E. Olson, A. Nikroo, P. M. Celliers, O. L. Landen, and D. D. Meyerhofer, *Phys. Plasmas* **17**, 012703 (2010).
- <sup>139</sup>K. K. M. Lee, L. R. Benedetti, R. Jeanloz, P. M. Celliers, J. H. Eggert, D. G. Hicks, S. J. Moon, A. Mackinnon, L. B. Da Silva, D. K. Bradley, W. Unites, G. W. Collins, E. Henry, M. Koenig, A. Benuzzi-Mounaix, J. Pasley, and D. Neely, *J. Chem. Phys.* **125**, 014701 (2006).
- <sup>140</sup>S. D. Baton, M. Koenig, E. Brambrink, H. P. Schlenvoigt, C. Rousseaux, G. Debras, S. Laffite, P. Loiseau, F. Philippe, X. Ribeyre, and G. Schurtz, *Phys. Rev. Lett.* **108**, 195002 (2012).
- <sup>141</sup>T. Caillaud, E. Alozy, M. Briat, P. Cornet, S. Darbon, A. Dizièrre, A. Duval, V. Drouet, J. Fariaut, D. Gontier, O. Landoas, B. Marchet, I. Masclet-Gobain, G. Oudot, G. Soullié, P. Stemmler, C. Reverdin, R. Rosch, A. Rousseau, B. Rossé, C. Rubbelynck, P. Troussel, B. Villetle, F. Aubard, S. Huelvan, R. Maroni, P. Llavador, V. Allouche, M. Burillo, C. Chollet, C. D'Hose, B. Prat, C. Trosseille, J. Raimbourg, C. Zuber, J. P. Lebreton, S. Perez, J. L. Ulmer, T. Jalinaud, J. Jadaud, J. L. Bourgade, R. Wrobel, X. Rogue, and J. L. Miquel, *Proc. SPIE* **9966**, 996606 (2016).
- <sup>142</sup>N. Hopps, K. Oades, J. Andrew, C. Brown, G. Cooper, C. Danson, S. Daykin, S. Duffield, R. Edwards, D. Egan, S. Elsmere, S. Gales, M. Girling, E. Gumbrell, E. Harvey, D. Hillier, D. Hoarty, C. Horsfield, S. James, A. Leatherland, S. Masoero, A. Meadowcroft, M. Norman, S. Parker, S. Rothman, M. Rubery, P. Treadwell, D. Winter, and T. Bett, *Plasma Phys. Controlled Fusion* **57**, 064002 (2015).
- <sup>143</sup>J. Galbraith, K. Austin, J. Baker, R. Bettencourt, E. Bliss, J. Celeste, T. Clancy, S. Cohen, M. Crosley, P. Datte, D. Fratanduono, G. Frieders, J. Hammer, J. Jackson,



- D. Johnson, M. Jones, D. Koen, J. Lusk, A. Martinez, W. Massey, T. McCarville, H. McLean, K. Raman, S. Rodriguez, D. Spencer, P. Springer, and J. Wong, *Proc. SPIE* **10390**, 1039002 (2017).
- <sup>144</sup>R. M. Malone, J. R. Bower, D. K. Bradley, G. A. Capelle, J. R. Celeste, P. M. Celliers, G. W. Collins, M. J. Eckart, J. H. Eggert, B. C. Frogget, R. L. Guyton, D. G. Hicks, M. I. Kaufman, B. J. MacGowan, S. Montelongo, A. W. N. B. Edmund, R. B. Robinson, T. W. Tunnell, P. W. Watts, and P. G. Zapata, *Proc. SPIE* **5580** (2004).
- <sup>145</sup>S. G. Glendinning, J. Bolstad, D. G. Braun, M. J. Edwards, W. W. Hsing, B. F. Lasinski, H. Louis, A. Miles, J. Moreno, T. A. Peyser, B. A. Remington, H. F. Robey, E. J. Turano, C. P. Verdon, and Y. Zhou, *Phys. Plasmas* **10**, 1931 (2003).
- <sup>146</sup>R. L. Kauffman, H. N. Kornblum, D. W. Phillion, C. B. Darrow, B. F. Lasinski, L. J. Suter, A. R. Theissen, R. J. Wallace, and F. Ze, *Rev. Sci. Instrum.* **66**, 678 (1995).
- <sup>147</sup>M. Takeda, H. Ina, and S. Kobayashi, *J. Opt. Soc. Am.* **72**, 156 (1982).
- <sup>148</sup>M. R. Charest, P. Torres, C. T. Silbernagel, and D. H. Kalantar, *Rev. Sci. Instrum.* **79**, 10F546 (2008).
- <sup>149</sup>J. Oh, A. J. Schmitt, M. Karasik, and S. P. Obenschain, *Phys. Plasmas* **28**, 032704 (2021).
- <sup>150</sup>J. L. Peebles, S. X. Hu, W. Theobald, V. N. Goncharov, N. Whiting, P. M. Celliers, S. J. Ali, G. Duchateau, E. M. Campbell, T. R. Boehly, and S. P. Regan, *Phys. Rev. E* **99**, 063208 (2019).
- <sup>151</sup>A. M. Saunders, S. J. Ali, H. S. Park, J. Eggert, F. Najjar, C. Huntington, T. Haxhimali, B. Morgan, Y. Ping, and H. G. Rinderknecht, *AIP Conf. Proc.* **2272**, 120025 (2020).
- <sup>152</sup>D. A. Callahan, N. B. Meezan, S. H. Glenzer, A. J. MacKinnon, L. R. Benedetti, D. K. Bradley, J. R. Celeste, P. M. Celliers, S. N. Dixit, T. Döppner, E. G. Dzenitis, S. Glenn, S. W. Haan, C. A. Haynam, D. G. Hicks, D. E. Hinkel, O. S. Jones, O. L. Landen, R. A. London, A. G. MacPhee, P. A. Michel, J. D. Moody, J. E. Ralph, H. F. Robey, M. D. Rosen, M. B. Schneider, D. J. Strozzi, L. J. Suter, R. P. J. Town, K. Widmann, E. A. Williams, M. J. Edwards, B. J. MacGowan, J. D. Lindl, L. J. Atherton, G. A. Kyrala, J. L. Kline, R. E. Olson, D. Edgell, S. P. Regan, A. Nikroo, H. Wilkins, J. D. Kilkenny, and A. S. Moore, *Phys. Plasmas* **19**, 056305 (2012).
- <sup>153</sup>B. Koziowski, B. Bachmann, A. Do, and R. Tommasini, *Rev. Sci. Instrum.* **94**, 041102 (2023).
- <sup>154</sup>R. J. Ellis, J. E. Trebes, D. W. Phillion, J. D. Kilkenny, S. G. Glendinning, J. D. Wiedwald, and R. A. Levesque, *Rev. Sci. Instrum.* **61**, 2759 (1990).
- <sup>155</sup>M. C. Weisskopf, B. Brinkman, C. Canizares, G. Garmire, S. Murray, and L. P. Van Speybroeck, *Publ. Astron. Soc. Pac.* **114**, 1 (2002).
- <sup>156</sup>J. R. Fein, D. J. Ampleford, J. K. Vogel, B. Koziowski, C. C. Walton, M. Wu, C. R. Ball, A. Ames, J. Ayers, P. Bell, C. J. Bourdon, D. Bradley, R. Bruni, G. S. Dunham, P. D. Gard, D. Johnson, K. Kilaru, C. Kirtley, P. W. Lake, A. Maurer, L. Nielsen-Weber, L. A. Pickworth, M. J. Pivovarov, B. Ramsey, O. J. Roberts, G. A. Rochau, S. Romaine, and M. Sullivan, *Rev. Sci. Instrum.* **89**, 10G115 (2018).
- <sup>157</sup>P. R. Champey, J. Kolodziejczak, B. Koziowski, J. Davis, C. Griffith, T. Kester, K. Kilaru, A. Meekham, J. Menapace, B. Ramsey, O. J. Roberts, J. Sanchez, P. Singam, W. Scott Smith, C. Speegle, M. Stahl, T. Suratwala, N. Thomas, M. Young, and J. K. Vogel, *Rev. Sci. Instrum.* **93**, 113504 (2022).
- <sup>158</sup>D. Ress, R. A. Lerche, R. J. Ellis, S. M. Lane, and K. A. Nugent, *Science* **241**, 956 (1988).
- <sup>159</sup>D. N. Fittinghoff, N. Birge, and V. Geppert-Kleinrath, *Rev. Sci. Instrum.* **94**, 021101 (2023).
- <sup>160</sup>G. L. Morgan, R. R. Berggren, P. A. Bradley, F. H. Cverna, J. R. Faulkner, P. L. Gobby, J. A. Oertel, F. J. Swenson, J. A. Tegtmeier, R. B. Walton, M. D. Wilke, D. C. Wilson, and L. Disdier, *Rev. Sci. Instrum.* **72**, 865 (2001).
- <sup>161</sup>G. P. Grim, N. Guler, F. E. Merrill, G. L. Morgan, C. R. Danly, P. L. Volegov, C. H. Wilde, D. C. Wilson, D. S. Clark, D. E. Hinkel, O. S. Jones, K. S. Raman, N. Izumi, D. N. Fittinghoff, O. B. Drury, E. T. Alger, P. A. Arnold, R. C. Ashbranner, L. J. Atherton, M. A. Barrios, S. Batha, P. M. Bell, L. R. Benedetti, R. L. Berger, L. A. Bernstein, L. V. Berzins, R. Betti, S. D. Bhandarkar, R. M. Bionta, D. L. Bleuel, T. R. Boehly, E. J. Bond, M. W. Bowers, D. K. Bradley, G. K. Brunton, R. A. Buckles, S. C. Burkhardt, R. F. Burr, J. A. Caggiano, D. A. Callahan, D. T. Casey, C. Castro, P. M. Celliers, C. J. Cerjan, G. A. Chandler, C. Choate, S. J. Cohen, G. W. Collins, G. W. Cooper, J. R. Cox, J. R. Cradick, P. S. Datte, E. L. Dewald, P. Di Nicola, J. M. Di Nicola, L. Divol, S. N. Dixit, R. Dylla-Spears, E. G. Dzenitis, M. J. Eckart, D. C. Eder, D. H. Edgell, M. J. Edwards, J. H. Eggert, R. B. Ehrlich, G. V. Erbert, J. Fair, D. R. Farley, B. Felker, R. J. Fortner, J. A. Frenje, G. Frieders, S. Friedrich, M. Gatu-Johnson, C. R. Gibson, E. Giraldez, V. Y. Glebov, S. M. Glenn, S. H. Glenzer, G. Gururangan, S. W. Haan, K. D. Hahn, B. A. Hammel, A. V. Hamza, E. P. Hattouni, R. Hatarik, S. P. Hatchett, C. Haynam, M. R. Hermann, H. W. Herrmann, D. G. Hicks, J. P. Holder, D. M. Holunga, J. B. Horner, W. W. Hsing, H. Huang, M. C. Jackson, K. S. Jancaitis, D. H. Kalantar, R. L. Kauffman, M. I. Kauffman, S. F. Khan, J. D. Kilkenny, J. R. Kirkbrough, R. Kirkwood, J. L. Kline, J. P. Knauer, K. M. Knittel, J. A. Koch, T. R. Kohut, B. J. Koziowski, K. Krauter, G. W. Krauter, A. L. Kritcher, J. Kroll, G. A. Kyrala, K. N. L. Fortune, G. LaCaille, L. J. Lagin, T. A. Land, O. L. Landen, D. W. Larson, D. A. Latray, R. J. Leeper, T. L. Lewis, S. LePape, J. D. Lindl, R. R. Lowe-Webb, T. Ma, B. J. MacGowan, A. J. MacKinnon, A. G. MacPhee, R. M. Malone, T. N. Malsbury, E. Mapoles, C. D. Marshall, D. G. Mathisen, P. McKenty, J. M. McNaney, N. B. Meezan, P. Michel, J. L. Milovich, J. D. Moody, A. S. Moore, M. J. Moran, K. Moreno, E. I. Moses, D. H. Munro, B. R. Nathan, A. J. Nelson, A. J. Nelson, R. E. Olson, C. Orth, A. E. Pak, E. S. Palma, T. G. Parham, P. K. Patel, R. W. Patterson, R. D. Petrasso, R. Prasad, J. E. Ralph, S. P. Regan, H. Rinderknecht, H. F. Robey, G. F. Ross, C. L. Ruiz, F. H. Séguin, J. D. Salmonson, T. C. Sangster, J. D. Sater, R. L. Saunders, R. P. Town, A. J. Traille, B. V. Wotterghem, R. J. Wallace, S. Weaver, S. V. Weber, P. J. Wegner, P. K. Whitman, K. Widmann, C. C. Widmayer, R. D. Wood, B. K. Young, R. A. Zacharias, and A. Zylstra, *Phys. Plasmas* **20**, 056320 (2013).
- <sup>162</sup>P. L. Volegov, private communication (2019).
- <sup>163</sup>J. S. Ross, P. Datte, L. Divol, J. Galbraith, D. H. Froula, S. H. Glenzer, B. Hatch, J. Katz, J. Kilkenny, O. Landen, A. M. Manuel, W. Molander, D. S. Montgomery, J. D. Moody, G. Swadling, and J. Weaver, *Rev. Sci. Instrum.* **87**, 11E510 (2016).
- <sup>164</sup>J. Katz, R. Boni, C. Sorce, R. Follett, M. J. Shoup, and D. H. Froula, *Rev. Sci. Instrum.* **83**, 10E349 (2012).
- <sup>165</sup>F. Fiuza, G. F. Swadling, A. Grassi, H. G. Rinderknecht, D. P. Higginson, D. D. Ryutov, C. Bruulsema, R. P. Drake, S. Funk, S. Glenzer, G. Gregori, C. K. Li, B. B. Pollock, B. A. Remington, J. S. Ross, W. Rozmus, Y. Sakawa, A. Spitkovsky, S. Wilks, and H.-S. Park, *Nat. Phys.* **16**, 916 (2020).
- <sup>166</sup>J. D. Kilkenny, M. D. Cable, E. M. Campbell, L. W. Coleman, D. L. Correll, R. P. Drake, R. J. Ellis, S. G. Glendinning, C. W. Hatcher, S. P. Hatchett, J. P. Hunt, D. R. Kania, R. L. Kauffman, H. N. Kornblum, D. T. Kyrasiz, S. M. Lane, R. A. Lerche, J. D. Lindl, W. H. Lowdermilk, D. H. Munro, D. W. Phillion, D. B. Ress, D. R. Speck, E. Storm, L. J. Suter, G. L. Tietbohl, A. R. Thiessen, R. S. Thoe, R. E. Turner, J. D. Wiedwald, and F. Ze, in *Proceedings of the Twelfth International Conference on Plasma Physics and Controlled Nuclear Fusion Research* (IAEA Vienna, 1989), Vol. 3, p. 29, IAEA-CN-50/B-1-3.
- <sup>167</sup>J. D. Kilkenny, M. D. Cable, C. A. Clower, B. A. Hammel, V. P. Karpenko, R. L. Kauffman, H. N. Kornblum, B. J. MacGowan, W. Olson, T. J. Orzechowski, D. W. Phillion, G. L. Tietbohl, J. E. Trebes, B. Chrien, B. Failor, A. Hauer, R. Hockaday, J. Oertel, R. Watt, C. Ruiz, G. Cooper, D. Hebron, R. Leeper, J. Porter, and J. Knauer, *Rev. Sci. Instrum.* **66**, 288 (1995).
- <sup>168</sup>"National Ignition Facility functional requirements and primary criteria revision 1.3," Report NIF-LLNL-93-058 (Lawrence Livermore National Laboratory, 1994).
- <sup>169</sup>R. J. Leeper, G. A. Chandler, G. W. Cooper, M. S. Derzon, D. L. Fehl, D. E. Hebron, A. R. Moats, D. D. Noack, J. L. Porter, L. E. Ruggles, C. L. Ruiz, J. A. Torres, M. D. Cable, P. M. Bell, C. A. Clower, B. A. Hammel, D. H. Kalantar, V. P. Karpenko, R. L. Kauffman, J. D. Kilkenny, F. D. Lee, R. A. Lerche, B. J. MacGowan, M. J. Moran, M. B. Nelson, W. Olson, T. J. Orzechowski, T. W. Phillips, D. Ress, G. L. Tietbohl, J. E. Trebes, R. J. Bartlett, R. Berggren, S. E. Caldwell, R. E. Chrien, B. H. Failor, J. C. Fernandez, A. Hauer, G. Idzorek, R. G. Hockaday, T. J. Murphy, J. Oertel, R. Watt, M. Wilke, D. K. Bradley, J. Knauer, R. D. Petrasso, and C. K. Li, *Rev. Sci. Instrum.* **68**, 868 (1997).
- <sup>170</sup>T. J. Murphy, C. W. Barnes, R. R. Berggren, P. Bradley, S. E. Caldwell, R. E. Chrien, J. R. Faulkner, P. L. Gobby, N. Hoffman, J. L. Jimerson, K. A. Klare, C. L. Lee, J. M. Mack, G. L. Morgan, J. A. Oertel, F. J. Swenson, P. J. Walsh, R. B. Walton, R. G. Watt, M. D. Wilke, D. C. Wilson, C. S. Young, S. W. Haan, R. A. Lerche, M. J. Moran, T. W. Phillips, T. C. Sangster, R. J. Leeper, C. L. Ruiz, G. W. Cooper, L. Disdier, A. Rouyer, A. Fedotoff, V. Y. Glebov, D. D. Meyerhofer, J. M. Soares, C. Stöckl, J. A. Frenje, D. G. Hicks, C. K. Li, R. D. Petrasso, F. H. Séguin, K. Fletcher, S. Padalino, and R. K. Fisher, *Rev. Sci. Instrum.* **72**, 773 (2001).

- <sup>171</sup>J. A. Oertel, T. J. Murphy, R. R. Berggren, J. Faulkner, R. Schmel, D. Little, T. Archuleta, J. Lopez, J. Velarde, and R. F. Horton, *Rev. Sci. Instrum.* **70**, 803 (1999).
- <sup>172</sup>D. H. Edgell, D. K. Bradley, E. J. Bond, S. Burns, D. A. Callahan, J. Celeste, M. J. Eckart, V. Y. Glebov, D. S. Hey, G. Laccaille, J. D. Kilkenny, J. Kimbrough, A. J. Mackinnon, J. Magoon, J. Parker, T. C. Sangster, M. J. Shoup, C. Stoeckl, T. Thomas, and A. MacPhee, *Rev. Sci. Instrum.* **83**, 10E119 (2012).
- <sup>173</sup>S. F. Khan, P. M. Bell, D. K. Bradley, S. R. Burns, J. R. Celeste, L. S. Dauffy, M. J. Eckart, M. A. Gerhard, C. Hagmann, D. I. Headley, J. P. Holder, N. Izumi, M. C. Jones, J. W. Kellogg, H. Y. Khater, J. R. Kimbrough, A. G. MacPhee, Y. P. Opachich, N. E. Palmer, R. B. Petre, A. J. L. Porter, R. T. Shelton, T. L. Thomas, and J. B. Worden, *Proc. SPIE* **8505**, 850505 (2012).
- <sup>174</sup>A. B. Reighard, S. G. Glendinning, P. E. Young, W. W. Hsing, M. Foord, M. Schneider, K. Lu, T. Dittrich, R. Wallace, and C. Sorce, *Rev. Sci. Instrum.* **79**, 10E915 (2008).
- <sup>175</sup>A. S. Moore, T. M. Guymier, J. L. Kline, J. Morton, M. Taccetti, N. E. Lanier, C. Bentley, J. Workman, B. Peterson, K. Mussack, J. Cowan, R. Prasad, M. Richardson, S. Burns, D. H. Kalantar, L. R. Benedetti, P. Bell, D. Bradley, W. Hsing, and M. Stevenson, *Rev. Sci. Instrum.* **83**, 10E132 (2012).
- <sup>176</sup>J. Benstead, A. S. Moore, M. F. Ahmed, J. Morton, T. M. Guymier, R. Soufli, T. Pardini, R. L. Hibbard, C. G. Bailey, P. M. Bell, S. Hau-Riege, M. Bedzyk, M. J. Shoup, S. Reagan, T. Agliata, R. Jungquist, D. W. Schmidt, L. B. Kot, W. J. Garbett, M. S. Rubery, J. W. Skidmore, E. Gullikson, and F. Salmassi, *Rev. Sci. Instrum.* **87**, 055110 (2016).
- <sup>177</sup>A. S. Moore, A. B. R. Cooper, M. B. Schneider, S. MacLaren, P. Graham, K. Lu, R. Seugling, J. Satcher, J. Klingmann, A. J. Comley, R. Marrs, M. May, K. Widmann, G. Glendinning, J. Castor, J. Sain, C. A. Back, J. Hund, K. Baker, W. W. Hsing, J. Foster, B. Young, and P. Young, *Phys. Plasmas* **21**, 063303 (2014).
- <sup>178</sup>B. Yaakobi, T. R. Boehly, D. D. Meyerhofer, T. J. B. Collins, B. A. Remington, P. G. Allen, S. M. Pollaine, H. E. Lorenzana, and J. H. Eggert, *Phys. Rev. Lett.* **95**, 075501 (2005).
- <sup>179</sup>J. R. Rygg, J. H. Eggert, A. E. Lazicki, F. Coppari, J. A. Hawreliak, D. G. Hicks, R. F. Smith, C. M. Sorce, T. M. Uphaus, B. Yaakobi, and G. W. Collins, *Rev. Sci. Instrum.* **83**, 113904 (2012).
- <sup>180</sup>L. R. Benedetti, J. H. Eggert, J. D. Kilkenny, D. K. Bradley, P. M. Bell, N. E. Palmer, R. B. Petre, B. F. Heidl, J. R. Rygg, T. R. Boehly, G. W. Collins, and C. Sorce, *AIP Conf. Proc.* **1979**, 160004 (2017).
- <sup>181</sup>S. Stoupin, D. B. Thorn, N. Ose, L. Gao, K. W. Hill, Y. Ping, F. Coppari, B. Koziolowski, A. Krygier, H. Sio, J. Ayers, M. Bitter, B. Kraus, P. C. Efthimion, and M. B. Schneider, *Rev. Sci. Instrum.* **92**, 053102 (2021).
- <sup>182</sup>K. L. Baker, R. E. Stewart, P. T. Steele, S. P. Vernon, and W. W. Hsing, *Appl. Phys. Lett.* **101**, 031107 (2012).
- <sup>183</sup>D. A. Shaughnessy, C. A. Velsko, D. R. Jedlovec, C. B. Yeaman, K. J. Moody, E. Tereshatov, W. Stoeffl, and A. Riddle, *Rev. Sci. Instrum.* **83**, 10D917 (2012).
- <sup>184</sup>J. M. Gostic, D. A. Shaughnessy, K. T. Moore, I. D. Hutcheon, P. M. Grant, and K. J. Moody, *Rev. Sci. Instrum.* **83**, 10D904 (2012).
- <sup>185</sup>C. A. Back, J. D. Bauer, O. L. Landen, R. E. Turner, B. F. Lasinski, J. H. Hammer, M. D. Rosen, L. J. Suter, and W. H. Hsing, *Phys. Rev. Lett.* **84**, 274 (2000).
- <sup>186</sup>A. B. R. Cooper, M. B. Schneider, S. A. MacLaren, A. S. Moore, P. E. Young, W. W. Hsing, R. Seugling, M. E. Foord, J. D. Sain, M. J. May, R. E. Marrs, B. R. Maddox, K. Lu, K. Dodson, V. Smalyuk, P. Graham, J. M. Foster, C. A. Back, and J. F. Hund, *Phys. Plasmas* **20**, 033301 (2013).
- <sup>187</sup>T. M. Guymier, A. S. Moore, J. Morton, J. L. Kline, S. Allan, N. Bazin, J. Benstead, C. Bentley, A. J. Comley, J. Cowan, K. Flippo, W. Garbett, C. Hamilton, N. E. Lanier, K. Mussack, K. Obrey, L. Reed, D. W. Schmidt, R. M. Stevenson, J. M. Taccetti, and J. Workman, *Phys. Plasmas* **22**, 043303 (2015).
- <sup>188</sup>A. M. Manuel, M. Millot, L. G. Seppala, G. Frieders, Z. Zeid, K. Christensen, and P. M. Celliers, *Proc. SPIE* **9591**, 959104 (2015).
- <sup>189</sup>B. Yaakobi, F. J. Marshall, T. R. Boehly, R. P. J. Town, and D. D. Meyerhofer, *J. Opt. Soc. Am. B* **20**, 238 (2003).
- <sup>190</sup>S. R. Nagel, K. S. Raman, C. M. Huntington, S. A. MacLaren, P. Wang, M. A. Barrios, T. Baumann, J. D. Bender, L. R. Benedetti, D. M. Doane, S. Felker, P. Fitzsimmons, K. A. Flippo, J. P. Holder, D. N. Kaczala, T. S. Perry, R. M. Seugling, L. Savage, and Y. Zhou, *Phys. Plasmas* **24**, 072704 (2017).
- <sup>191</sup>A. Casner, C. Mailliet, S. F. Khan, D. Martinez, N. Izumi, D. Kalantar, P. Di Nicola, J. M. Di Nicola, E. Le Bel, I. Igumenshchev, V. T. Tikhonchuk, B. A. Remington, L. Masse, and V. A. Smalyuk, *Plasma Phys. Controlled Fusion* **60**, 014012 (2018).
- <sup>192</sup>T. J. Hilsabeck, J. D. Hares, J. D. Kilkenny, P. M. Bell, A. K. L. Dymoke-Bradshaw, J. A. Koch, P. M. Celliers, D. K. Bradley, T. McCarville, M. Pivovarov, R. Soufli, and R. Bionta, *Rev. Sci. Instrum.* **81**, 10E317 (2010).
- <sup>193</sup>A. Do, L. A. Pickworth, B. J. Koziolowski, A. M. Angulo, G. N. Hall, S. R. Nagel, D. K. Bradley, T. McCarville, and J. M. Ayers, *Appl. Optics* **59**, 010777 (2020).
- <sup>194</sup>G. P. Grim, P. A. Bradley, T. A. Bredeweg, A. L. Keksis, M. M. Fowler, A. C. Hayes, G. Jungman, A. W. Obst, R. S. Rundberg, D. J. Vieira, J. B. Wilhelm, L. A. Bernstein, C. J. Cerjan, R. J. Fortner, K. J. Moody, D. H. Schneider, D. A. Shaughnessy, W. Stoeffl, and M. A. Stoyer, *Rev. Sci. Instrum.* **79**, 10E503 (2008).
- <sup>195</sup>S. P. Vernon, M. E. Lowry, K. L. Baker, C. V. Bennett, J. R. Celeste, C. Cerjan, S. Haynes, V. J. Hernandez, W. W. Hsing, G. A. LaCaille, R. A. London, B. Moran, A. S. von Wittenau, P. T. Steele, and R. E. Stewart, *Rev. Sci. Instrum.* **83**, 10D307 (2012).
- <sup>196</sup>M. J. Haugh and M. Schneider, *Photodiodes - Communications, Bio-Sensings, Measurements and High-Energy Physics*, edited by J. W. Shi (Intechopen, Rijeka, Croatia, 2011).
- <sup>197</sup>J. D. Kilkenny, P. M. Bell, D. K. Bradley, D. L. Bleuel, J. A. Caggiano, E. L. Dewald, W. W. Hsing, D. H. Kalantar, R. L. Kauffman, D. J. Larson, J. D. Moody, D. H. Schneider, M. B. Schneider, D. A. Shaughnessy, R. T. Shelton, W. Stoeffl, K. Widmann, C. B. Yeaman, S. H. Batha, G. P. Grim, H. W. Herrmann, F. E. Merrill, R. J. Leeper, J. A. Oertel, T. C. Sangster, D. H. Edgell, M. Hohenberger, V. Y. Glebov, S. P. Regan, J. A. Frenje, M. Gatu-Johnson, R. D. Petrasso, H. G. Rinderknecht, A. B. Zylstra, G. W. Cooper, and C. Ruizf, *Fusion Sci. Technol.* **69**, 420 (2016).
- <sup>198</sup>A. B. Zylstra, C. Yeaman, S. Le Pape, A. MacKinnon, M. Hohenberger, D. N. Fittinghoff, H. Herrmann, Y. Kim, P. B. Radha, P. W. McKenty, R. S. Craxton, and M. Hoppe, *Phys. Plasmas* **27**, 124501 (2020).
- <sup>199</sup>S. Le Pape, L. Divol, L. B. Hopkins, A. Mackinnon, N. B. Meezan, D. Casey, J. Frenje, H. Herrmann, J. McNaney, T. Ma, K. Widmann, A. Pak, G. Grimm, J. Knauer, R. Petrasso, A. Zylstra, H. Rinderknecht, M. Rosenberg, M. Gatu-Johnson, and J. D. Kilkenny, *Phys. Rev. Lett.* **112**, 225002 (2014).
- <sup>200</sup>A. M. Cok, R. S. Craxton, and P. W. McKenty, *Phys. Plasmas* **15**, 082705 (2008).
- <sup>201</sup>E. K. Storm, H. G. Ahlstrom, and J. F. Holzrichter, "Exploding pusher targets illuminated using f/1 lenses at ~0.4 TW," Document No. 7127515, Palaiseau, France, 1976, see [OSTI.gov](http://OSTI.gov).
- <sup>202</sup>S. Glenn, P. M. Bell, L. R. Benedetti, D. K. Bradley, J. Celeste, R. Heeter, C. Hagmann, J. Holder, N. Izumi, J. D. Kilkenny, J. Kimbrough, G. A. Kyrala, N. Simanovskaia, and R. Tommasini, *Proc. SPIE* **8144**, 814409 (2013).
- <sup>203</sup>L. F. Berzak Hopkins, N. B. Meezan, S. Le Pape, L. Divol, A. J. Mackinnon, D. D. Ho, M. Hohenberger, O. S. Jones, G. Kyrala, J. L. Milovich, A. Pak, J. E. Ralph, J. S. Ross, L. R. Benedetti, J. Biener, R. Bionta, E. Bond, D. Bradley, J. Caggiano, D. Callahan, C. Cerjan, J. Church, D. Clark, T. Döppner, R. Dylla-Spears, M. Eckart, D. Edgell, J. Field, D. N. Fittinghoff, M. Gatu Johnson, G. Grim, N. Guler, S. Haan, A. Hamza, E. P. Hartouni, R. Hatarik, H. W. Herrmann, D. Hinkel, D. Hoover, H. Huang, N. Izumi, S. Khan, B. Koziolowski, J. Kroll, T. Ma, A. MacPhee, J. McNaney, F. Merrill, J. Moody, A. Nikroo, P. Patel, H. F. Robey, J. R. Rygg, J. Sater, D. Sayre, M. Schneider, S. Sepke, M. Stadermann, W. Stoeffl, C. Thomas, R. P. J. Town, P. L. Volegov, C. Wild, C. Wilde, E. Woerner, C. Yeaman, B. Yoxall, J. Kilkenny, O. L. Landen, W. Hsing, and M. J. Edwards, *Phys. Rev. Lett.* **114**, 175001 (2015).
- <sup>204</sup>J. S. Ross, D. Ho, J. Milovich, T. Döppner, J. McNaney, A. G. MacPhee, A. Hamza, J. Biener, H. F. Robey, E. L. Dewald, R. Tommasini, L. Divol, S. Le Pape, L. B. Hopkins, P. M. Celliers, O. Landen, N. B. Meezan, and A. J. Mackinnon, *Phys. Rev. E* **91**, 021101 (2015).
- <sup>205</sup>"2016 inertial confinement fusion program framework," Report No. DOE/NA-0044 (Department of Energy, NNSA, 2016).
- <sup>206</sup>S. Ross, "The National Diagnostic Plan (NDP) for HED science September 2021," Document No. 1823688 (Lawrence Livermore National Laboratory, 2021), see [OSTI.gov](http://OSTI.gov).
- <sup>207</sup>H. G. Ahlstrom, "Laser fusion experiments at LLL," Report No. UCID-18707 (1980).